ABSTRACT

PARAMETRIC STUDY OF HEAVY METAL PARTITIONING IN A PILOT-SCALE INCINERATOR BURNING SIMULATED MUNICIPAL SOLID WASTE

by
Sukrut S. Thipse

Incineration is a combustion process used to convert toxic waste to benign gases and residue in presence of excess air. The products of the incineration process are bottom ash, fly ash and the flue gas. Most of the metal-based phases formed in incineration are toxic and their emissions need to be strictly controlled. Therefore, behavior of metal species during incineration must be well understood. Such understanding is possible based on the experimental identification of the metal phases formed in the waste combustion and determination of their concentration in various incineration products.

A pilot-scale incinerator of 140,000 Btu/hr capacity was constructed, characterized and operated at NJIT. A synthetic fuel representative of the municipal solid waste in the United States was formulated and produced in 600 lb batches. The synthetic fuel was in the form of solid pellets and was characterized by standard ASTM tests. The solid fuel contained Fe and SiO_2, and was doped with trace amounts of Al, Ni, Cr, Hg and Pb. Several experiments were performed on the incinerator with varying fuel-air equivalence ratio and both gaseous and condensed products were sampled.

Atomic absorption spectroscopy was used to identify metal concentrations in the ashes and the flue gas. X-ray diffraction was used to identify metal phases in the bottom ash and the fly ash. Scanning electron microscope was used to study the morphology of the ash particles and energy dispersive X-ray spectroscopy was used to identify the spatial composition of the ash particles. Size distributions of the fly ash particles were

obtained using sieves and optical microscopy. It has been observed that the fly ash particles have bimodal size distribution and that the particles of different sizes have different elemental and phase compositions.

Thermodynamic equilibrium computations for the incineration process were conducted to obtain the adiabatic flame temperature and identify the metal phases produced at equilibrium conditions.

PARAMETRIC STUDY OF HEAVY METAL PARTITIONING IN A PILOT-SCALE INCINERATOR BURNING SIMULATED MUNICIPAL SOLID WASTE

by
Sukrut S. Thipse

A Dissertation
Submitted to the Faculty of
New Jersey Institute of Technology
in Partial Fulfillment of the Requirements for the Degree of
Doctor of Philosophy in Mechanical Engineering

Department of Mechanical Engineering

May 2001

APPROVAL PAGE

PARAMETRIC STUDY OF HEAVY METAL PARTITIONING IN A PILOT SCALE INCINERATOR BURNING SIMULATED MUNICIPAL SOLID WASTE

Sukrut S. Thipse

Dr. Edward L. Dreizin, Dissertation Advisor **Date**
Associate Professor of Mechanical Engineering, NJIT, Newark

Dr. Rong Y. Chen, Dissertation Committee Chair **Date**
Professor of Mechanical Engineering, NJIT, Newark

Dr. Peter B. Lederman, Committee Member **Date**
Research Professor of Chemical Engineering and Environmental Policy, NJIT, Newark

---

Dr. Joseph W. Bozzelli, Committee Member **Date**
Distinguished Professor of Chemistry, NJIT, Newark

Dr. Pushpendra N. Singh, Committee Member **Date**
Assistant Professor of Mechanical Engineering, NJIT, Newark

Dr. Michael R. Booty, Committee Member **Date**
Professor of Mathematics, NJIT, Newark

BIOGRAPHICAL SKETCH

Author: Sukrut S. Thipse

Degree: Doctor of Philosophy

Date: May 2001

Undergraduate and Graduate Education :

- Doctor of Philosophy in Mechanical Engineering,
  New Jersey Institute of Technology, Newark, 2001
- Master of Science in Mechanical Engineering,
  Bradley University, Peoria, Illinois, 1997
- Bachelor of Engineering in Mechanical Engineering,
  University of Poona, Pune, India, 1994

Major : Mechanical Engineering

Presentations and Publications:

Thipse, S.S., Sheng, C., Sun, H., Bozzelli J.W., Booty, M.R., and Magee, R.S., 1999. A Pilot-Scale Incinerator for Evaluating the Combustion of Co-fired Plastics, *Proceedings of the Joint meeting of the U.S sections of the Combustion Institute,* Vol. 1, 857-860, George Washington University, Washington, D.C.

Thipse, S.S., and Sheng, C., 1999. Evaluation and Comparison of Heat of Combustion Values for Synthetic RDF, *Proceedings of the meeting of the Eastern sections of the Combustion Institute,* Vol. 1, 224-227, North Carolina State University, Raleigh, NC.

Thipse, S.S., Sheng C., Booty M.R., Magee R.S. and Dreizin E.L., 2001. Characterization of a Synthetic Fuel for the Imitation of Municipal Solid Waste, *Chemosphere* (In Press).

Thipse, S.S., and Dreizin E.L., 2001. Metal Partitioning in Products of Incineration of Municipal Solid Waste, *Chemosphere* (Submitted).

BIOGRAPHICAL SKETCH
(Continued)

Thipse, S.S., Booty, M.R., Sheng, C., Magee, R.S., and Bozzelli, J.W., 2001. Chemical Makeup and Physical Characterization of a Synthetic fuel and Methods of Heat Content Evaluation for Studies on MSW Incineration, *Fuel* (Submitted).

Thipse, S.S., and Dreizin E.L., 2001. Size Distribution and Morphology of MSW Incinerator Fly Ash, *Fuel Processing Technology* (Submitted).

Thipse, S.S., and Dreizin, E.L., 2001. Morphology of the Fly Ash Particles Produced in Incineration of Municipal Solid Waste, *Proceedings of the Second Joint Meeting of the US Sections of the Combustion Institute*, Oakland Marriott, Oakland, CA.

Sheng, C., Thipse, S.S., Magee, R.S., Booty, M.R., and Bozzelli, J.W., 1999. Evaluation of Combustion of Co-Fired Plastics by a Pilot-Scale Incinerator, *Proceedings of the IT3 International Conference on Waste Incineration*, Miami, FL.

This dissertation is dedicated to my loving parents and my younger brother who provided the inspiration and support.

ACKNOWLEDGEMENT

I would like to express my sincere gratitude towards my advisor Dr. Edward Dreizin for his valuable guidance and continuing support. I also express my gratitude towards Dr. Richard Magee and Dr. Rong Chen for their guidance and support. I am deeply indebted to Dr. Joseph W. Bozzelli for his continuing guidance and support. I thank him for giving me the opportunity to work with the members of his research group. Without his valuable support this dissertation would not have been completed. Heartfelt thanks to Dr. Michael Booty for his contributions and support. I would like to express my sincere gratitude towards Dr. Lederman and Dr. Singh for serving as members of my dissertation committee.

I appreciate the active support and input of my friends and colleagues Dr. Yuri Shoshin, Chad Sheng, Roman Brukh, Samuel Chern, Dr. Byung-Ik Park, Ruslan Mudryy, Hongyan Sun, and Alexandre Ermoline. I am grateful to Dr. Ronald Kane and Dr. Daniel Watts for their encouragement and the financial support throughout my tenure at NJIT. I would also like to acknowledge the encouragement and help of Mr. John Griscavage, Mrs. Margaret Griscavage, Mr. Chandrakant Patel, Mr. Thomas Boland and Mr. Clinton Brockway from the HSMRC. Last but not the least, I would like to acknowledge the heartfelt gratitude I feel towards my family and reaffirm my faith in the all mighty.

TABLE OF CONTENTS

TABLE OF CONTENTS
(Continued)

TABLE OF CONTENTS
(Continued)

TABLE OF CONTENTS
(Continued)

LIST OF TABLES

LIST OF FIGURES

LIST OF FIGURES
(Continued)

CHAPTER 1

LITERATURE REVIEW

1.1 Introduction

Incineration is a thermal combustion process to reduce the volume of solid waste while producing benign gases and sterilized residue. The use of this process in solving problems of waste disposal in general and disposal of municipal solid waste (MSW) in particular cannot be underestimated. From both industrial and municipal sources, the United States generates about 10 billion metric tons of solid waste per year (Kiser, 1991). According to the *Scientific American Journal* "Every five years an average American discards directly or indirectly an amount of waste equal in weight to the Statue of Liberty" (O'Leary et al., 1988). The primary strategy of disposal of MSW from antiquity to modern times was landfilling. Nowadays, due to the stringent regulations in the U.S. and increased environmental awareness of people, incineration appears to have become a more and more viable means of waste treatment in the United States. Incineration, as a process, has evolved from widely distributed small incinerators, which were essentially open fires for destruction of waste materials, to highly sophisticated technological plants. Table 1.1 shows the current applications of incineration and competing technologies. The major advantages of incineration are: volume reduction of waste, detoxification of some harmful wastes, energy recovery, and environmental impact mitigation.

Table 1.1 Current applications of incineration and competing technologies.

Types of Waste	Reasons for incineration	Competing Technologies
Biomass	Energy recovery, Substitution for fossil fuels	Composting, Landfilling
Municipal solid waste	Conservation of land space, energy recovery	Landfilling, Biodegradation.
Medical Waste	Destruction of drugs, pathogens and syringes	Steam sterilization and subsequent landfilling
Hazardous waste	Destruction of hazardous chemicals in the waste	Biological treatment Pyrolysis

The major disadvantages of incineration are high capital cost, high operating costs along with the technical risks, and public opinion which tends to resist the technology for the fear of impact on the environment (Wallis and Watson, 1994). The major concern over the increased use of incineration has to do with the produced toxic emissions (Wallis and Watson, 1994). However, it has been shown that with the currently available control facilities and techniques, the air, land and water pollution can be minimized to increase the role of incineration in hazardous waste management.

With the increased use of incineration for disposal of various wastes, the problems of emission and pollution control need to be continuously addressed. It is especially important to develop pollution prevention and control techniques that would be adequate for treatment of wastes with continuously evolving compositions. It has also been observed that metal and plastic contents of municipal wastes have steadily increased with excessive use of metals and plastics in daily life (Gupta and Rohrbach, 1992). Industrial processes also produce a variety of solid metal-bearing waste materials including slags, fly ash, abrasive wastes, spent catalysts and construction waste containing refractory bricks (Brunner, 1989). Metal contaminated wastes are either landfilled or incinerated. Surface water infiltrating in landfills can pass through wastes

Therefore incineration can be a better alternative for the metal containing wastes if it immobilizes the heavy metals in ash.

In this study, an attempt has been made to address the concerns regarding metal emissions by characterizing the metal species in bottom ash and the fly ash of a waste pilot-scale incinerator. It was necessary to study the behavior of different metals contained in the waste during incineration. This was essential in understanding their impact on the environment. Although a lot of literature has been published on metal partitioning, many critical questions are still unanswered. These deficiencies in the literature include information on species distribution of metals in incineration products, link between metal species distribution and ash particle size and morphology. No attempt has been made to develop a standard fuel for metal partitioning analysis, which could be repeatable and easily fabricated. This study attempts to remove those deficiencies.

1.2 Metal Emissions and Their Toxicity

It is important to know which metallic species are present in various wastes in order to understand their behavior during combustion, predict combustion products and their effect on the environment. A list of the metal-containing compounds most often present in MSW and formed during the incineration are presented in Table 1.2. The most common metals of concern in municipal solid waste are lead, mercury, nickel and chromium (Brunner, 1989). They are toxic in solid or gaseous species in the elemental form or as oxides, chlorides or sulfides. Metals like aluminum and iron are also occur in the waste in increasing proportions due to increased disposal of packing items, soda cans and various consumer electronics and kitchenware (Wallis and Watson, 1994).

The concern over the emissions of heavy metals from the incineration process to the environment is well known. In particular, the volatile toxic metals like Pb and Hg pose a health hazard if released directly in gaseous form (ASME, 1979). In order to devise means to control the concentration of metals in air, it is essential to understand the fundamental thermal behavior of these metals in the incineration process. It is also important to study the link between the operating parameters of the incinerator and the volatilization behavior of metals. Because chemical, physical and toxicological properties of metal species are different, speciation has important implications in explaining emissions and ultimate environmental risks. Metals are distributed in the flue gas, bottom ash and fly ash as different species and this process is called metal partitioning.

Table 1.2 Metal species considered in the incineration processes.

Metal Name	Species Formula	Melting Point (C)	Boiling Point (C)	Species Toxicity	Reference Book
Chromium	Cr	1907	2671	Toxic	1
	CrN	1700	2010	Toxic	2
	Cr_2O_3	2435	4000	Toxic	1
	$CrCl_2$	824	1100	Toxic	2
	$Cr(NO_3)_3$	60	100	Toxic	2
	$Cr(Cl)_3$	1150	1300	Toxic	2
	CrS	1550	1715	Toxic	3
	$Cr_2(SO_4)_3$	100	235	Toxic	3
	$Cr(CO)_6$	110	210	Toxic	2
Lead	Pb	327.5	1744	Toxic	1
	PbO	888	1025	Toxic	1
	PbO_2	290	456	Toxic	2
	Pb_2O_3	370	578	Toxic	1
	Pb_3O_4	500	890	Toxic	2
	$PbCl_2$	501	950	Toxic	2
	$PbCl_4$	-15	105	Toxic	2
	PbS	1114	1325	Toxic	2
	$PbSO_4$	1170	1400	Toxic	3
	$PbCO_3$	315	420	Toxic	3
	$Pb(NO_3)_2$	470	552	Toxic	2

Mercury	Hg	-38.87	356.58	Toxic	1
	$HgCl_2$	276	302	Toxic	2
	HgCl	354	412	Toxic	2
	Hg_2Cl_2	400	612	Toxic	2
	HgO	500	724	Toxic	1
	HgS	583.5	616	Toxic	2
	$HgCO_3$	130	215	Toxic	2
	$Hg(NO_3)_2$	70	95	Toxic	3
	$Hg(CN)_2$	117	135	Toxic	3
	$HgSO_4$	1056	1187	Toxic	2
Nickel	Ni	1453	2732	Toxic	1
	NiO	1990	2810	Toxic	1
	$NiSO_4$	848	1574	Toxic	3
	$NiCl_2$	973	1001	Toxic	2
	$Ni(OH)_2$	230	440	Toxic	2
	$NiCO_3$	165	254	Toxic	3
Aluminum	Al	660.2	2467	Non-toxic	1
	Al_2O_3	2045	2980	Non-toxic	1
	$AlCl_3$	190	182	Non-toxic	2
	Al_2S_3	1100	1500	Non-toxic	2
	$Al(OH)_3$	300	510	Non-toxic	3
	AlN	2000	2200	Non-toxic	2
	Al_2SO_4	770	1025	Hazardous	3
Iron	Fe	1535	3000	Non-toxic	1
	FeO	1420	2630	Non-toxic	3
	Fe_2O_3	1565	2850	Non-toxic	1
	Fe_3O_4	1538	2120	Non-toxic	1
	$Fe(OH)_3$	136	310	Non-toxic	2
	FeS	1193	1634	Non-toxic	3
	$FeCO_3$	80	112	Non-toxic	3
	$FeCl_2$	670	815	Non-toxic	2
	$FeCl_3$	37	280	Non-toxic	2
	$Fe(CO)_5$	-21	102.8	Hazardous	2
	$FeSiO_4$	1503	1980	Non-toxic	2
	Fe_2C	1837	2345	Non-toxic	3
	$FeNO_3$	60.5	85	Non-toxic	2
Silicon	Si	1410	2355	Non-toxic	1
	SiO	1702	1880	Non-toxic	2
	SiO_2	1703	2230	Non-toxic	1
	SiC	2700	3895	Non-toxic	3
	$SiCl_2$	815	970	Non-toxic	2

Key: 1) JANAF, 1991 2) CRC, 1998 3) Miller, 1990

Ideally the non-volatile metals (Al, Ni, Cr, Fe) and their compounds should be immobilized in the bottom ash and the volatile metals (Pb and Hg) and their compounds should be immobilized in the fly ash with no metal or metal compounds escaping to the

flue gas. During the actual incineration process, however, some metal does escape to the flue gas and this fraction constitutes a heath hazard (Niessen, 1995). Also some fraction of the incinerator fly ash in the form of sub-micron particulate matter escapes capture by the fabric filters or electrostatic precipitators and is emitted to the environment. Minimization of these metal fractions is thus the practical goal of the majority of research conducted in metal partitioning. While these concerns have been well understood and addressed in the literature, the metals that are captured in the ash are usually considered immobile (Niessen, 1995). However, depending on the size, composition and morphology of the metal-containing ash particles, this may or may not be true. Thus the important scientific goals of this study are to understand the process of metal partitioning and characterize metallic species produced at different stages of incineration. Since metal contents are different for various types of waste, experimental research should focus at a particular kind of waste. The current project deals with metal partitioning in the products of incineration of municipal solid waste.

1.3 The Origin of Metals in MSW

The toxic metals addressed in this study are mercury (Hg), lead (Pb), chromium (Cr), and nickel (Ni). All of these metals are commonly found in municipal solid waste (USEPA, 1996) and are selected in this study due to their toxicity. Toxic metals like As and Cd also exist in MSW, but were not chosen for this study as their partitioning has been thoroughly discussed in the literature (Linak and Wendt, 1993). The significant inorganic species present in MSW contain Si, Fe and Al, therefore partitioning of these elements has also been addressed. Literature studies on Al, Fe and Si partitioning are

almost absent. Information about these metals and their sources in the waste is discussed below.

Chromium: Chromium (Cr) is a silver-gray lustrous non-volatile metal found mainly in the earth's crust as chromite ($Fe_2Cr_2O_4$) mineral. It occurs in this compound form and is extracted commercially. The estimated consumption of chromium in the United States is 435,000 metric tons annually (Niessen, 1995). Chromium is contained in stainless steel and thus ends up in MSW via discarded stainless steel items. It also occurs as Cr (III) oxide or Cr (VI) oxide in scrap residue in municipal solid waste and both oxides are toxic (Brunner, 1989). Chromium coatings also present an important source of waste chromium.

Lead: Lead (Pb) is a bluish-white, silvery semi-volatile metal that is highly lustrous. It is very soft and malleable and can be cast, rolled and extruded. Lead occurs as oxide in batteries or in elemental form in paints. The consumption of lead in the U.S is approximately 1,220,000 metric tons annually (Niessen, 1995). The major source of lead in municipal waste is lead acid batteries (around 80%). Flameproof curtains, waste paint cans containing certain paints with lead as an ingredient are some other sources. Lead is also contained in the solder used in electronic chips. All lead-containing species are toxic.

Mercury: Mercury (Hg) is a silvery volatile liquid at room temperature. Mercury is commonly found in the earth's crust as the ore, cinnabar (HgS). Mercury is used in thermometers and in other analytical instruments. The total use of mercury in the US is approximately 621 metric tons annually (Niessen, 1995). The common sources of mercury in waste are spent batteries, mercury vapor lamps, switches, dental amalgams,

measuring devices, control instruments and electrolytic refining wastes. Mercury is also used in the production of chlorine and ends up in the waste as a byproduct. All compounds of mercury are toxic and carcinogenic (Niessen, 1995).

Aluminum: Aluminum (Al) is a lustrous silvery non-volatile metal. Aluminum content in the solid wastes in the United States increases every year (Niessen, 1995). The most common source of aluminum in the MSW is soda cans. The other sources are packaging, cigarette foils and candy wrappers. Aluminum accounts for 0.6% of the total waste by mass. 1,960,000 tons of aluminum is produced and consumed annually in the U.S. Except for hazardous sulfate species, most of the aluminum compounds are non-toxic.

Nickel: It is a non-volatile element of concern due to its toxicity. Nickel is commonly used as a component of stainless steel and in the production of wires. 1,400,000 tons of nickel is consumed annually in the U.S. Nickel content in the solid wastes in the United States increases every year (Niessen, 1995). All nickel species are toxic and carcinogenic.

Iron: Iron is a non-volatile heavy metal, which usually ends up in municipal solid waste as scrap metal. Cast iron pipes, iron shavings are commonly found in waste. Iron occurs in elemental form as well as in the oxide form as FeO or Fe_2O_3. Except for hazardous carbonyl species most of the iron species are non-toxic.

Silicon: Silicon is a non-volatile semiconductor element used in electronic and computer applications. It ends up in waste through discarded electronic, computer equipment and television tubes and waste sand and glass from construction sites. Most of the silicon present in the waste is in form of silicon dioxide (SiO_2) commonly known as silica.

Silica is a chemically inert material and is the major constituent of sand. All silicon species are non-toxic (Niessen, 1995).

1.4 Factors Influencing Metal Partitioning

The release of toxic metal containing species in refuse incineration depends on high temperature chemical mechanisms and on phase composition of non-metallic products dominating the incinerator exhaust. Statistically metals are fairly uniformly distributed in the solid waste entering the municipal solid waste (MSW) incinerator (Brunner, 1989). The concentration of metals in the waste is usually lower than the levels considered hazardous. However, due to the overall lower volatility of metal-containing species as compared to that of the majority of organic combustion products, the percentage of metal containing species in ash becomes much higher than that in MSW. This concentration increase of metals in ash is one factor contributing to the classification of some of the ash residues from MSW incineration as hazardous.

Metal partitioning is studied by analyzing products of the incineration process, namely the bottom ash, the fly ash and the flue gas. The greater part of the ash residue formed in an incinerator during combustion tends to remain on the grate and is referred to as the bottom ash. The remainder of the ash that is formed becomes entrained in the gas flow through the combustor and is carried downstream with reacting gases. It is known as the fly ash. The main factors identified in the literature (Niessen, 1995), affecting metal partitioning are: 1) Incinerator design; 2) Primary combustion chamber temperature; 3) Fuel-air equivalence ratio (ϕ); 4) Residence time of the fuel on the grate; 5) Residence time of the flue gas in the secondary combustion chamber; 6) Metal

characteristics; 7) Exhaust gas temperature; 8) Waste content of metal volatilizing species, especially chlorine.

1.5 Metal Partitioning Literature

Metal partitioning research can be divided in two main sections, namely experimental and theoretical. The experimental research can be further subdivided into three groups depending on the type and size of the incineration equipment used in the study. Most of the work has been carried out using large-scale commercial incinerators as summarized in the literature (Niessen, 1995). Clearly, the capabilities of control of the process parameters, variation in fuel composition, and establishing correlation between the incineration process and metal partitioning are very limited for this type of research. The other group of incineration studies employ the bench scale units, which comprise of small tubular reactors (Park et al., 2000). While providing much more detailed diagnostics and instrumentation capabilities, these units have limitations, such as lack of turbulence and solid fuel feeding system. The third category is the pilot-scale incinerator, in which the fewest studies by far, have been carried out. The units here range from 100,000 to 150,000 Btu/hr in capacity (Niessen, 1995). These units are large enough to replicate all the significant incineration conditions, but at the same time, are sufficiently small to enable one to operate them in a carefully controlled manner. The design and building of such units is costly and therefore, the experimental data sets produced using this kind of facilities are limited than with full-size units (see review by Linak and Wendt, 1993).

In most of the previous studies of incineration metal partitioning, metals were introduced into the combustion system as a spray of metal nitride solutions in a natural

gas flame (Bool et al., 1995). Such experiments poorly represent the behavior of metals in actual incinerators where they are introduced as solid particles within a solid waste matrix. A synthetic waste fuel used in the laboratory studies should better imitate MSW with metal content. Only in a very few studies, (Ho et al., 1994) did researchers attempt to develop or use such a synthetic fuel. Another experimental difficulty is the achievement of continuous fuel feed, similar to industrial incinerators. Because of many experimental difficulties, only few researchers have been able to compare the amounts of metals fed to and exiting from the incinerator (Ho et al., 1994). For the large-scale units the input metal concentration could not be controlled. The loss of metals was also high within the unit due to the adhesion to the walls and heat exchanger tubes (Ho et al., 1994).

Numerous studies have been published, focused on partitioning of a few toxic metals like Hg, Pb, Cr, Cd, As and Ni and have been reviewed by Brunner, 1989. Most of the times, the partitioning results for the metals have been reported as percentage distribution in bottom ash, fly ash and flue gas without discussing the species of metals distributed. This is due to the difficulties in identifying the trace metal species and measuring concentrations usually in the order of parts per million (ppm). Effects of some of the experimental conditions, such as chlorine content, combustion temperature, and incinerator design on metal partitioning have been extensively studied (Linak and Wendt, 1993). In many of the theoretical studies of metal partitioning, equilibrium analysis predictions have been made (Wu and Biswas, 1993) using various equilibrium codes such as NASA code (Gordon and McBride, 1991), CHEMKIN code (SANDIA, 1995) and Air Force Code (Selph and Hall, 1993). The effects of incinerator operating

parameters e.g., combustion temperature, chlorine content of the fuel, and flue gas residence time on metal phase distribution have been discussed based on the results of the equilibrium modeling (Linak and Wendt, 1993). However, in most cases the fuels used by researchers in equilibrium modeling did not have chemical formulae representing the MSW.

The kinetic data available for chemical transformations occurring during incineration in general and metal reactions in particular is very limited (Fernandez et al., 1992). As a first approximation, partitioning behavior of Fe, Hg, Al, Ni, Cr, Pb, Al and Si can be predicted based on their physical properties, e.g. volatility at the incineration temperatures. Fe, Al, Ni, Cr and Al are partitioned in the bottom ash whereas Hg and Pb are partitioned in the fly ash.

1.6 Experimental Literature

Metal partitioning was addressed in a number of studies using different incineration equipment and different fuels. Table 1.3 shows summary of the experimental conditions used in the literature discussed below. It is necessary to point out here that the synthetic fuel used in this study was doped with five trace metal species Hg, Pb, Al, Ni, and Cr (each 0.01 % by mass). These metals occur naturally in the MSW in similar trace amounts. The main advantage of doping the fuel with metal species is to replicate the entry of metals in the solid form in waste incinerators. Also the metals can be uniformly distributed and introduced in a controlled measured amount in the incinerator, which helps to achieve a better mass balance. Although the actual metal distribution in waste incinerators is highly heterogeneous, reasonable heterogeneity is obtained in the synthetic fuel.

Table 1.3 Summary of experimental studies

Researchers	Reactor	Fuel Used	Grate	PCC Temp Degree C	Addition-al Info	Country
Jakob et al., 1995	Full-Scale	MSW	Fixed	670 to 1300		Switzerland
Chiang et al., 1998	Full-Scale	MSW	Fixed	650 to 900	0.8 % Cl	Taiwan
Nakamura et al., 1996	Full-Scale	MSW	Fixed	1000 to 1100		Japan
Wang and Chiang, 1999	Full-Scale	MSW	Fixed	650 to 850	Phi 0.2-0.5	Taiwan
Biswas and Wu, 1998	Full-Scale	MSW	Fixed	827 to 1227	0.6 % Cl	USA
Brunner and Monch, 1986	Full-Scale	MSW	Fixed	900 to 1200	Phi 0.5-1	Switzerland
Vogg et al., 1986	Full-Scale	MSW	Fixed	900 to 1000	0.7 % Cl	Germany
Bergstrom, 1986	Full-Scale	MSW	Fixed	1000 to 1100		Sweden
Reimann, 1986	Full-Scale	MSW	Fixed	800 to 1000		Germany
Ho et al., 1994	Full-Scale	MSW	Rotary	870 to 1100	1.5 % Cl	USA
Binner et al., 1997	Full-Scale	MSW	Rotary	900 to 1500		Denmark
Carroll et al., 1995	Full-Scale	Synthetic Fuel	Rotary	538 to 927	3.4 % Cl	USA
Wey et al., 1998	Full-Scale	Synthetic Fuel	Fluidized	700 to 900	10 % Cl	Taiwan
Lind et al., 1999	Full-Scale	Forest Waste	Fluidized	780 to 880		Sweden
Linak and Wendt, 1993	Full-Scale	MSW +Coal	Fixed	750 to 1100		USA
Eckert et al., 1999	Full-Scale	MSW +Coal	Fixed	1000 to 1200		USA
Senior et al., 1999	Full-Scale	Coal	Fixed	1100 to 1175		USA
Bool and Wendt, 1995	Pilot-Scale	Coal	Fixed	1100 to 1500	Phi 0.8-1.3	USA
Karimanal et al., 1996	Bench-Scale	Metals	Fixed	450 to 900		USA

1.6.1 Mercury Partitioning

A) Overall Distribution and Species: Mercury is a volatile metal and most researchers agree that high amounts of mercury are found in the flue gases (Chen et al., 1998). However, there is no agreement on the specific amount of Hg present in the flue gas. For example, approximately 80% of Hg occurred in the gaseous state and about 20 % was deposited on the fly ash at flue gas temperatures between 200 and 230°C in experiments by Vogg et al., 1986. A slightly different distribution was reported by Brunner and Monch, 1986: 72 % of Hg occurred in the flue gas, 24% occurred in the fly ash and 4 % occurred in the bottom ash. Reimann, 1986 reported that for primary combustion chamber temperatures in the range of 800°C to 1000°C, 80 to 90% of mercury was present in the flue gas and observed that the bottom ash and fly ash contained small amounts of mercury.

In the case of speciation of Hg, there is disagreement between different researchers, partly due to the differences in fuel and incineration conditions. Vogg et al., 1986 predicted the formation of gaseous $HgCl_2$ and further reduction to gaseous HgCl at incineration temperatures around 1000°C. Brunner and Monch, 1986 experimentally observed that higher carbon, chlorine and sulfur contents in the fuel caused the formation of mercury carbonate $HgCO_3$, mercury chloride $HgCl_2$ and mercury sulfate $HgSO_4$ in the flue gas. Bergstrom, 1986 noted that if chlorine was absent in the fuel, mercury existed both in elemental and oxide forms in the flue gases. Carroll et al., 1995 observed experimentally that increased chlorine content in waste caused higher concentration of $HgCl_2$ (g) in the flue gas but also observed presence of elemental Hg and mercury oxide HgO in the flue gas in the absence of chlorine in the fuel similar to

Bergstrom, 1986. However, Wang and Chiang, 1999 experimentally observed Hg oxides formed in the incinerator in the temperature range of 650 to 850°C, even though chlorine was present in the waste fuel. XRD analysis confirmed the presence of HgO in the bottom ash.

B) Effect of incinerator operating conditions: Brunner and Monch, 1986 reported that the combustion temperature and the equivalence ratios affected the overall Hg partitioning between the flue gas and fly ash. They predicted a trend of increasing Hg concentration in the flue gas and decreasing of the Hg concentration in fly ash at the increased combustion temperatures from 900°C to 1200°C and equivalence ratios from 0.5 to 1.0. Bergstrom, 1986 experimentally observed that mercury concentration in the flue gases of MSW incinerator increased with increasing flue gas residence time in the incinerator. Wang and Chiang, 1999 reported that an increase in incinerator temperature, and waste chlorine content increased $HgCl_2$ formation, which increased the mercury content in the flue gas. Linak and Wendt, 1993 observed that increasing the combustion temperature, waste chlorine content and flue gas residence time increased the mercury content in the flue gas.

1.6.2 Lead Partitioning

A) Overall Distribution and Species: Brunner and Monch, 1986 reported Pb concentration of 58 % in the bottom ash, 37 % in the fly ash and 5 % in the flue gas for a MSW incinerator operated at a maximum primary combustion chamber temperature of 1200°C. Nakamura et al., 1996 reported the distribution for Pb in bottom ash, fly ash, and flue gas of the MSW incinerator as 66 %, 33 % and 1% respectively. Brunner and

Monch, 1986 show higher concentration of Pb in the fly ash and lower Pb concentration in the bottom ash than that of Nakamura et al., 1996. This can be explained due to the higher equivalence ratios (0.5 to 1.0) used by Brunner and Monch, which leads to higher primary combustion chamber temperatures (around 1200°C) in their experiments. Higher temperatures cause higher Pb volatility and hence increase the concentration of Pb in the flue gas and the fly ash. Wey et al., 1998 reported Pb distribution in the bottom ash, fly ash and flue gases of the MSW incinerator to be 82 %, 9.2 % and 5.3 % respectively. This distribution is in a contrast to the one observed experimentally by Brunner and Monch, mostly due variation of waste composition in Taiwan and Germany.

There is agreement among researchers as to which species of lead are observed in the bottom ash and fly ash/flue gas during incineration. Brunner and Monch, 1986 observed presence of lead oxide (PbO) in the bottom ash. This observation was in agreement with that of Karimanal and Hall, 1996 who also observed lead oxide (PbO) in the bottom ash. Wang and Chiang, 1999 identified lead oxide (PbO) and elemental lead (Pb) in the bottom ash and lead chloride ($PbCl_2$) in the fly ash by XRD. Linak and Wendt, 1993 observed gaseous lead chloride $PbCl_2$ in the flue gas, which condensed downstream at lower temperatures and ended up in the fly ash as $PbCl_2$ (s).

B) Effect of incinerator operating conditions: Wang and Chiang, 1999 noted that an increase in the incinerator temperature and waste chlorine content promoted the formation of volatile lead chloride $PbCl_2$ which was partitioned in the flue gas. Eckert et al., 1999 observed a correlation of the Pb concentration in the waste and the bottom ash unlike Wang and Chiang, 1999 who observed no correlation. Karimanal and Hall, 1996

concluded experimentally that increase in the temperature, airflow velocity increased the volatilization of metal Pb in the incinerator environment.

1.6.3 Chromium Partitioning

A) Overall Distribution and Species: Wey et al., 1998 reported the experimental percentage distribution of Cr in bottom ash, fly ash and flue gases of MSW incinerator operated at 600°C to be 92 %, 5.2 %, and 2.6 % respectively. Binner et al., 1997 reported experimental percentage distributions for Cr in bottom ash, fly ash and flue gases of a MSW incinerator to be 97.64 %, 1.19 % and 1.16% respectively. The difference in distributions can be explained on the basis of higher chlorine content 5 % in the experiments of Wey et al., 1998, which causes the formation of volatile chromium chlorides increasing the concentration in the fly ash.

In case of species distribution, Wu and Biswas, 1993 noted that chromium oxides and chromium hydroxides were observed in bottom ash and chromium chlorides were present in the fly ash. Similar results were obtained by Wang and Chiang, 1999 who identified chromium oxides in the bottom ash and chromium chlorides in the fly ash using x-ray diffraction.

B) Effect of operating conditions: Wang and Chiang, 1999 outlined the important parameters affecting Cr partitioning as the incinerator temperature, the fuel-air equivalence ratios and the initial chromium content of waste. They experimentally found higher concentration of Cr in the bottom ash (94 to 96 %) with increasing fuel-air equivalence ratios (0.2 to 0.5) and combustion temperature (650°C to 850°C).

1.6.4 Nickel Partitioning

A) Overall distribution and Species: Binner et al., 1997 reported experimental percentage distributions for Ni in bottom ash, fly ash and flue gas of a MSW incinerator to be 94.48 %, 3.72 % and 1.8 % respectively. Data about species distribution is not available in the literature.

B) Effect of operating conditions: Binner et al., 1997 experimentally observed higher concentration of Ni in the bottom ash (92 to 94.5) % with increasing combustion temperature (900°C to 1500°C). Wu and Biswas, 1993 also observed a similar trend.

1.6.5 Aluminum Partitioning

A) Overall Distribution and Species: Senior et al., 1999 measured 97 % of Al in the incinerator bottom ash. Wang and Chiang, 1999 experimentally measured percentage of Al in the incinerator fly ash as 4.47 % by energy dispersive x-ray (EDX) analyses. It was observed that aluminum oxidized during incineration producing the stable aluminum oxide Al_2O_3 (Senior et al., 1999).

B) Effect of operating conditions: Brunner and Monch, 1986 experimentally observed a trend of increasing Al concentration in the bottom ash (90 to 94 %) with increasing fuel air equivalence ratios (0.5 to 1.0) and combustion temperature from 900° to 1200°C.

1.6.6 Iron Partitioning

A) Overall Distribution and Species: Brunner and Monch, 1986 reported experimental percentage distribution for Fe between bottom ash, fly ash and flue gases of the incinerator to be 99 %, 1 % and 0.02 %. Wang and Chiang, 1999 experimentally

measured percentage of Fe in the incinerator fly ash to be 3.95 % by energy dispersive x-ray (EDX) analysis. Bool and Wendt, 1995 observed that iron in the coal oxidized to form iron oxide Fe_2O_3. This was a two step reaction and the equations are written as 2 $Fe + O_2 \rightarrow 2\ FeO$ and $2\ FeO + O_2 \rightarrow Fe_2O_3 + O$.

B) Effect of operating conditions: Brunner and Monch, 1986 observed a trend of increasing Fe concentration in the bottom ash (98 % to 99 %) with increasing fuel-air equivalence ratios (0.5 to 1.0) and the combustion temperatures (900°C to 1200°C).

1.6.7 Silicon Partitioning

A) Overall Distribution and Species: Wang and Chiang, 1999 experimentally measured percentage of Si in the incinerator fly ash as 9.79 % by energy dispersive x-ray (EDX) analysis. Silicon is expected to be present as silicon dioxide SiO_2 in incinerator ashes. However Wey et al., 1998 observed that in the oxidizing atmosphere of the incinerator chamber, local oxygen depleted reduction zones were formed. This could account for the volatilization of refractory silicon oxides in ash by reduction to form volatile suboxides or pure elements. For example silica (SiO_2) can be reduced as $SiO_2 + CO \rightarrow SiO + CO_2$ and then $SiO + CO \rightarrow Si + CO_2$.

This completes a brief review of the experimental literature available for metal partitioning in incineration. One can note from this review that there is need for research addressing the following specific problems. 1) Link between metal partitioning and morphology of fly ash and bottom ash. 2) Link between metal partitioning and species are present in the fly ash and bottom ash.

1.7 Theoretical Literature

The incineration process has been studied and researchers have performed two types of theoretical analyses namely, 1) equilibrium modeling and 2) kinetic modeling. Equilibrium modeling determines adiabatic flame temperature and adiabatic product distribution. kinetic modeling considers in detail the reaction rates and predicts the possible chemical reactions and products. In this study only equilibrium modeling was used and the adiabatic product distribution for each metal is discussed separately in the following review. Refer to Table 1.4 for the list of equilibrium codes used by various researchers.

Table 1.4 Summary of Equilibrium Computations

Researchers	Code Used	Metals Analyzed	Fuels Considered
Binner et al., 1997	NASA	Hg and Pb	MSW, Denmark
Barton et al., 1998	NASA	Cr and Ni	MSW, USA
Wu and Biswas, 1993	STANJAN	Hg, Pb and Cr	MSW, USA
Chen et al., 1998	STANJAN	Pb and Cr	MSW, Taiwan
Fernandez et al., 1992	CHEMKIN	Pb, Al and Fe	MSW, Spain
Reimann, 1989	CHEMSAGE	Hg, Pb, Cr and Ni	MSW, Germany
Verhulst et al., 1996	CHEMSAGE	Hg, Pb, Ni, Al and Fe	MSW, Germany
Ljung and Nordin, 1995	CHEMSAGE	Pb, Cr and Ni	Biomass, Sweden
Furimsky, 2000	EQUILIB	Hg and Pb	Coal, Canada

1.7.1 Mercury Partitioning

Binner et al., 1997 reported that according to his computations, mercury formed volatile $HgCl_2$ in the flue gas for temperatures up to 1500°C. This prediction was in agreement with the prediction of Verhulst et al., 1996 who also observed $HgCl_2$ (g) above 700°C. However, predictions of both Binner et al., 1997 and Verhulst et al., 1996 disagreed with the prediction of Reimann, 1989 that mercury formed gaseous HgO above 800°C. The reason for this discrepancy was the higher Cl content of 2 to 3 % in the MSW considered by Binner et al., 1997 and Verhulst et al., 1996 as compared to 0.5 % of Cl used by Reimann, 1989. Wu and Biswas, 1993 predicted gaseous mercury oxide HgO formation at higher temperatures and gaseous mercury chloride $HgCl_2$ formation at higher Cl concentrations. This prediction was in agreement with that of Furimsky, 2000 who predicted the formation of HgO (g) and volatile $HgCl_2$ (g) in his equilibrium output.

1.7.2 Lead Partitioning

Ljung and Nordin, 1997 predicted from their equilibrium computations that lead formed lead oxide PbO (g) above 800°C. This prediction was in agreement with that of Furimsky, 2000 and Reimann, 1989 who predicted formation of PbO (g) in their equilibrium output. Binner et al., 1997 however predicted that the predominant lead species formed was $PbCl_2$ (g). Verhulst et al., 1996 also observed in their computations that Pb volatilized as $PbCl_2$ (g) above 800°C. The formation of chloride was due to higher chlorine content in the MSW used by Binner et al., 1997 and Verhulst et al., 1996. Wu and Biswas, 1993 predicted PbO (g) formation at higher temperatures and $PbCl_2$ (g) formation at higher Cl concentrations.

1.7.3 Chromium Partitioning

Chen et al., 1998 predicted that Cr_2O_3(s) was formed in a Cr-oxygen system, whereas CrO_2Cl_2(s) was formed in a Cr-oxygen-chlorine system. This prediction was in agreement to that of Wu and Biswas, 1993 who predicted the formation of Cr_2O_3(s) and CrO_2Cl_2(s) formation in the computations conducted without and with chlorine respectively. Reimann, 1989 predicted that chromium formed oxide Cr_2O_3 above 800°C. Ljung and Nordin, 1997 also predicted formation of Cr_2O_3 (s) upto 1000°C. In addition they predicted formation of CrO_3 (g) above 1000°. For the high chlorine containing wastes, Barton et al., 1998 predicted formation of $CrCl_2$ (g).

1.7.4 Nickel Partitioning

Equilibrium computations by Riemann, 1989 predicted that Ni formed nickel oxide NiO(s) above 800°C. This prediction was in agreement with that of Verhulst et al., 1996. Ljung and Nordin, 1997 also predicted formation of NiO(s) upto 1500°C and in addition, predicted formation of $NiCl_2$ (g) over 1500°C. Barton et al., 1998 however only predicted the formation of nickel chloride $NiCl_2$ (g), in their output due to the high chlorine content (5 to 10 %) in their waste. They also noted that an additional 10 % increase in the waste chlorine content had no effect on the species distribution.

1.7.5 Aluminum Partitioning

Verhulst et al., 1996 predicted from his equilibrium computations that Al_2O_3 was the stable oxide and $AlCl_3$ was the stable chloride formed under incineration conditions. They noted that the aluminum chloride volatilized and entered the flue gas and

subsequently condensed in the fly ash. Fernandez et al., 1992 predicted by kinetic calculations that aluminum reacted to form stable alumina (Al_2O_3) in the combustion chamber. 4/3 Al + O_2 ➔ 2/3 Al_2O_3. They also predicted the formation of $AlCl_3$ or $AlSO_4$, for wastes with higher chlorine and sulfur contents.

1.7.6 Iron Partitioning

Verhulst et al., 1996 predicted by equilibrium computations that hematite, Fe_2O_3 and $FeCl_2$ were the stable species formed during incineration. This prediction was in agreement with the kinetic predictions of Fernandez et al., 1992 that iron produces iron oxide (Fe_2O_3) and volatile iron chloride ($FeCl_2$) during incineration. The reactions can be written as 4/3 Fe + O_2 ➔ 2/3 Fe_2O_3 and 2 Fe + O_2 + 4 HCl ➔ 2 $FeCl_2$ + 2 H_2O. Fernandez et al., 1992 also predicted the transport of iron to the fly ash by mechanical entrainment of Fe_2O_3 and volatilization of $FeCl_2$.

1.8 Summary

It can be observed from the literature review that the equilibrium computations have focussed on the chloride, oxide and sulfide species of metals. No work has addressed the formation of metal nitrides or carbides in case of nitrogen rich or carbon rich fuels. Equilibrium computations have considered the effect of temperature, air to fuel ratio, chlorine/sulfur content in fuel. Kinetic data available for metal reactions and organic-metal reactions are very limited. Only a few research groups such as the Wendt research group in university of Arizona and Fernandez research group in Spain have performed kinetic modeling of metal partitioning process (Linak and Wendt, 1993; Fernandez et al., 1992).

CHAPTER 2

SYNTHETIC FUEL

2.1 Introduction

This chapter explains the development and testing of a synthetic fuel, which emulates municipal solid waste in the United States. Research on waste combustion and products of solid waste incinerators has been active (e.g., Abe et al., 1997, Binner, et al., 1997, Karimanal and Hall, 1996). Most of the relevant research efforts have been focused at analyses of operation of industrial incinerators (Hinton and Lane, 1991). Often, the results of such studies are hard to reproduce and interpret in terms of mechanistic understanding of incineration processes. Recently, detailed mechanisms of waste incineration processes have been addressed in experiments using laboratory burners and incinerator models (e.g., Davis et al., 1998, Linak et al, 1996, Chiang, et al., 1997, Shin and Choi, 2000, Blumenstock et al., 2000). Even though the number of relevant studies has become significant, meaningful comparison of the reported results, especially describing the compositions of effluent gas and particulate matter is not straightforward largely due to the differences in the compositions of the actual and simulated wastes used in different studies and differences in the construction of the experimental incinerators. Often, different kinds of wood are used as a simulated waste or biofuel (Andersson and Marklund, 1998, Shin and Choi, 2000, Blumenstock, et al., 2000). In a recent study by Wang et al., (1999), a simulated municipal solid waste (MSW) was developed based on the Taipei's MSW statistics. Unfortunately, the preparation of the simulated MSW was not described in sufficient detail for reproducing in different

experiments, in addition the composition of the simulated MSW described by Wang et al., (1999) did not correlate well with that of the typical US MSW (USEPA, 1997).

Analysis of the current research indicates that in order to adequately characterize operation of the industrial "waste to energy" facilities, both an appropriate scale, well-instrumented incinerator facility and a well-characterized, reproducible fuel simulating waste (or refuse derived fuel) are required. Recently, a pilot-scale, continuous operation, incinerator facility has been developed at NJIT (described in detail in Chapter 3) that is capable of reproducing the operation of industrial incinerators while enabling detailed characterization and control of combustion processes and products (Thipse et al., 1999). The second component, "synthetic waste" fuel, is required for successful experiments. It needs to be well characterized, reproducible, and easy to modify so that various experimental conditions including feed variations can be assessed and compared. The developing trend in separating different wastes, e.g., in MSW, medical wastes, chemical industrial wastes, etc., somewhat simplifies the problem and allows one to start preparing a synthetic fuel replicating a particular kind of waste used in the incineration plants. MSW presents the most significant portion of the incinerated wastes worldwide and this work is aimed at production and characterization of a synthetic fuel that imitates MSW for experimental studies of the processes affecting its incineration.

2.2 Synthetic Fuel Formulation

The composition of MSW has been traced over the years by the US Environmental Protection Agency (EPA) and it is summarized in the EPA reports (USEPA, 1997). The MSW composition is shown in Table 2.1 according to the latest available EPA report. Previous research has also determined a number of physical and chemical parameters of

MSW that play important role in the incineration processes and should, therefore, be adequately reproduced in the synthetic fuel. These parameters of MSW are presented in Table 2.2 together with respective literature references.

The synthetic fuel that imitates MSW must be reproducible and its components should be readily available and inexpensive. Based on these considerations, the data presented in Table 2.1, and on discussions with the members of American Plastics Council (Goodman et al., 1997), the following components have been chosen for the synthetic fuel:

1. Paper, 35 weight %. The newsprint paper strips of 4 – 5 inches long with no ink or printing on them are obtained from Vanguard Offset Printers, Hillside NJ.
2. Hardwood mulch, 17 weight %. This component imitates both wood and yard trimming in MSW. Although this may not accurately represent all forms of garden waste such as grass clippings, it replicates the cellulose component of the waste. The mulch is obtained from Pecquanock Lumber Mill, NJ. The size of mulch particles is 2 to 3 mm. Moisture content in the mulch was determined by measuring the mulch sample weight reduction after annealing in a flow of air in a convection oven at 110°C for two hours. The experimental moisture content was found to be 8 mass percent that is in fair agreement with the wood moisture content of about 10 % reported in the literature (White, 1987).
3. Low-density polyethylene (LDPE), 14 weight %. This plastic is the one that is most widely used in consumer products. The LDPE for the synthetic fuel was obtained from Chevron Polyethylene Resins, it is 98% pure granular powder with particles of about 0.5 mm diameter. An increased weight percent of plastic was used in the

synthetic fuel as compared to the plastic content in MSW, reflecting a trend to increased amounts of plastics in wastes noted in (USEPA, 1997).

4. Iron, 8 mass %. Since most of the metal in MSW is ferrous, iron has been chosen to serve as a representative component in synthetic fuel. Iron filings with the particle size range of 0.2 - 0.5 mm and purity of 99% have been obtained from Fisher Chemicals.
5. Animal feed, 5 weight %. This component has been chosen to represent the food waste. Recreational horse food was obtained from Agway, Inc.
6. Sand, 1 weight %. Sand represents glass and miscellaneous inorganic waste content of the fuel. The sand was obtained from a construction supplier in Ironbound, NJ; the size of sand particles is less than 0.2 mm. In preliminary experiments, greater amounts of sand (3 – 7 %) were used, but sand clusters were observed to form and clog the incinerator grates.

Table 2.1 EPA statistics on MSW content (US EPA, 1997)

COMPONENT	MASS %
Paper and Paperbound	39.2
Yard Trimming	14.3
Wood	7.1
Plastics	9.1
Metals: Ferrous 5.6 % Aluminum 1.4 % Other nonferrous 0.6 % Total	7.6
Food Wastes	6.7
Glass	6.2
Textiles	3.6
Rubber and Leather	2.9
Miscellaneous Inorganic Wastes	1.5
Other	1.7

2.3 Synthetic Fuel Preparation

A fuel batch of about 270 kg is usually prepared. That is sufficient for 3 experiments using the NJIT pilot scale incinerator as described in Chapter 3 (Thipse et al., 1999). The components are weighed out separately, mixed and then shredded in a small hammer-mill shredder (12" flakebreaker by Jacobson Inc.). The shredder reduces the size of paper, mulch, and animal feed to a fluffy mixture of particles of less than 1 mm size. The mixture is placed in airtight, plastic drums. To imitate the moisture content of MSW, 20 weight % of water is added to the fluff before compaction. The mixture is compacted into cylindrical pellets of 2.5 cm diameter and average 5 cm length using a HYFLO California Pellet Mill. This pellet size has been chosen based on preliminary experiments in which different size pellets were burned in air in an electric furnace at 750°C. The selected size of the pellets corresponded to a volatilization time of about 20 min, close to the experimental residence time of MSW in the primary combustion chamber (Table 2.2).

2.4 Synthetic Fuel Characterization

A summary of the results of the fuel characteristics is presented in Table 2.2. The detailed description of the techniques used to characterize the fuel and the characterization result discussion are presented below.

The density of the synthetic fuel is obtained by measuring the mass of the bulk fuel sample filling a closed volume chamber. The variation in the density was in the range of 538 ± 13 kg/m^3. The measurements of the fuel density and the described below tests determining contents of various fuel components are conducted for each prepared

batch of the synthetic fuel. The comparison of results for different fuel batches confirmed repeatability and uniformity of the fuel compositions.

2.4.1 Physical Characterization (Proximate Analysis)

A series of sequential tests developed by ASTM for refuse-derived fuels (ASTM, 1996) was conducted to determine moisture, volatile matter, fixed carbon and ash contents of the synthetic fuels. The moisture content of the fuel is determined by heating the fuel to 110°C and maintaining it at this temperature for 1 hour and measuring the weight loss, according to the ASTM test E949-88. It is found that as prepared, the fuel contains 19.5 ± 0.5 weight % of moisture. The volatile matter content is determined according to the ASTM test E897-88, by measuring the weight loss of the moisture reduced fuel sample when it is inserted for 7 minutes in an electric furnace in air at 950°C. It is found that the synthetic fuel contains 55.7 ± 2 weight % of volatile matter. In the following test, the fixed carbon content is determined as a weight loss of the fuel residue from the volatile matter test after its burning in air at 750°C for 30 minutes (ASTM test E830-88). The test shows that the fixed carbon content in the fuel is 1.02 ± 0.05 % and the final residue is qualified as ash and its content is 21 ± 1.5 % of the total fuel mass.

2.4.2 Chemical Characterization (Ultimate Analysis)

Sulfur, chlorine and nitrogen contents in the synthetic fuel are determined using the ASTM standard chemical analysis tests, E775-87, E776-87 and E778-87, respectively (ASTM, 1996). The sulfur content of the fuel is determined by igniting a fuel sample with Barium Chloride and the Eschka mixture ($MgO + Na_2CO_3$) and precipitating barium sulfate. The sulfur content based on the weight of the precipitate is 0.3 ± 0.05%.

The chlorine content is determined by combusting the sample with oxygen in a closed volume. As a result of combustion, chlorine is converted into hydrogen chloride, which is absorbed in an alkaline solution of NaOH and is quantified by titration. The synthetic fuel contains 0.57 ± 0.10 mass % of chlorine. The nitrogen content is determined by reaction of the fuel sample with concentrated sulfuric acid. As a result of reaction, nitrogen is converted to ammonium salts. The salts are decomposed with a hot alkaline solution of sodium hydroxide to recover ammonia by distillation. This ammonia distillate is then titrated to determine the nitrogen content. The nitrogen content detected in the synthetic fuel was 0.4 ± 0.04 mass %. Comparison of the results of the fuel component measurements with the component content of MSW presented in Table 2.2 shows that the synthetic fuel composition imitates well that of MSW.

Table 2.2 Characterization of MSW and synthetic fuel

PARAMETER	SYNTHETIC FUEL	MSW	
		VALUE	REFERENCE
Heat of Combustion	4565 ± 35 cal/g	2000 - 4200 cal/g	(Gupta and Rohrbach, 1991)
Density (compacted MSW)	524 to 551 kg/m^3	500 – 1000 kg/m^3	(Niessen, 1995)
Residence time in the primary combustion chamber	20 min	20 min	
Fuel Components (weight %)			
Moisture Content (E949-88)	19.5 ± 0.5	32	(Gupta and Rohrbach, 1991)
Volatile Matter (E897-88)	55.7 ± 2	39.6	
Ash Content (E830-88)	21 ± 1.5	21.6	
Sulfur (E775-87)	0.3 ± 0.05	0.01-0.4; 0.23	(ASME, 1979; Niessen, 1995)
Chlorine (E776-87)	0.57 ± 0.10	0.13-0.95	(ASME, 1979)
Nitrogen (E778-87)	0.4 ± 0.04	0.44	(Gupta and Rohrbach, 1991)
Fixed Carbon (E830-88)	1.02 ± 0.05	5.45	(Niessen, 1995)

2.5 Evaluation of Heat of Combustion

The heat of combustion of synthetic fuel is determined according to the standard ASTM method E711-87 using a standard bomb calorimeter. The sample for calorimetry should be in the powder-like form and thus the fuel pellets are size reduced to 0.5 mm particles in a grinder. The powder is air-dried and loaded into the calorimeter. The experiment is conducted in a sealed vessel in the model 1108 Parr Instrument Company calorimeter in pure oxygen at a pressure of 30 atmospheres. The energy equivalent of the calorimeter is determined by combusting standard benzoic acid pellets. The heat of combustion value is determined from the measured temperature rise resulting from the fuel combustion. Appropriate thermo-chemical corrections including the heat of combustion of the fuse wire, and heats of formation of nitric acid and sulfuric acid due to the presence of moisture and sulfur in the fuel are computed. The heat of combustion for the synthetic fuel was measured using the prepared fuel pellets and the individual fuel components. In addition, an estimate of the expected heat of combustion was made as described below.

2.5.1 Heat of Combustion of Synthetic Fuel Pellets by Standard Bomb Calorimetry

The heat of combustion obtained by this method is the higher heating value (HHV). This is due to the inclusion of latent heat of condensation of water vapor formed during combustion. Most of the heat content values reported in the literature are higher heating values. In practice however, the steam in the flue gas may not condense, so the latent heat of condensation is not released. The heating value obtained neglecting the latent heat of condensation is referred to as the lower heating value (LHV). The obtained synthetic fuel heat of combustion values are averaged over five runs. The average value obtained is 4565 cal/g $\pm$ 35 cal/g. A sample calculation for heat of combustion by

standard bomb calorimetry is shown below. Specific chemicals and their amounts are given in the calorimeter manual.

A) Determination of Thermochemical Corrections

m = Mass of pellet sample = **0.85** g

c1 = Volume of alkali used for titration of bomb washing liquid = **22** ml

c2 = percentage of sulfur in sample measured by ASTM method E775-87 = **0.29** %

c3 = length of fuse wire consumed = **10** cm

e1 = correction in calories for heat of formation of HNO_3

= c1 as 0.0709N alkali was used for titration yields **22** cal.

e2 = correction in calories for heat of formation of H_2SO_4

= 13.7 (cal/g) x c2 x m (g) = **3.37** cal.

e3 = correction in calories for heat of combustion of fuse wire

= 2.3 (cal/cm) x c3 (cm) for Parr 45C10 Ni-Cr fuse wire (Parr, 1994) = **23** cal.

T = corrected temperature rise for synthetic fuel = **2.08** °C

B) Determination of energy equivalent (W)

H = heat of combustion of benzoic acid = **6318** cal/g

mb = mass of benzoic acid pellet = **1.02** g

t = corrected temperature rise for benzoic acid pellet = **3.42** °C

W = Energy Equivalent of Bomb Calorimeter = [H (mb) + e3]/t = **1891.04** Cal/°C

C) Computing Gross heat of combustion (Hg)

$$Hg = \text{Gross heat of combustion of synthetic fuel} = \frac{(T)(W) - e1 - e2 - e3}{m}$$

Hg = **4570.58** Cal/g = **8227.04** Btu/lb.

2.5.2 Heat of Combustion for Individual Components of the Synthetic Fuel by Standard Bomb Calorimeter

In this method each of the fuel components is burned separately in the calorimeter. The individual component heating values weighted by their mass fractions are shown in Figure 2.1. The heat of combustion for the synthetic fuel can be calculated by multiplying experimentally determined values for each of the components by their mass fraction and then summing up the fractions. This leads to a calculated value of 4428 ± 22 cal/g. The difference between this and the experimentally determined value for the entire synthetic fuel is less than 5 %. Therefore the size reduction and compaction steps of fuel preparation have negligible influence on the heat of combustion value.

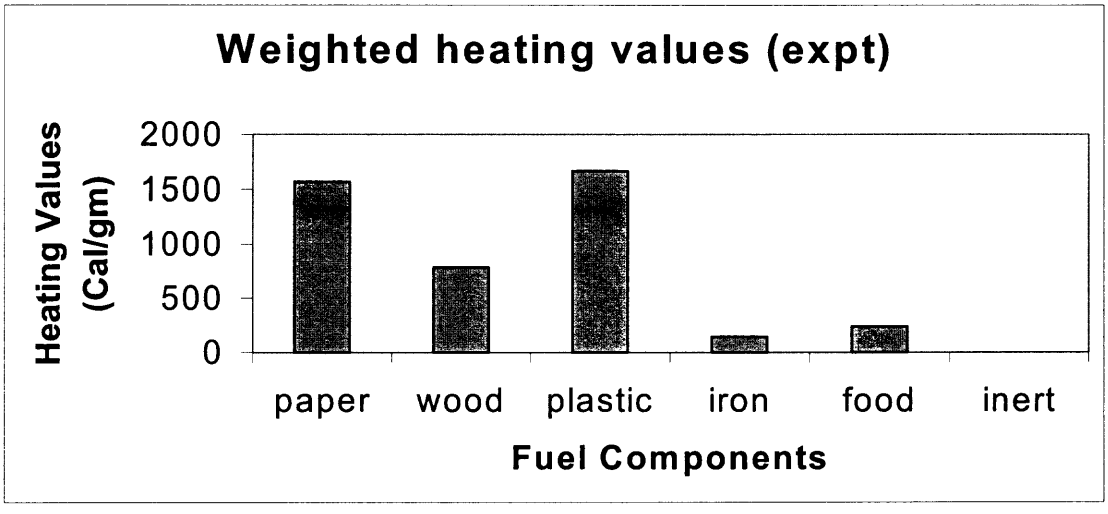

Figure 2.1 Experimental Weighted Heat of Combustion Values

2.5.3 Heat of Combustion of Synthetic Fuel Estimated from Literature Values

The estimate involves using the heat of combustion values for components of our synthetic fuel obtained from literature sources (Niessen, 1995). The literature values used are for the materials whose descriptions best fit those of separate components of the

synthetic fuel. For example, animal feed used to simulate waste food in the synthetic fuel consists mostly of mixed cereal grains with some fat, whereas literature data available is for dried vegetable waste. This organic feed is the source of the nitrogen content of the fuel (Reger et al., 1993). Materials like newsprint and wood contain a high proportion of cellulose (White, 1987), so their values of heat of combustion are assumed to be similar to that of cellulose.

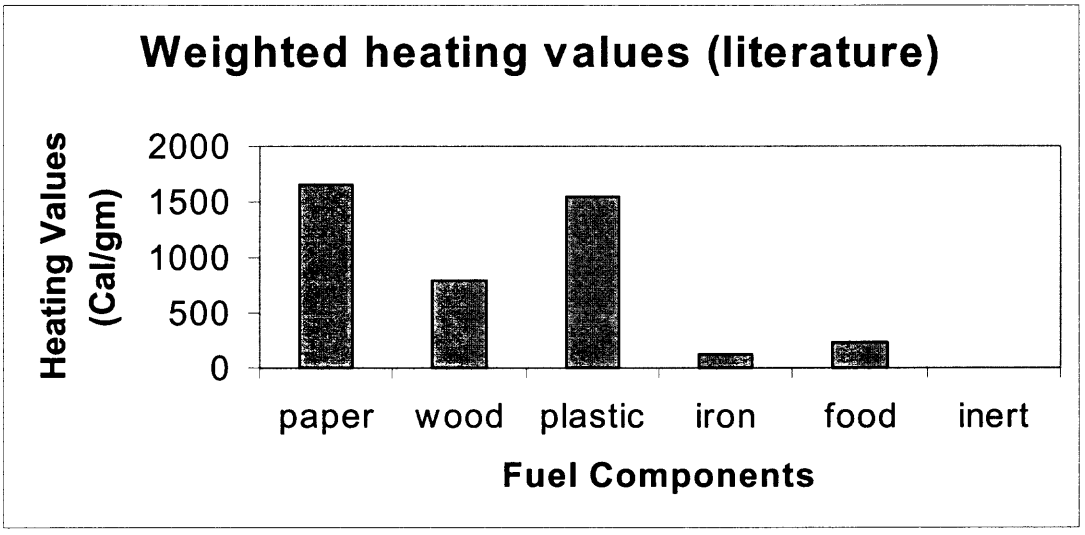

Figure 2.2 Literature Weighted Heat of Combustion Values

The heat of combustion value for our synthetic fuel can be calculated by multiplying the literature values of heat of combustion for the individual components by the mass fractions and then summing. The value obtained by this method is 4370 cal/g and is in reasonable agreement with the calorimetric measurements. The individual component literature heating values (ASME, 1979) weighted by their mass fractions are shown in Figure 2.2.

2.5.4 Discussion of Results

The obtained literature value of 4370 cal/g for the heat of combustion of our synthetic fuel is slightly higher (around 4 %) than the maximum value for MSW found in the literature (4200 cal/g). The literature values given for the heat of combustion of refuse-derived fuels (USEPA, 1997) vary in a broad range because of the varied compositions of the waste fuel samples. Mostly, this is due to the heterogeneous nature of real waste, including quantities of inert species, which can be altered by recycling and waste fuel processing (Shin and Choi, 2000). One of the heat of combustion values for MSW available in the literature is from Delaware Reclamation Project (Gupta and Rohrbach, 1991). The value for heat of combustion of MSW after some recycling is in the range of 2,000 cal/g to 4,200 cal/g with the average near 2,700 cal/g. Data are given in (ASME, 1979) for the heat of combustion of MSW sampled from U.S. cities in the early 1970s as ranging from 1,300 cal/g to 4,200 cal/g with the average near 2,800 cal/g. The data are given on an `as fired' (i.e., wet basis) and much of the variation seems to be due to the variation in the moisture contents between samples. If the experimental dry basis for our synthetic fuel is adjusted for 20% moisture, then a wet basis (as fired) value of 3,650 cal/g is obtained. Overall there is good agreement between the heat of combustion values (HHV) for the synthetic fuel determined by the three methods in this study (4565 cal/g, 4428 cal/g and 4370 cal/g).

2.5.5 Comparison with NIST Standard Reference Material

The National Institute of Standards and Technology (NIST) has certified certain materials for use as standards in calibration of combustion bomb calorimeters. The NIST reference material number 1657 is the standard for synthetic refuse-derived fuel (NIST,

1993). This standard material is composed of 80% cellulose, 15% silica, and 5% alumina. This material has a heat of combustion value of 5963 ± 107 Btu/lb or 3312 ± 59 cal/g on a dry basis, which is lower by 25 % as compared to the heat of combustion values for our synthetic fuel. This is due to the fact that our synthetic fuel contains polyethylene, which causes an increase in its heating value. The NIST value is closer to the 'as fired' heating value of 3650 cal/g for our fuel that includes the moisture content of the fuel.

2.6 Experimental Testing of Synthetic Fuel

Synthetic fuel was burned in the pilot-scale NJIT incinerator (Thipse et al., 1999) in a steady-state regime. Synthetic fuel is fed to the PCC at a rate of 10 to 13 kg/hr and the fuel residence time on the grate ranges from 20 to 30 minutes. Underfire air is introduced to the PCC through holes distributed uniformly under the grate surface. Overfire air is introduced through stainless steel nozzles positioned in the chamber wall above the grate. The SCC provides the flue gas residence time of 1-2 seconds that is usually sufficient for the complete gas phase reactions when temperature is 900°C. The typical duration of an experimental run varied from 6 to 7 hours. The lean conditions with equivalence ratio varied around 0.2 – 0.3 were produced in the combustion chamber, in agreement with the usual practice of operating the practical combustors with 50 to 100% excess air (Niessen, 1995). The temperatures in the primary and secondary combustion chambers varied in the ranges of 800 – 1000°C and 745 – 825°C, respectively. After initial warm up and ignition period of 2 hours, the pilot burner flame extinguished automatically and constant temperatures were established in the

incinerator. This operation state known as the 'steady-state' was achieved and reproduced when the same fuel feed rates and airflows were used.

While it has been shown that the ratio of the underfire to overfire air could affect combustion significantly (Tuttle, 1998), this effect has not been addressed in these experiments in which the underfire airflow was always significantly greater than the overfire airflow. The continuous gas emissions monitoring system determined concentrations of O_2, CO, and NO at the exit of the secondary combustion chamber. Experimental concentrations of O_2, CO, and NO at different experimental fuel/air ratios were compared with the respective computed equilibrium concentrations at adiabatic flame temperatures, as discussed below.

2.7 Estimated Flame Conditions at Equilibrium

Adiabatic flame temperatures and equilibrium product species were computed using a one-dimensional isentropic equilibrium code (Selph and Hall, 1992). The fuel species used in thermodynamic equilibrium computations and their standard enthalpies of formation $\Delta H_{f\,(298)}$ are listed in Table 2.3. Cellulose was used as the main constituent of both paper and mulch, polyethylene was used to represent plastic, its enthalpy of formation was estimated as the enthalpy of formation of ethylene corrected by the enthalpy of polymerization of -93.6 kJ/mole of ethylene (Whiteley et al., 1992). Amine group molecular compounds are often considered as a good representation of bio-chemicals, such as food wastes (Reger et al., 1993). Therefore, methanamine was selected to represent the animal feed. In addition, water was added to the initial fuel species to represent both the moisture contained in wood (White, 1987) and any other

moisture accumulated in the fuel. Air represented by a 20/80 oxygen/nitrogen mixture was used as oxidizer.

Table 2.3 Synthetic fuel components, representative species and their enthalpies of formation used in thermodynamic equilibrium computations

Fuel component	Species	Formula	Enthalpy of Formation, kJ/mole
Newsprint (paper)	Cellulose	$C_6H_{10}O_5$ (s)	- 906.3 (Brunner, 1989)
Hardwood mulch			
Moisture	Water	H_2O (l)	- 285.8 (Eremenko et al., 1998)
Low Density Polyethylene	Polyethylene	$(C_2H_4)_n$ (s)	- 51.2 (Cox and Pilcher, 1970)
Iron	Iron	Fe (s)	0.012 (Eremenko et al., 1998)
Animal Feed	Methanamine	CH_3NH_2 (s)	- 47.3 (Cox and Pilcher, 1970)
Sand	Silica	SiO_2 (s)	- 910.9 (Eremenko et al., 1998)

In a series of computations, the amounts of the fuel species introduced in the proportion reflecting the synthetic fuel composition were unchanged, whereas the amount of air varied in a wide range. Resulting adiabatic flame temperature and major product species are shown in Figure 2.3 as a function of fuel/air mole ratio. The maximum adiabatic flame temperature of 1821°C corresponds to the stoichiometric fuel/oxidizer ratio and the respective reaction is given by Eq. (1).

$$C_6H_{10}O_5 + 0.28\ (C_2H_4)_n + 0.1\ CH_5N + 6.75\ O_2 \rightarrow$$

$$5.68\ H_2O + 6.05\ CO_2 + 0.61\ CO + 0.13\ H_2 + 0.1\ NO \qquad (1)$$

Equation (1) shows no iron and silica participation in the reaction. In other words, these species supplied as a fuel are compensated in the computation by equal amounts of the same species in the products. This stoichiometric condition is achieved at the overall fuel/air molar ratio of 1/17 (equivalence ratio $\varphi = 1$). The ratio includes both active and

inert fuel and air components, therefore the comparison of this ratio with the experimental one is straightforward. At fuel-lean conditions, comparable to those used in the experiments (equivalence ratio $\varphi = 0.3$), the adiabatic flame temperature is 830°C and the reaction suggested by equilibrium computations is:

$$C_6H_{10}O_5 + 0.28\ (C_2H_4)_n + 0.1\ CH_5N + 0.16\ Fe + 21.79\ O_2 \rightarrow$$

$$14.56\ O_2 + 5.81\ H_2O + 6.66\ CO_2 + 0.1\ NO + 0.08\ Fe_2O_3 \quad (2)$$

The amount of the input oxygen in this reaction is not balanced with that in the products, and the unreacted O_2 appears in the right part of Eq. (2). Other features of the equilibrium reaction occurring in the lean mixture and at lower temperature are the negligibly small amounts of CO, H_2, and NO produced, and the formation of iron oxide. The computed concentrations of CO, O_2, and NO are compared with those determined experimentally at the exit from the secondary combustion chamber in Table 2.4. One can see that the concentration of unreacted oxygen is significantly over-predicted by the equilibrium computations, whereas experimental concentrations of CO significantly exceed the equilibrium prediction. This discrepancy is most likely due to the very fast kinetics of formation of CO [$k=5.8 \times 10^{13}(cm^3s)\ \exp(-576(cal/mol)/RT)$] versus the relatively slow kinetics of formation of CO_2 [$k=2.5\ 10^{12}(cm^3s)\ \exp(-47800(cal/mol)/RT)$] (Burgess et al., 1996). Thus experimental data (Table 2.4) indicate that a large portion of the CO produced in the combustion as an intermediate product ($C+O_2 \rightarrow CO + O$) does not continue with the reaction ($O_2 + CO \rightarrow O + CO_2$) and remains in the exhaust. This indicates residence time of the synthetic fuel on the grate is insufficient. Also at higher temperatures, CO_2 decomposes to form CO. The predicted and measured NO concentrations appear to be fairly close. This comparison implies that

more detailed measurements and a more detailed analysis including both chemical kinetics and thermodynamic equilibrium considerations are needed to interpret processes occurring in MSW combustion.

TABLE 2.4 Comparison of experimental and equilibrium concentrations of some gas species in the synthetic fuel combustion products

Flame Equivalence ratio	Species Concentrations (moles)							
	CO		NO		NO/NO_x		O_2	
	Equilibr	Experim	Equilibr	Experim	Equilibr	Experim	Equilibr	Experim
0.270	1.46E-12	1.26E-03	3.34E-05	2.96E-06	0.700	0.989	1.35E-01	2.50E-03
0.262	7.48E-12	8.68E-04	2.75E-05	3.33E-06	0.735	0.991	1.37E-01	2.74E-03
0.254	7.45E-12	5.60E-04	2.45E-05	4.73E-06	0.761	0.988	1.39E-01	2.87E-03
0.210	5.18E-14	4.20E-04	6.37E-06	5.16E-06	0.871	0.992	1.49E-01	3.12E-03

2.8 Summary

A synthetic fuel has been developed for experimental studying MSW combustion. The fuel includes all the typical components of MSW, its parameters and composition are characterized using standard ASTM methods developed for the refuse-derived fuels. Density, heat of combustion, and composition of the synthetic fuel are found to be similar to those of MSW. Preliminary combustion experiments were conducted using synthetic fuel and pilot-scale incinerator research facility and it has been observed that steady state operation regimes can be achieved and reproduced using repeatable fuel feed rates and airflows.

Thus, the new synthetic fuel can be used in the future experiments aimed at the parametric characterization of the MSW incineration processes. Thermodynamic equilibrium computations were conducted for a wide range of fuel/air ratios using chemical species representative of each synthetic fuel component. Comparisons of the

equilibrium computation results with the limited experimental measurements of the combustion product gas species show that chemical kinetics must be considered for an adequate modeling of the MSW incineration processes.

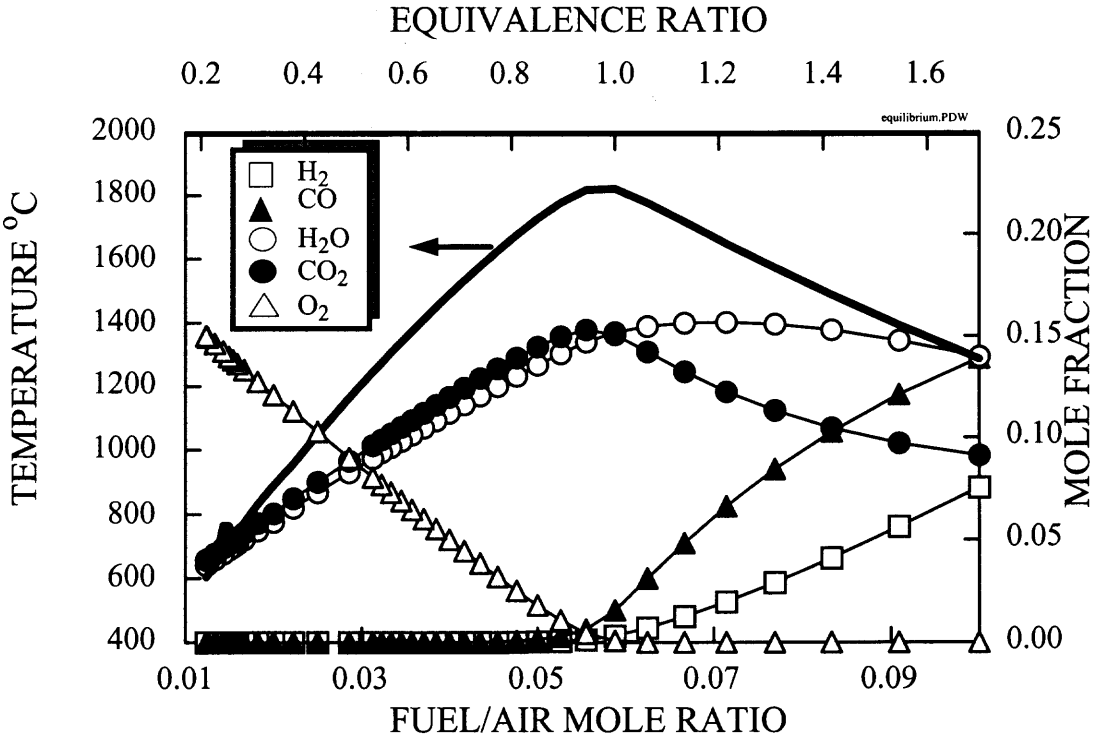

Figure 2.3 Adiabatic flame temperatures (solid line) and combustion product species predicted for MSW (or synthetic fuel) combustion at thermodynamic equilibrium at different fuel/air ratios.

CHAPTER 3

PILOT-SCALE INCINERATOR

3.1 Introduction

The pilot-scale incinerator facility at New Jersey Institute of Technology has a capacity of 140,000 Btu/hr. No other institution in the U.S. possesses similar pilot-scale apparatus and that makes this facility unique. This incinerator was designed and manufactured by Enercon Systems, Elyria, Ohio in collaboration with the incinerator research group at NJIT. The incinerator was assembled and setup in lab 103 at Otto.H.York Center for Environmental Engineering and Science at NJIT, Newark. The incinerator has a continuous fuel feed system and inputs for natural gas, city water and compressed air. The analytical equipment for the incinerator facility consists of continuous emissions monitoring system (CEMS), which includes gas analyzers and gas chromatographs. The measured data from the incinerator is recorded by a Fluke data logger and Labview software. Minichrom software is used to acquire chromatograms.

3.1.1 Commercial Incinerators

Numerous technologies have been developed to incinerate the vast array of wastes produced as a consequence of industrial activity. The MSW incinerators destroy around 20 % of the municipal solid waste generated in the United States as reported by Niessen, 1995. Various companies such as E.I. Dupont, Dow Chemical, Eastman Kodak and General Electric use special purpose commercial incinerators (Mannien et al., 1997). In order to meet the wide technical requirements of general purpose incineration, different types of incinerators have been developed that include rotary kiln, stationary grate, moving grate and fluidized bed (Tillman et al., 1989). Dempsey and Oppelt, 1993 report

that all of these technologies meet 99.99 % destruction removal efficiency for hazardous substances. Refer Table 3.1 for comparison of pilot-scale and large-scale incinerators.

Table 3.1 Comparison of Pilot-Scale and Large-Scale Incinerators.

Parameter	**Pilot-Scale Incinerator** (Thipse et al., 1999)	**Large-Scale Incinerator** (Niessen, 1995)
Flue Gas Residence time	1-2 seconds	2-3 seconds
PCC Temperatures	800 to 1000 C	900 to 1200 C
Exhaust Temperature	90-100 C	100 C
Fuel Grate Residence Time	20 to 25 min	25 to 30 min
Fuel Feed Rate	12 to 15 Kg/hr	1000 to 15,000 Kg/hr
Filter Used	Fabric Filter	Electrostatic Precipitator
Overfire/Underfire Air Supply	Fan	Blower
Capacity	41 kW	10 to 15 MW
Feed Mechanism	Continuous	Batch/Continuous
Density of Waste Burned	510 to 550 Kg/m3	80 to 240 Kg/m3
Heating Value of Waste Burned	4500 to 4600 cal/g	2800 to 4500 cal/g
Type of Grate	Stationary with moving fingers	Stationary/Rotating/ Fluidized bed

3.2 Incinerator Components and Operation

The pilot-scale NJIT incinerator is designed to emulate the conditions of large-scale commercial or municipal incinerators. It is of a sufficient scale to obtain experimental data in a manner that is representative of full scale MWCs, but at the cost and experiment time frame of pilot plant equipment. Figure 3.1 is a block diagram of the incinerator. The details of the main components of this incinerator are explained below.

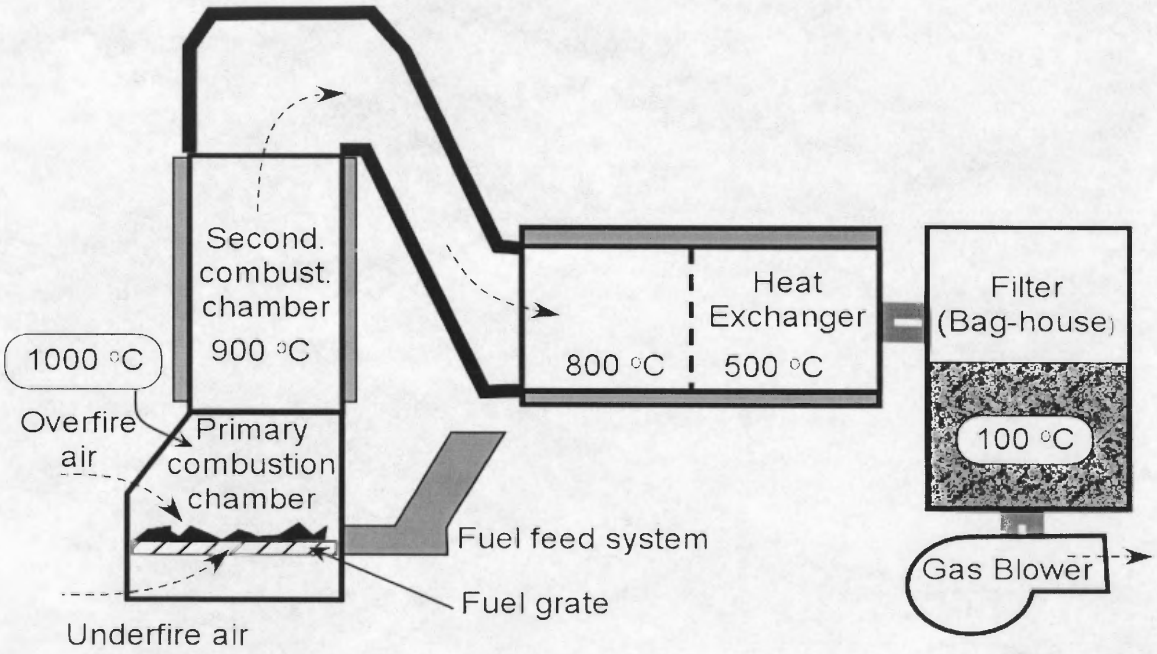

Figure 3.1 Block Diagram of the Incinerator

3.2.1 Primary Combustion Chamber (PCC)

This is the primary component of the incinerator where the actual combustion process takes place. The volume of the primary chamber is 0.25 m^3 and its walls are insulated with refractory material to withstand the high temperatures in the combustion process. Operating temperatures are around 800°C to 1000°C, but temperatures as high as

1200°C can be achieved easily in the unit. The capabilities of the unit to reproduce data and achieve a steady state operation have been experimentally established (Thipse et al., 1999). A sketch of the PCC is shown in Figure 3.2.

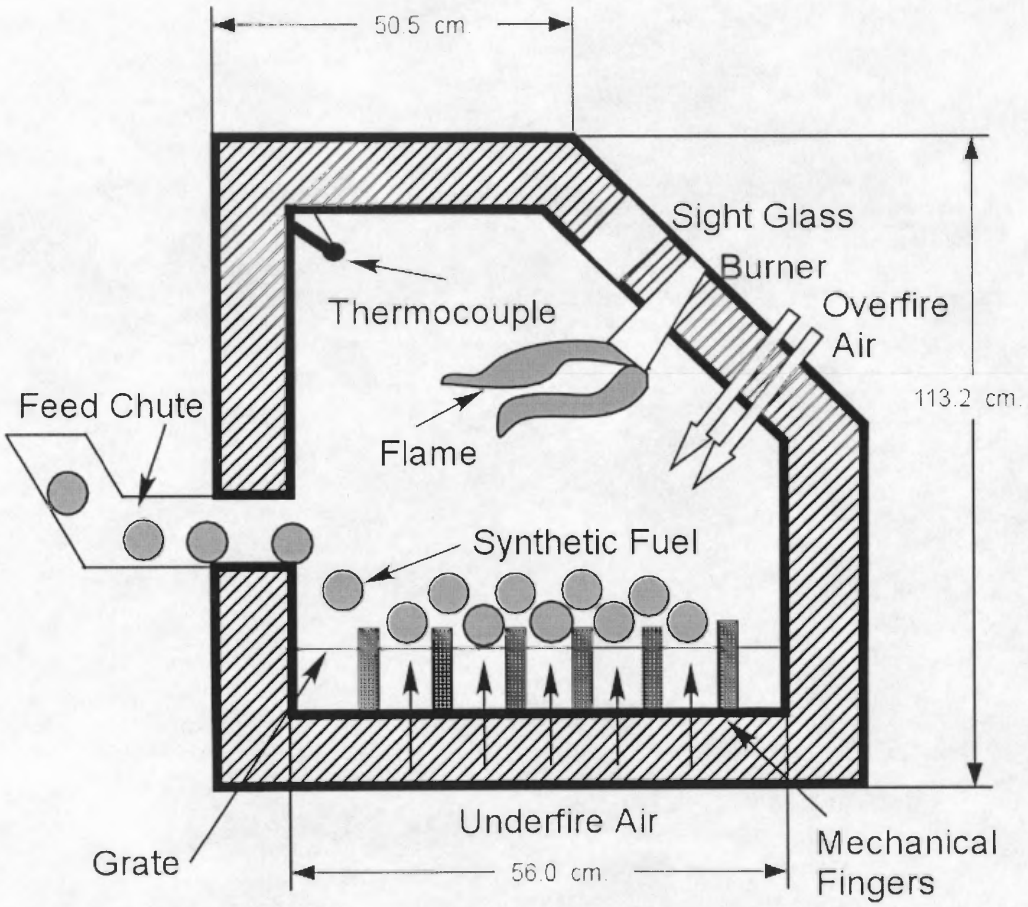

Figure 3.2 Details of the primary combustion chamber

The synthetic fuel is added to the PCC via a chute located on the inlet of the incinerator. Pneumatic rams with an adjustable time period are used to push solid fuel on to the grate at a rate of 10-13 kg/hr. The PCC has a stationary grate 0.26 m wide and 0.56 m long with moving fingers to direct the fuel movement along the grate. Solid fuel

residence time on the grate is adjustable over a range from 20 minutes to 30 minutes. The grate is made of stainless steel and is water-cooled.

Air supply to the incinerator unit is comprised of the overfire and the underfire air flows. The underfire air is introduced to the grate through holes distributed uniformly under its surface, and overfire air is introduced by two opposed banks of 0.6 outer diameter (OD) stainless steel jets located on the primary combustion chamber front wall about 30 cm above the grate. Each bank has five stainless steel jets. The underfire air flow rate is measured by a magnahelic and is regulated manually from 50 to 70 SCFM by a butterfly valve. The overfire air rate is measured by a Dwyer rotameter type flow meter in the range of 1 to 11 SCFM with an automatic flow control from the main control panel with a solenoid valve.

The PCC is equipped with a natural gas premixed flame burner as shown in Figure 3.2. The natural gas flow is regulated by a supply valve, located on the supply pipeline. The burner is used for ignition of the solid fuel and initial warm up and is shut down after the steady combustion regime is achieved. Additional features of the PCC include wall mounted external cooling fans, glass window for visual inspection, a plenum chamber to collect ash and access panels for cleaning the grate. Measurement devices such as an industrial thermocouples to measure the PCC temperature and a portable magnahelic gauge to measure the static pressure drop across the PCC are provided.

3.2.2 Secondary Combustion Chamber (SCC)

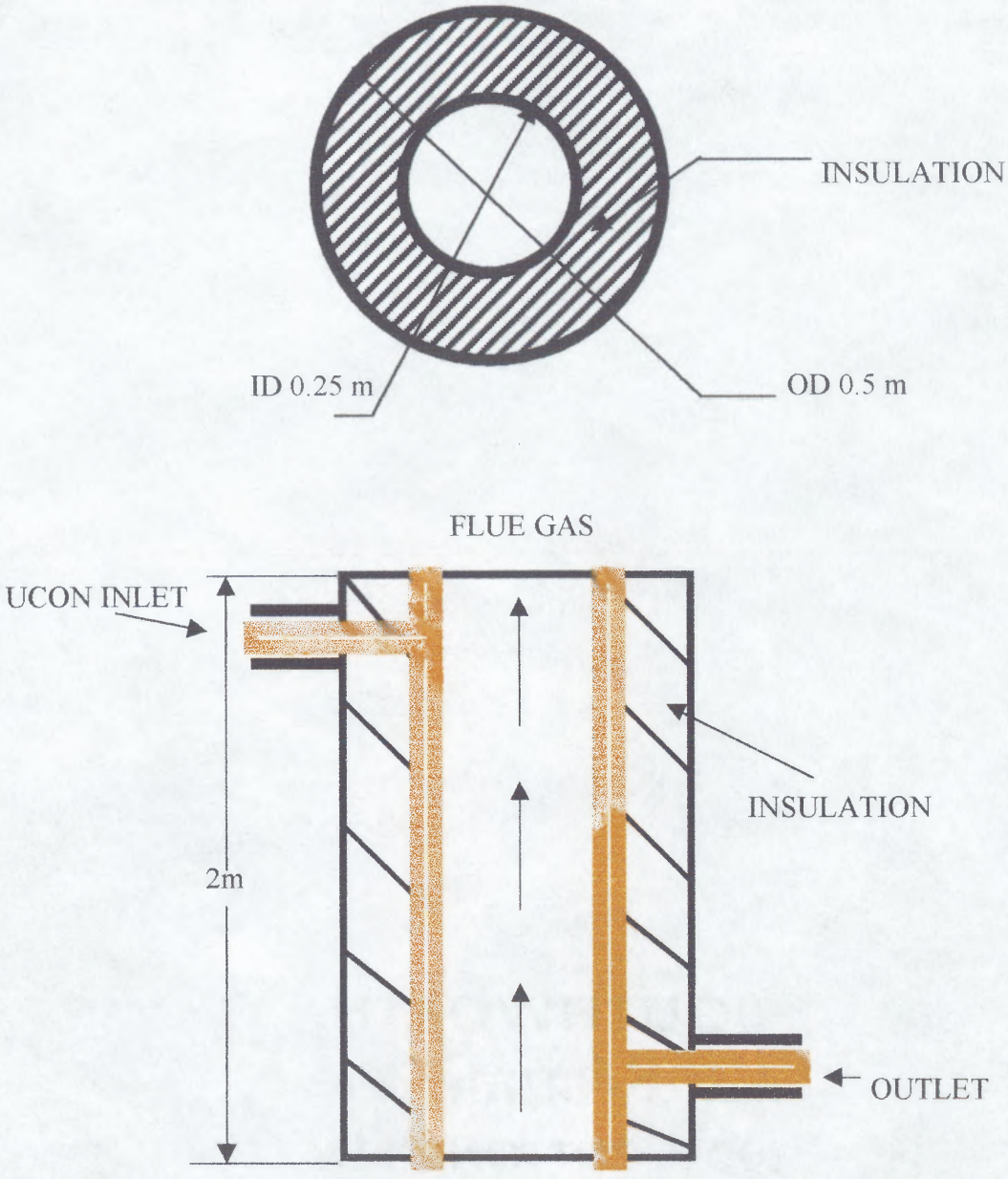

Figure 3.3 Cross-section View of the Secondary Combustion Chamber

Gas effluent from the primary combustion chamber passes into the secondary combustion chamber. This chamber is a long vertical section of a pipe (length 2 m and outer diameter 0.5 m) insulated both within and outside as shown in Figure 3.3. The residence time of the flue gases in the secondary combustion chamber is about two

seconds, similar to commercial incinerators. This allows sufficient time for the chemical reactions to go to completion in the flue gases. The secondary chamber temperature measured by a K-type thermocouple are about 100°C lower than the PCC.

3.2.3 Heat Exchangers

The flue gas temperature is reduced by means of two heat exchangers, which are designed to provide a temperature profile similar to municipal incinerators. The heat exchangers are cross flow type stainless steel units coated with fiberglass insulation on the outside (see Figure 3.4).

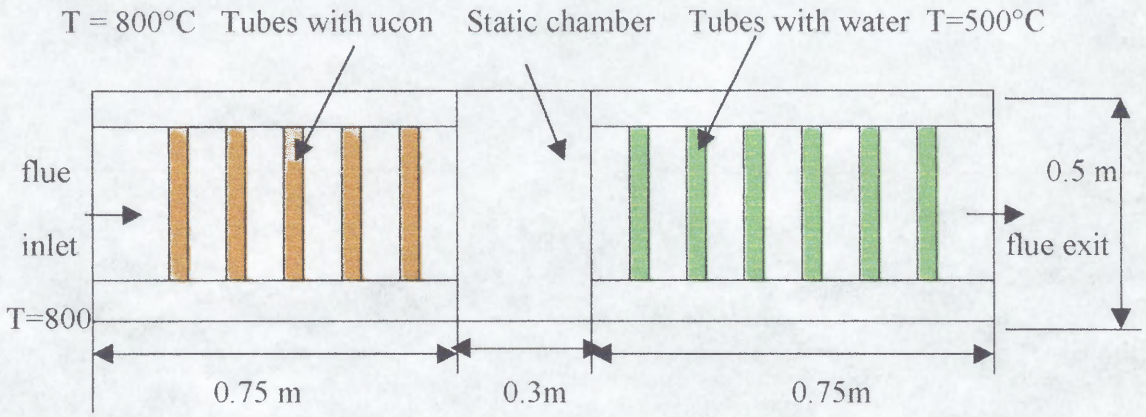

Figure 3.4 Heat Exchanger Construction

The two heat exchangers use two different fluids and are joined together by a static chamber. The flue gas from the SCC enters the heat exchangers at a temperature of about 800°C. The flue gases are then cooled to 500°C by the heat exchangers before entering the baghouse. Poly-alkylene glycol (ucon) and water are used as the heat transfer fluids in the first and second heat exchangers respectively.

External heating and circulation of the heat transfer fluids is done by the two supertrol units designed by Enercon Inc. which are located near the two heat exchangers. This facilitates bringing the heat exchangers to operating temperature quickly. Each

supertrol unit consists of a compressor, a heater, a cooler and operating valves. The heat exchangers are of sufficient capacity to maintain effluent gas temperatures during steady state operation within +/-3 °C at all three CEMS sampling ports. An injection port is located at the exit of second heat exchanger for injection of lime in the flue gases to neutralize acid components. A butterfly valve is located after the second heat exchanger to control the static pressure drop by regulating the draft through the incinerator.

3.2.4 Fabric Filter Baghouse

This is a fabric filter device used to collect the fly ash from the flue gases. Refer to Figure 3.5 for details of the baghouse. Fly ash is removed from the gases by the P-84 fabric filter bags. A pneumatic cylinder located at the top section of the baghouse is filled with compressed air. The pressure is released through five strokes executed in fixed time sequence regulated from the main control panel. These vibration trap strokes cause the filter bags to vibrate and the fly ash is collected at the bottom of the baghouse. After each run the fly ash is removed from the baghouse. The exit gas flow rate and temperature are measured by an S-type Pitot tube and a thermocouple located downstream of the baghouse.

3.2.5 CEMS Equipment

In order to derive qualitative and quantitative performance analysis from the pilot scale incinerator, continuous emissions monitoring equipment (CEMS) is installed and operated. Three sampling ports are located along the unit: port 1, at the downstream end of the annular flue in the secondary combustion chamber extension; port 2, immediately downstream of the second heat exchanger and port 3, between the baghouse and exhaust induced draught (ID) fan.

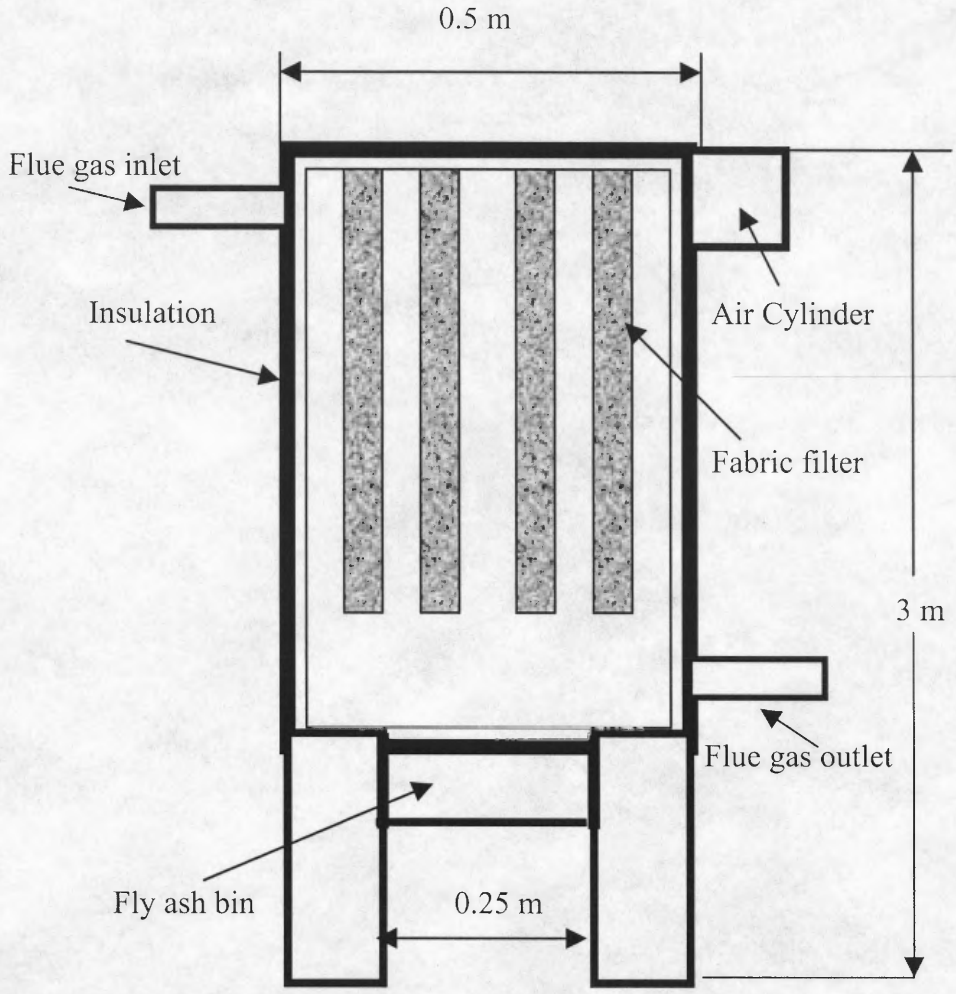

Figure 3.5 Construction of the Fabric Filter Baghouse

Thermocouples are used for temperature measurement, and flowmeters are used for flow measurement. A California Instruments CO analyzer, O_2 analyzer, and a NO_x analyzer, are installed. The CO analyzer uses infrared radiation absorption principle and is capable of reading between 0 and 1000 ppm. The O_2 analyzer uses the paramagnetic property of O_2 to measure its concentration. The NO_x analyzer uses chemiluminesence to detect the presence of NO_x and has a built-in ozonator using ambient air to produce the needed ozone reactant. All data from the CEMS equipment are recorded simultaneously by a 20 channel Fluke FL 2026A data acquisition unit. The data

acquisition unit is connected to a personal computer (PC) running Labview software for the storage, analysis and presentation of data.

Three gas chromatographs (GCs) are used to sample hydrocarbon (HC) species. A Gow-Mac GC, model number 580 is used to detect total hydrocarbons, and is referred to as the total HC analyzer. The Gow-Mac uses a flame ionization detector (FID), with 3 mm OD stainless steel tubing, a gas sampling valve with 1 ml sampling loop and no column or stationary phase. The sample gas flows continuously through the sampling valve and is injected to the GC at 10 minute intervals. The second GC is a Varian 3700, with a flame ionization detector (FID) and 2 m x 3 mm OD packed column with standard material Super-Q as its stationary phase. This GC is used to detect the presence of low molecular weight hydrocarbons, such as C1 to C4 hydrocarbons and oxyhydrocarbons. Samples are injected into the GC column through a 6-port gas sampling valve and 1 ml loop. The third GC is a Varian 3600 with a capillary column (AT5 or DB1) for the detection of higher molecular weight hydrocarbon and oxygenated hydrocarbon species as well as chlorocarbons. The resulting data from all GCs are recorded into a separate PC via a Lab Systems VG Chromatography Server, and the Minichrom software used for GC peak integration and peak area conversion to concentration.

3.3 Experimental Results and Discussion

Each experiment carried out on the pilot-scale incinerator was termed as a "run." The data for all incinerator runs is listed in Table 3.2.

Table 3.2 Incinerator Experimental Data

Run	Feed rate	Eq Ratio	PCC	SCC	Port 1	Port 2	Port 3	O2 conc	CO conc	NO conc	NOX conc	NO/NOX
Number	lb/hr	Phi	Temp C	Temp C	Temp C	Temp C	Temp C	Moles	Moles	Moles	Moles	Ratio
1	15	0.21	830	738	623	232	85	3.12E-03	4.20E-04	2.96E-06	2.98E-06	0.992
2	15	0.242	860	754	635	235	90	3.01E-03	5.17E-04	3.13E-06	3.13E-06	0.991
3	19	0.254	882	776	605	239	94.5	2.87E-03	5.60E-04	3.37E-06	3.37E-06	0.988
4	19	0.262	893	779	630	239	94	2.74E-03	8.68E-04	4.77E-06	4.77E-06	0.991
5	27	0.27	993	878	709	255	98.5	2.50E-03	1.26E-03	5.21E-06	5.21E-06	0.989
6	27	0.283	998	882	712	260	99	2.42E-03	1.74E-03	5.48E-06	5.48E-06	0.988
7	24	0.226	926	820	653	250	96	2.63E-03	1.02E-03	4.99E-06	5.06E-06	0.987
8	24	0.242	951	832	661	252	97	2.61E-03	1.09E-03	5.11E-06	5.20E-06	0.983
9	24	0.276	938	818	658	249	96	2.67E-03	1.04E-03	5.07E-06	5.15E-06	0.985

3.3.1 Effect of Equivalence Ratios on Incinerator Temperatures

The fuel feed rate was kept at a fixed value throughout the duration of each of the incinerator runs. Total nine runs were conducted on the incinerator excluding the initial trials and fuel feed rates of 15, 19, 24 and 27 lb/hr were used. The fuel–air equivalence ratios for these feed rates ranged from 0.210 to 0.283. As the equivalence ratio increased from 0.210 to 0.283, the primary combustion chamber temperatures increased from 860°C to 998°C and the secondary combustion chamber temperature increased from 754°C to 882°C. This trend is logical as a higher feed rate causes more heat to be released during combustion. Figure 3.6 displays the relationship between fuel-air equivalence ratio and primary combustion chamber temperature. For each incinerator run, a drop of 100°C was observed in the temperature of flue gases after they reached the secondary combustion chamber from the primary combustion chamber. Temperatures were also recorded at three sampling ports located after the SCC, heat exchanger and the bag house. Temperatures at all these ports also increased along with increasing equivalence ratios. However the temperature rise decreased in magnitude as the flue gases moved downstream. The temperature of port 1 increased from 635°C to 712°C, temperature of port 2 increased from 192°C to 216°C, and temperature of port 3 increased from 92°C to 97°C.

3.3.2 Effect of Equivalence Ratios on Gaseous Emissions

An increase in the equivalence ratios from 0.21 to 0.283 caused an increase in the CO concentration from 19 to 46 ppm and a simultaneous decrease in the O_2 percentage from 8.9 % to 7.4 %. Also with an increasing fuel feed rate from 19 lb/hr to 27 lb/hr a decrease was observed in the NO and NO_X concentration from 146 to 97 ppm and 148 to

100 ppm respectively. The NO/NO_X ratio however remained fairly constant (~ 0.98) inspite of changing the feed rate.

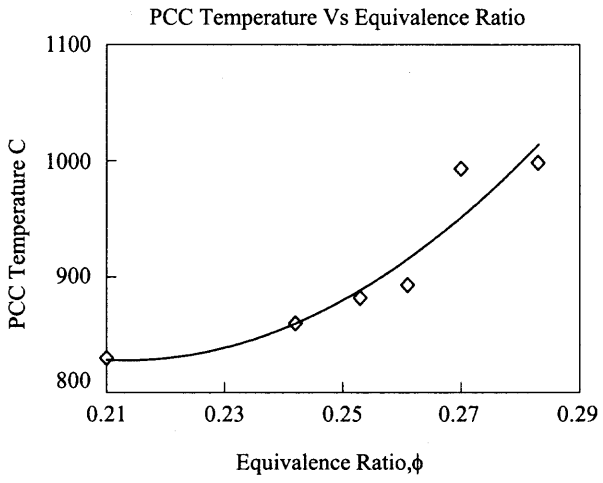

Figure 3.6 Relationship between experimental ϕ and PCC Temperature.

3.3.3 Effect of Fuel Grate Residence Time on Unburned Carbon

The fuel grate residence time is the amount of time taken by the solid fuel to traverse the entire length of the grate. This time was measured manually for three runs and values of 20, 25 and 30 minutes were recorded. The residence time can be increased or decreased by speeding or slowing the controlled reciprocating movement of the moving fingers from the main control panel. The bottom ash samples were analyzed by the standard ASTM test for determining the unburned carbon also known as fixed carbon in the bottom ash. The tests revealed that for increase of residence time from 20 to 30 minutes the unburned carbon reduced from 1.5 % to 0.8 %. This trend is anticipated because an increase in the grate residence time allows longer time for conversion of the fixed carbon in the fuel to CO or CO_2.

3.4 Optical Temperature Measurements

The temperature from the primary combustion chamber of the incinerator was measured by an industrial thermocouple located in the chamber and was designated as the PCC temperature. However, it was expected that the actual flame temperature could exceed the thermocouple measurements because of the spatial non-uniformity of the flame and, therefore the temperature field within the PCC. Thus, two additional types of temperature measurements were made on the PCC flame zone during a single experimental run. The measured PCC temperature displayed on the main control panel (thermocouple readout) was **845°C ± 10°C.**

In the first measurement, a three-color optical pyrometer was used. The individual color radiation signals a (red), b (green), and c (blue) were recorded using a multichannel data acquisition system. Interference filters at 510, 568 and 615 nanometers were used to separate radiation regimes. Ten separate measurement files were recorded. A strip lamp setup was used to calibrate the pyrometer over a wide range of temperatures by varying the filament current of a NIST-certified strip lamp. The resulting calibration curves, are shown in Figure 3.7.

The a/c and b/c curves were taken as a reference for measurement. The a/c and b/c ratios generated by the pyrometer measurement on the incinerator flame were around 3.6 ± 0.1 and 21.2 ± 0.2. Referring both the curves for those ratios, the flame temperature obtained was **890°C ± 5°C** (standard deviation). This temperature was higher by almost 40°C than the primary combustion chamber temperature measured by the thermocouple.

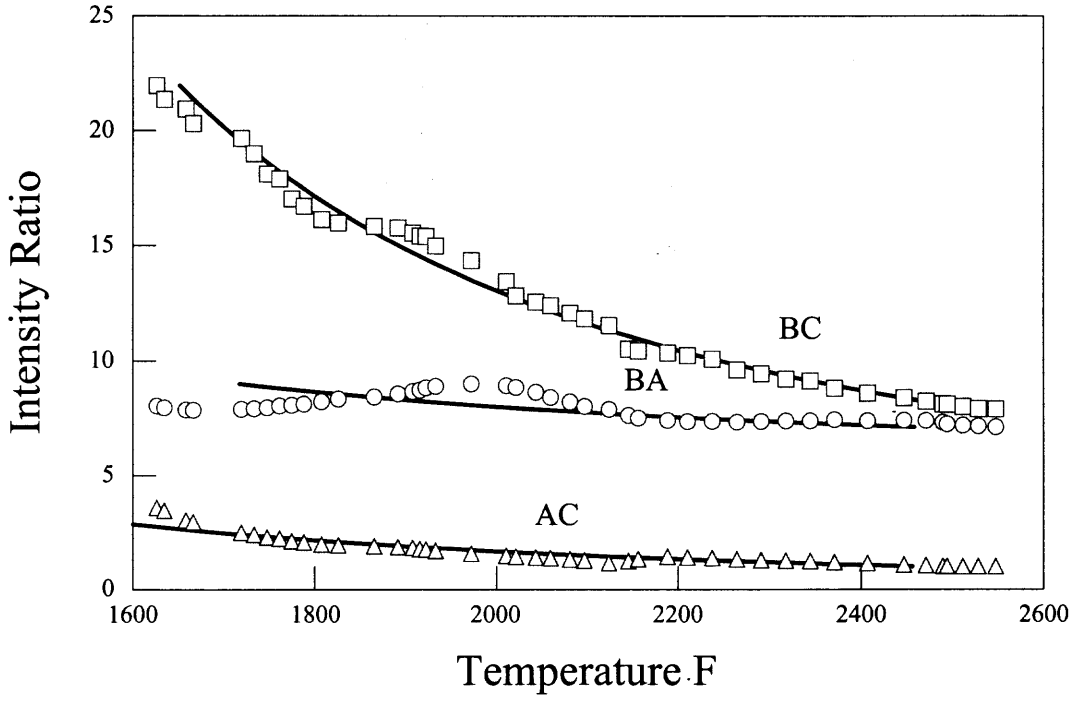

Figure 3.7 Pyrometer Calibration Curves

The second technique used was based on the comparison of flame radiation determined using a digital camcorder. Digital images were captured frame by frame from the camera to a computer "Image Capture" image processing software. Subsequently these images were analyzed by "Tracker" software, which measured the minimum, maximum and average intensity of the flame images. The intensities were either measured by a rectangular cursor to obtain combined intensity or by the line method, which provided the three distinct intensity profiles on three channels (green, red and blue). The camcorder was also calibrated using the strip lamp apparatus to obtain the calibration curves of temperature Vs intensity and the calibration curve obtained is shown in Figure 3.8. The settings for the exposure (1/250) and the diaphragm (9) were maintained constant both for the calibration and flame imaging.

Ten different images of the incinerator flame were analyzed by the tracker software and their minimum, average and maximum intensities were recorded. The average intensity of the images varied considerably from minimum of 75 to maximum of 200 averaging 125. The flame temperature obtained form the calibration curves ranged from **860°C to 950°C**. This temperature range is in reasonable agreement with the temperature measured by the pyrometer and exceeds the thermocouple measurement.

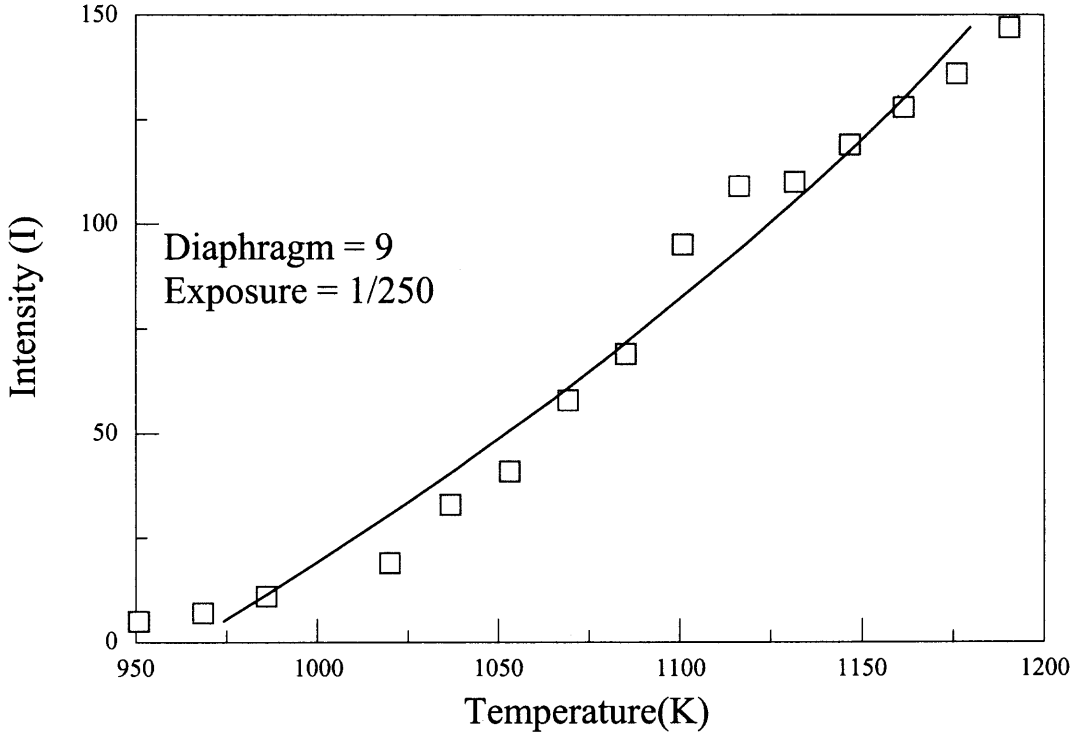

Figure 3.8 Calibration curve for Camcorder

3.5 Summary

A pilot-scale incinerator has been constructed for emulating large-scale incinerators. The capability of the unit to operate at steady state conditions after a transient startup phase has been demonstrated. The ability of the unit to replicate data for similar operating conditions has been established during recent runs.

CHAPTER 4

METAL PARTITIONING IN MSW INCINERATION PRODUCTS

4.1 Introduction

Research on the mechanisms of metal partitioning in the products of waste incinerators has been active (e.g., Wu and Biswas, 1993, Linak and Wendt, 1993) due to the toxicity of many metal species found in the incineration products. Most of the relevant experimental efforts have addressed the operation of industrial incinerators (Niessen, 1995). However, the results of such studies are hard to reproduce and interpret in terms of the mechanistic understanding of the metal partitioning processes. Metal partitioning in waste incineration has also been studied using laboratory scale burners and incinerator models (Karimanal et al., 1996, Linak and Wendt, 1993), which are much better instrumented, but only partially simulate the conditions and processes occurring in industrial facilities.

Most of the reported results specify amounts of different metals in the incineration products in terms of elemental metal mass or atomic fractions (e.g., Reimann, 1989, Nakamura et al., 1996, Binner et al., 1997). Such information is valuable, but often is not sufficient for the adequate processing of the incineration products. Specifically, the behavior of metals in the landfills and in the materials made using the incineration ash (e.g., cement) depends on the types of the metal species present in the ash and on the morphology of the metal-containing particles. Even though the number of relevant studies has become significant, identification of the metal species and morphology of the metal-containing particles in the incineration products is still lacking. Partially, the lack of this information is due to the extreme complexity of the

processes occurring in a practical incinerator and difficulties in the producing the laboratory imitations or models of such processes.

In order to adequately characterize different metal species formed in the incineration products, a well-instrumented, continuous feed, pilot scale 140,000 Btu/hr (41 kW) incinerator facility has been recently developed (Thipse et al., 1999). In addition, a well-characterized and reproducible synthetic fuel has been developed that closely simulates municipal solid waste (Thipse et al., 2001). Therefore, laboratory experimental studies of processes, mechanisms, and products of waste incineration can now be conducted that represent industrial incineration technologies much better than was possible in the past. The objective of this research is to exploit the new facility and classify and characterize various types of metal species produced in the incineration products and their distribution between the generated bottom ash and fly ash. The results of this work and their implications are discussed below and compared with some of the available information on metals partitioning in municipal solid waste incineration.

4.2 Technical Approach

4.2.1 Experimental Procedure

The combustion experiments have been conducted with equivalence ratio varied around 0.2 – 0.3 to simulate the lean conditions used normally in the practical combustors (Niessen, 1995). Bottom ash was collected from the incinerator grate and the fly ash was collected in the fabric filter. In addition, the flue gas was sampled and analyzed for volatile metals (Pb and Hg) using a sampling port located at the exit of the bag-house. Metal contents in the condensed combustion products (bottom ash and fly ash) were

analyzed using atomic absorption spectroscopy (flame AA, Thermo Jarrel Ash Inc., metal digestion using nitric acid solution). Metal species have been determined using an X-ray diffractometer (a Phillips X'pert model).

The flue gas samples were collected using a gas-sampling manifold connected to three different sampling ports. To limit the sample loss and condensation in the transfer lines, the sample collection lines were heated to 110 – 130 °C and maintained at a pressure of 4 to 7 kPa above the atmospheric pressure. The flue gas was bubbled through an impinger solution 400 ml of 1.5 % potassium permanganate in 10 % (3.6 Normal) sulfuric acid (Korpiel and Vidic, 1997). This solution was later analyzed by atomic absorption spectroscopy to determine the concentrations of Hg, Pb, and other metals in the flue gas.

4.2.2 Thermodynamic Equilibrium Estimates

The expected equilibrium combustion products produced at different equivalence ratios have been predicted using a thermodynamic equilibrium code (Selph and Hall, 1992). In the computations, the synthetic fuel was treated as a combination of representative species. In addition, trace amounts of metals doped to the synthetic fuel (Al, Ni, Cr, Pb, Hg) as well as up to 0.5 % of Cl were added to the fuel in different computation runs. The effect of chlorine on the predicted metal partitioning was found to be negligible at the low chlorine contents that are typical of the US MSW. The higher chlorine contents were observed to affect significantly the metal species and their distribution among the combustion products, but were not of interest to this investigation aimed at the characterization of the products of MSW incineration. The results of equilibrium computations performed in a wide range of equivalence ratios and some comparisons of

comparisons of the computed results versus the measured gas species concentrations have been discussed elsewhere (Thipse et al., 2001). In this chapter, the focus is placed at the equilibrium prediction of the metal-containing species and comparisons of the computations with the new experimental measurements. Therefore, the equilibrium computations were conducted only for the experimental fuel-air equivalence ratios (ϕ) ranging from 0.210 to 0.283.

Two sets of computations have been performed for each equivalence ratio. In the first computation, the adiabatic flame temperature was computed and the product species at these conditions were found. It has been assumed that the predicted species that are condensed at the adiabatic flame temperature can be considered as those forming the bottom ash. The gaseous products of the first computation have been considered as a fuel for the second computation (with the initial temperature equal to the adiabatic flame temperature), for which the final temperature has been pre-set to 373 K (the exhaust temperature of the incinerator). The goal of the second computation was to compare the composition and species of the cooled product species with those determined experimentally by analyzing the fly ash and flue gases exiting the incinerator.

The results of the equilibrium code computation are produced as mole fractions of various species, C_i^{Eq}, where I is the species counter. For a particular metal containing species, the equilibrium computation produced mole fraction C_{ms}^{Eq}. In order to compare this result with the atomic absorption measurement that produces the weight fraction, of a metal (as element) in the sample being analyzed, m_{me}^{AA}, the following re-normalization of the computational results was conducted. The computed (by the equilibrium code) mass percentage of each elemental metal m_{me}^{Eq}, was calculated as:

$$m_{me}^{Eq} = \frac{\mu_{ms} \times C_{ms}^{Eq}}{\sum_{i=1}^{N} \mu_i \times C_i^{Eq}} \cdot \frac{\rho_{ms}}{\rho_{me}} \cdot 100\% \qquad (4.1)$$

where μ is the molar weight, ρ is density, subscript *ms* shows the predicted by the equilibrium code metal species (in most cases, metal oxides), and subscript *me* shows the elemental metal. Therefore, the calculated metal weight fraction, m_{me}^{Eq}, could be compared directly with the metal weight fraction measured using atomic absorption techniques, m_{me}^{AA}.

4.2.3 Metal consumption rate estimates

The metal species fed into the primary combustion chamber react through two main processes: heterogeneous oxidation and volatilization. The rates of these two processes need to be compared to the rate at which the metals are fed into the incinerator in order to evaluate the expected contents of various metal species in the combustion products. At the temperatures characteristic of the primary combustion chamber (around 1000 K), the group of metals including Fe, Ni, Cr, and Al are primarily oxidized heterogeneously, whereas Hg and Pb are volatilized. Therefore, to make a magnitude estimate for the volatile metals, their feed rates are compared to the expected rate of their volatilization based on a simplified energy balance approach. For the non-volatile metals, the feed rates are compared to the expected rates of their heterogeneous oxidation estimated at the temperature in the primary combustion chamber.

A) Non-volatile metals: The synthetic fuel was doped with trace amounts (0.1 mass %) of Al, Ni and Cr, in solid powder form so that at different experimental fuel feed rates, the mass feed rates for these metals, $\dot{m}_f$, varied in the range of 0.113 – 0.205 g/s. The

fuel contained 8 mass % of iron, so that the experimental feed rate for Fe varied in the range of 9.04 - 16.4 g/s. At the experimental temperature range of the primary combustion chamber, 1073 – 1273 K, the oxidation process for each of the non-volatile metals present in the fuel is best described by the parabolic law (Kubachewski, 1962):

$$\left(\frac{m_{ox}}{A}\right)^2 = K_p \cdot \Delta t \tag{4.2}$$

where m_{ox} is the mass of the metal that has been oxidized during the time interval Δt, A is the metal surface area, and k_p is the parabolic rate coefficient. For a simple estimate, we assumed $\Delta t = 1\ s$, so that the estimated m_{ox} per second could be directly compared to the metal feed rate, $\dot{m}_f$, also normalized per second. The following expressions were used to estimate the rate coefficient k_p at the primary chamber temperatures:

Metal	Rate Coefficient, $g^2\ cm^{-4}\ s^{-1}$	Reference
Fe:	$k_p = 0.37\ exp\ (-33{,}000/RT)$	(Stanley et al., 1951)
Ni:	$k_p = 1.2 \times 10^2\ exp\ (-68{,}300/RT)$	(Kubachewski, 1962)
Al:	$k_p = 2 \times 10^{-5}\ exp\ (-33{,}000/RT)$	(Kubachewski, 1962)
Cr:	$k_p = 61.5\ exp\ (-64{,}630/RT)$	(Gulbransen & Andrew, 1958)

Where R is the universal gas constant with units (Cal/g°C).

The surface area for each metal was estimated as

$$A = 4\pi r^2 N = \frac{3\dot{m}_f}{r\rho} \tag{4.3}$$

where r is the average radius of the metal particles, ρ is the metal density, and N is the number of particles fed to the incinerator per second estimated as

$$N = \frac{\dot{m}_f}{4/3 \pi r^3 \rho} \tag{4.4}$$

The average particle sizes for each metal used in the synthetic fuel were determined using particle size distributions obtained from the optical microscopy measurements. The final results of these estimates i.e., the oxidation rates of non-volatile metals are shown in Table 4.1. The results indicate that at the primary combustion chamber temperature range, iron is oxidized at a rate comparable to its feed rate and a more accurate estimate is needed to predict what portion of iron found in the bottom ash will be oxidized. Nickel and chromium can be oxidized at a noticeably faster rate than they are fed to the incinerator, therefore, it is expected that these metals be primarily contained in the bottom ash as respective oxides. For aluminum, the oxidation rate is slower than the feed rate, thus aluminum metal specie is expected to remain in the bottom ash.

Table 4.1 Feed and Oxidation rates for Non-Volatile Metals

Metal	Feed rate, g/s		Oxidation rate, g/s	
	T = 1073 K	T = 1273 K	T = 1073 K	T = 1273 K
Fe	9.04	16.40	14.327	19.204
Ni	0.113	0.205	2.029	3.732
Al	0.113	0.205	0.019	0.026
Cr	0.113	0.205	1.782	3.185

B) Volatile metals **:** For these metals, their volatilization rate was compared with the feed rate. To estimate the volatilization rate, the heat required to preheat the metal to the boiling point and the latent heat of evaporation were balanced with the convective heat flow to the metal-containing particles. Different mechanisms of volatilization were considered for Hg and Pb.

Metallic mercury was added to the synthetic fuel and a simple boiling model was used for mercury. The expected rate of mercury evaporation, $\dot{m}_{Hg}$, was estimated using the heat balance equation for mercury particles:

$$4\pi r_{Hg}^2 N_{Hg} h\left(T_{pcc} - T_{boil,Hg}\right) = \frac{\dot{m}_{Hg}}{M_{Hg}}\left[C_{p,Hg}\left(T_{boil,Hg} - T_0\right) + L_{Hg}\right] \tag{4.5}$$

where r is the particle size, N is the number of "particles" fed to the primary combustion chamber per second, estimated using Equation 4.4 above, M is the species molar mass, T_{pcc}, is the temperature in the primary combustion chamber, varied from 1073 to 1273 K, $T_{boil,Hg}$ is the mercury boiling point, T_0 is the initial fuel temperature, C_p is the molar heat capacity, L is the molar latent heat of vaporization, and h is the heat transfer coefficient, determined as $k \cdot Nu / 2r_{Hg}$, where k is the air thermal conductivity, and Nusselt number Nu is estimated using Whitaker equation (Çengel, 1997):

$$Nu = 2 + \left[\left(0.4\,Re^{1/2} + 0.06\,Re^{2/3}\right) Pr^{0.4} \left(\mu_\infty / \mu_s\right)^{1/4}\right] \tag{4.6}$$

where Re is the Reynolds number estimated using particle size and gas flow velocity in the combustion chamber, $Pr = 0.69$ is Prandtl number for air (Mills, 1995), and μ_∞ and μ_s are the air viscosities at the primary combustion chamber temperature and particle surface temperature, respectively.

The addition of lead to the synthetic fuel was in the form of condensed PbO, and according to the literature data, PbO in presence of oxygen is further oxidized and volatilized as PbO_2 at a temperature of $T_{vol,PbO2}$ = 673 K (Kubachewski, 1962). Therefore, lead volatilization was considered as a two-step process. In the first step, the

condensed PbO_2 formed as a result of PbO reaction with oxygen, and in the second step, the PbO_2 was volatilized:

$$PbO\ (s) + \tfrac{1}{2}\ O_2 \rightarrow PbO_2\ (s) \qquad (4.7)$$

$$PbO_2(s) \rightarrow PbO_2\ (g) \qquad (4.8)$$

Both reactions are assumed to occur at 673 K, so that the heat balance equation used was:

$$4\pi r_{PbO}^2 N_{PbO} h\left(T_{pcc} - T_{vol,PbO_2}\right) = \frac{\dot{m}_{PbO}}{M_{PbO}}\left[C_{p,PbO}\left(T_{vol,PbO_2} - T_0\right) + \Delta H + L_{PbO_2}\right] \qquad (4.9)$$

where the notation is similar to that used in Eq. 4.5 above and ΔH is the enthalpy of reaction (Equation 4.7), estimated using enthapies of formation of all reagents to be -75.94 KJ/mol. The parameters used in the estimates are listed in Table 4.2 and the results of these estimates are summarized in Table 4.3. It is observed that both Hg and Pb can be volatilized noticeably faster than they are fed in the incinerator, so that it is expected that almost none of these metals should be found in the bottom ash.

4.3 Results and Discussion

4.3.1 Overall ash compositions

Iron and silicon contents in the ash were determined using atomic absorption measurements; carbon, chlorine, hydrogen, nitrogen, and sulfur contents were obtained using standard ASTM chemical tests (ASTM, 1996). The remaining mass balance was assumed to be oxygen. The resulting compositions for both bottom ash and fly ash are illustrated in Figure 4.1. In addition to the main elements, the ash percentage composed of the trace metals is lumped together and shown as the overall trace metal content labeled M. Compositions of the bottom and fly ashes predicted by the equilibrium

computations are shown in Figure 4.2. The relative metal contents in the ash predicted by equilibrium computations are much higher than the observed experimental metal concentrations.

Table 4.2 Quantities used in Estimates of Metal Volatilization Rates.

Quantity	Symbol	Value	Units	Reference
Prandtl number air	Pr	0.69		Mills, 1995
Reynolds number, Pb	Re_{Pb}	11.01 to 14.23		Estimated
Reynolds number, Hg	Re_{Hg}	55.01 to 71.18		Estimated
Nusselt number, Pb	Nu_{Pb}	3.42 to 3.58		Estimated
Nusselt number, Hg	Nu_{Hg}	5.36 to 5.75		Estimated
Reaction enthalpy, Hg	ΔH_{Hg}	-75.94	KJ/mol	Estimated
Latent heat, PbO_2	L_{PbO2}	178	KJ/mol	Winter, 2000
Latent heat, Hg	L_{Hg}	59.3	KJ/mol	Winter, 2000
Heat capacity, Hg	Cp_{Hg}	20.78	J/mol K	Eremenko et al, 1998
Heat capacity, PbO	Cp_{PbO}	37.31	J/mol K	Eremenko et al, 1998
Boiling temp, Hg	T_{boilHg}	629.5	K	Eremenko et al, 1998
Temperature PCC	T_{pcc}	1073 to1273	K	Measured
Initial fuel temp	T_0	300	K	Measured
Surface temp	T_s	1173	K	Estimated
Air viscosity (Tpcc)	μ_∞	41 to 46 x 10^{-6}	Kg/ms	Mills, 1995
Air viscosity (Ts)	μ_s	43.98 x 10^{-6}	Kg/ms	Mills, 1995
Molar mass, PbO	M_{Pb0}	239	g	Eremenko et al, 1998
Molar mass, Hg	M_{Hg}	200	g	Eremenko et al, 1998
Particle size, Pb	r_{Pb}	0.00005	m	Measured
Particle size, Hg	r_{Hg}	0.00025	m	Estimated
Particle number, Pb	N_{Pb}	29949	s^{-1}	Estimated
Particle number, Hg	N_{Hg}	230	s^{-1}	Estimated

Table 4.3 Feed and Volatilization Rates for Volatile Metals

Metal species	Metal feed rate, g/s		Metal volatilization rate, g/s	
	T = 1073 K	T = 1273 K	T = 1073 K	T = 1273 K
Hg	0.113	0.205	0.188	0.847
PbO	0.113	0.205	0.96	3.07

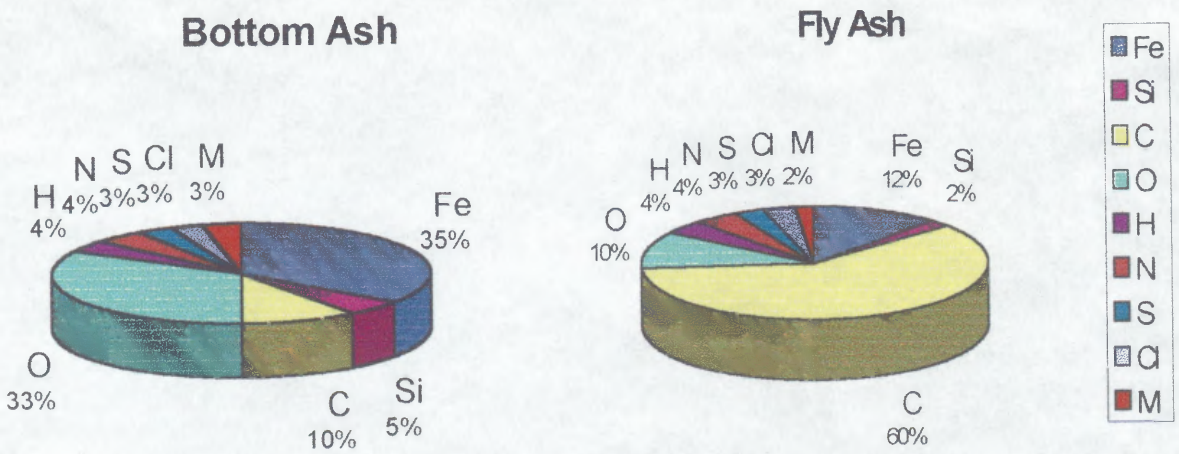

Figure 4.1 Experimental Bottom Ash and Fly Ash Composition

The main reason for this discrepancy is that the equilibrium computations predict higher concentration of CO_2 do not predict the formation of carbon (soot) in the ash, whereas significant amounts of soot (and carbon) are found in both bottom and fly ash samples.

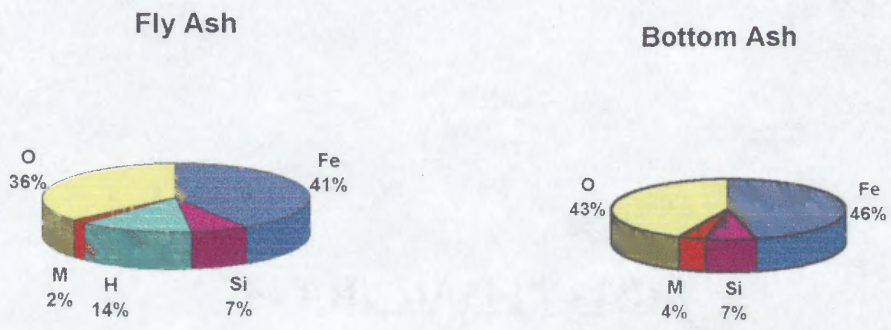

Figure 4.2 Compositions of the bottom and fly ashes predicted by the equilibrium computations

Once this discrepancy is recognized, a superficial correction of the experimental bottom ash and fly ash contents can be suggested in which the elements that never appear in the predicted equilibrium ash composition, e.g., C, N, S and Cl, are removed from the experimental ash composition. Such "corrected' ash compositions can be

compared versus the equilibrium computation results in order to approximately balance the overall quantities of metal-containing compounds and, most importantly, compare the magnitudes of their relative changes as a function of equivalence ratio. The recomputed experimental elemental compositions for the bottom ash and fly ash are shown in Figure 4.3.

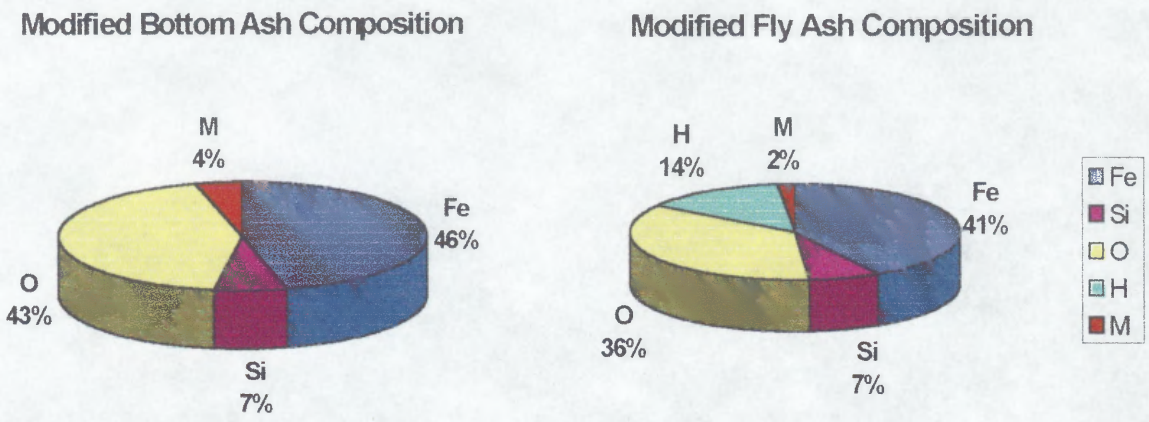

Figure 4.3 Modified experimental composition of the produced bottom and fly ashes

After each experimental run, the total masses of bottom ash M_b and fly ash M_f, were measured. The total mass of the produced flue gas M_g was calculated as $M_g = v \cdot A \cdot \rho \, t$, where v is the flue gas velocity measured at the system exhaust using a pitot tube, A is the area of the pipe cross-section where the velocity measurement was made, ρ is the density of flue gas at a temperature of 373 K, and t is the duration of the run. The gas density was estimated assuming that the gas composition was close to that predicted for the gaseous combustion products by an equilibrium computation conducted at the final temperature set to 373 K. Using the total masses of each of the combustion product component (fly ash, bottom ash and flue gas), and the measured concentrations of metal species in each of the components, the overall distributions of each metal

between different combustion products were found. The results of this analysis are shown in Figure 4.4 along with the results predicted by the thermodynamic equilibrium computations and some data reported in the literature. It can be noted that for all the metals except for Ni, our experimental data indicate higher metal species contents in the flue gas as compared to the other data sets reported in the literature. An interpretation of this could be that in most of the referred works, electrostatic precipitators have been used, that are more efficient in capturing the ultra fine particles than the fabric filters used in this research. Therefore, it is likely that some of the fine and ultra-fine particles escaped the fabric filter and remained aerosolized in the flue gas. Some of that fine particulate matter could be captured during the gas sampling and, therefore, increased concentrations of metal species in the flue gas could be detected by the atomic absorption spectroscopy measurements.

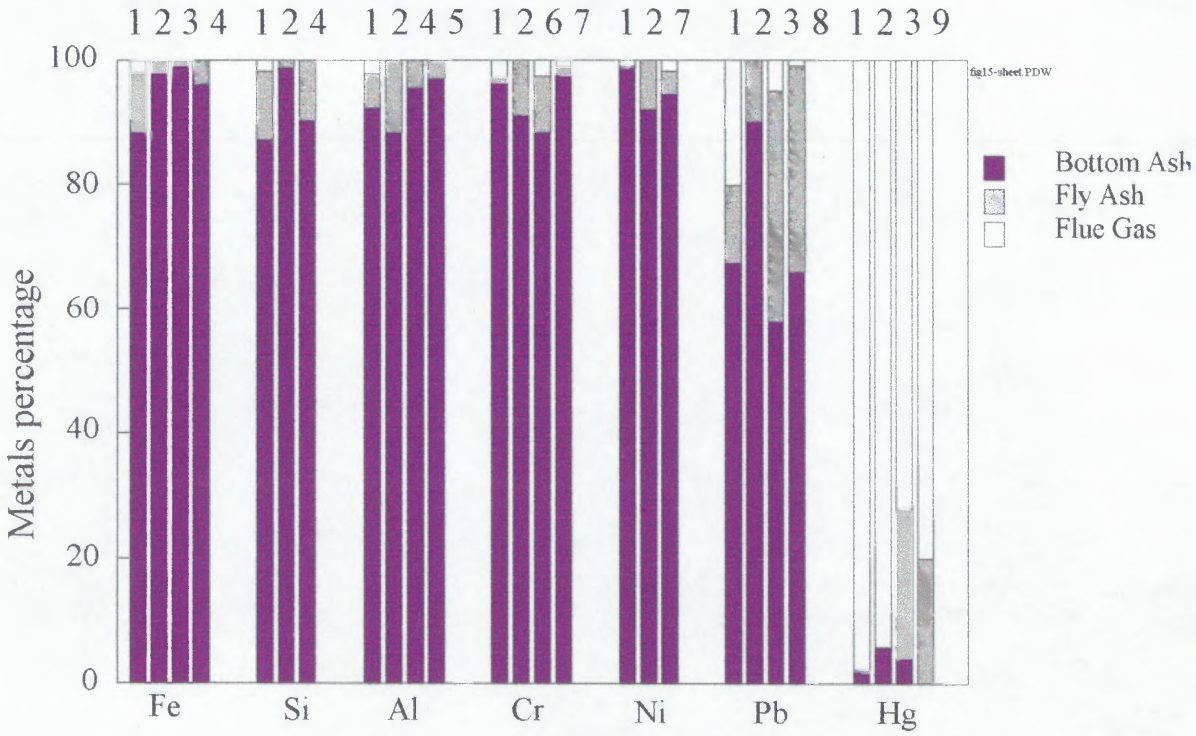

Figure 4.4 Distribution of metals in incineration products

Where, 1 Experimental results of this research; 2. Equilibrium computation predictions Brunner and Monch, 1986; 4. Wang et al., 1999; 5. Verhulst, et al., 1996; 6 Wey et al., 1998; 7. Binner, et al., 1997; 8. Nakamura, et al., 1996; 9 Vogg, et al., 1986.

The overall amounts of the metals entering the system as a part of the fuel have been balanced with the respective metal contents in the combustion products determined using the total mass and atomic absorption measurements for the flue gas and fly and bottom ash. The results of comparison of the overall amounts of metals in the input and output of the incinerator are illustrated in Figure 4.5.

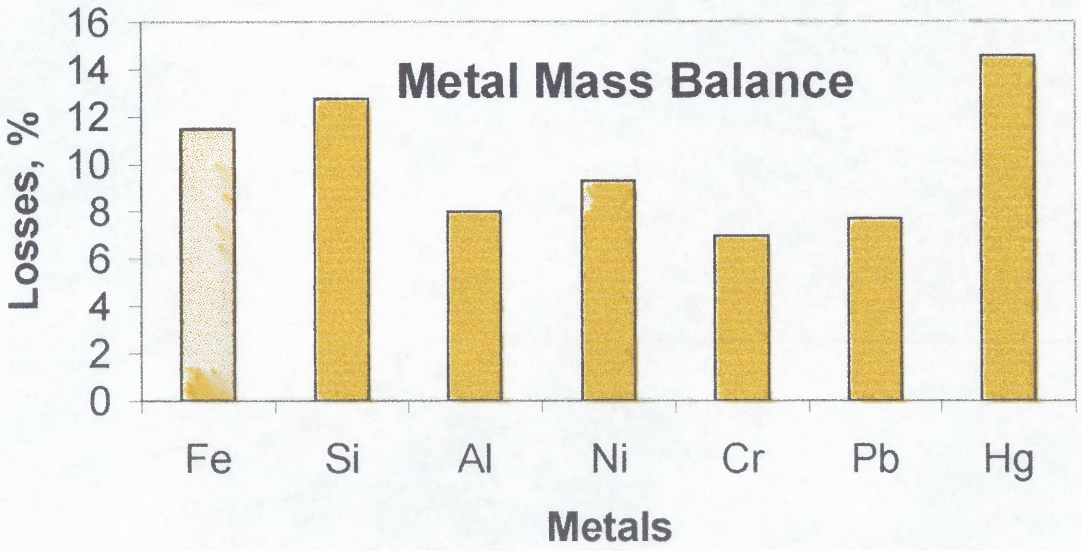

Figure 4.5 Percentages of metal-containing species not accounted in the overall metal mass balance in this research.

Estimates show that the experimental errors in the analyses of the ash metals contents can account for approximately 10 % of the difference between the metal mass

input and output. As shown in Figure 4.5, the observed discrepancy in highest for mercury. The discrepancy for all metals is due to the ultra-fine particles that escaped the bag-house filter and have not been effectively captured during the flue gas sampling.

The species present in the bottom ash and fly ash have been identified based on the x-ray diffraction measurements. Typical x-ray diffraction patterns for the bottom ash and fly ash samples are presented in Figure 4.6 and Figure 4.7. Analyses of such patterns produced by the ash samples have not been straightforward due to a large number of peaks resulting from the complex specie composition. Therefore, only the strongest peaks have been accounted for and respective species are marked in Figure 4.6 and Figure 4.7. A more detailed discussion of the observed metal species follows below.

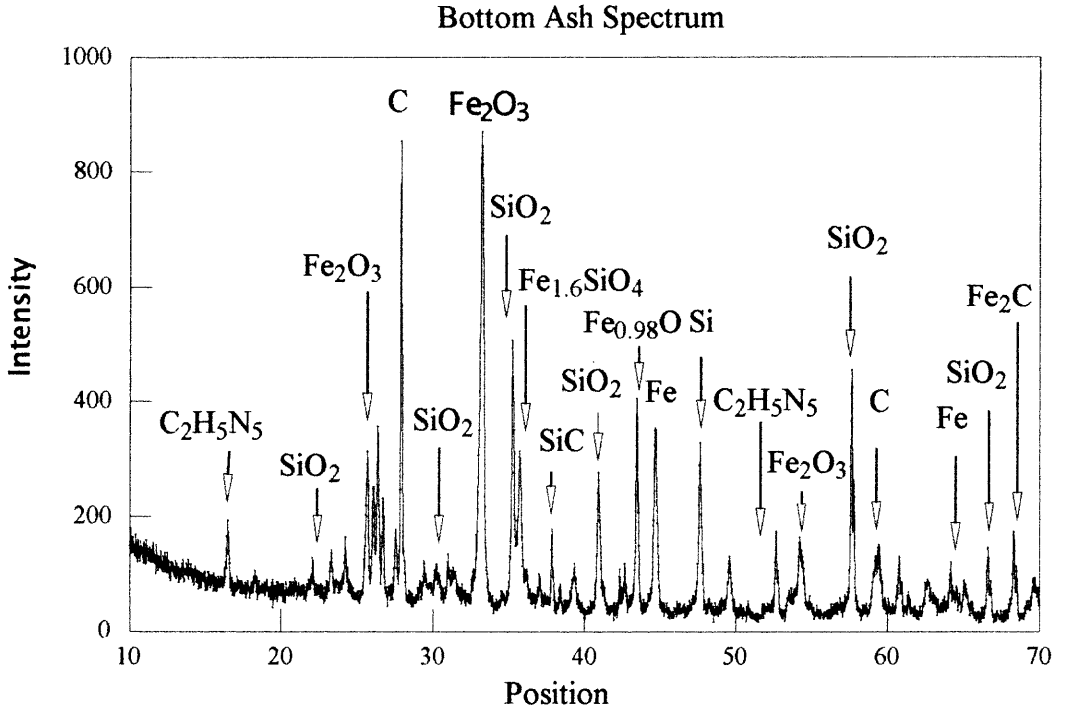

Figure 4.6 X-ray diffraction pattern of the produced bottom ash

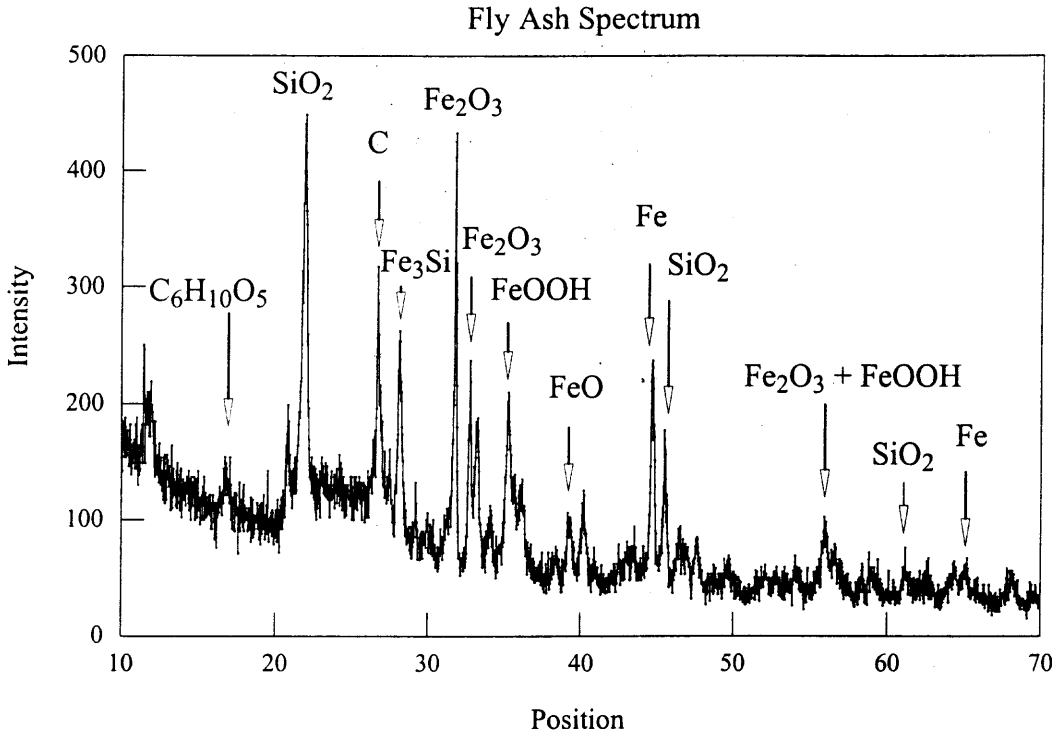

Figure 4.7 X-ray diffraction pattern for produced fly ash

4.3.2 Metal species and partitioning in the combustion products

Iron: Iron is a non-toxic, environmentally benign element and often the researchers motivated to determine the environmental and health hazards of the combustion products do not consider its partitioning and species found in the ash. However, iron in one of the most significant constituents of the produced ash and, therefore, the understanding of the formation mechanisms and distribution of the iron species is important for understanding of the behavior of toxic trace metal elements.

The equilibrium computations predicted formation of Fe_2O_3 as the only iron-containing species in the bottom ash and FeOOH as the only iron-containing species in the fly ash. In each case, the computations predicted the presence of only one iron-containing condensed species, even though the thermodynamic data for a number of compounds, including FeO, Fe_3O_4, $FeCl_2$, and $FeCl_3$, were included in the

thermodynamic database (the data for iron silicates are not included). Some of the equilibrium computations reported in the literature suggest the formation of additional iron-containing species, such as $FeCl_2$ and $FeSO_4$, e.g., Verhulst et al., 1996. The main difference between the equilibrium computations conducted in this project and those by Verhulst et al., 1996 is in the initial chlorine content. The chlorine fuel content used in our computations (and experiments) was 0.5 %, the reported chlorine content of MSW in the United States, whereas up to 3 % of chlorine was added to the fuel in the equilibrium computations by Verhulst et al., 1996.

In terms of the iron partitioning between the fly ash and bottom ash, our equilibrium computations are in fair agreement with the earlier measurements by Brunner and Monch, 1986, and Wang et al., 1999, as illustrated in Figure 4.4. However, as shown in Figure 4.4, our AA measurements indicate significantly higher iron contents in both fly ash and flue gas as compared to the literature contents. (Please note, that here and below the results of the atomic absorption measurements are the corrected ones as shown in Figure 4.3). One possible reason for such a discrepancy has been discussed by Wu et al., 1994, based on the possibility of the mechanical entrainment of non-volatile metal particles into the turbulent gas flows. This effect could be more significant in our experiments than in industrial incinerators because relatively small iron particles (800 μm average diameter) were added to the synthetic fuel as opposed to large bulk iron pieces often contained in the municipal waste. The estimated settling velocity for the iron particles is about 10 m/s, which is less than the gas velocity in the combustion chamber of about 15 m/s, so that the entrainment of the particles could indeed occur.

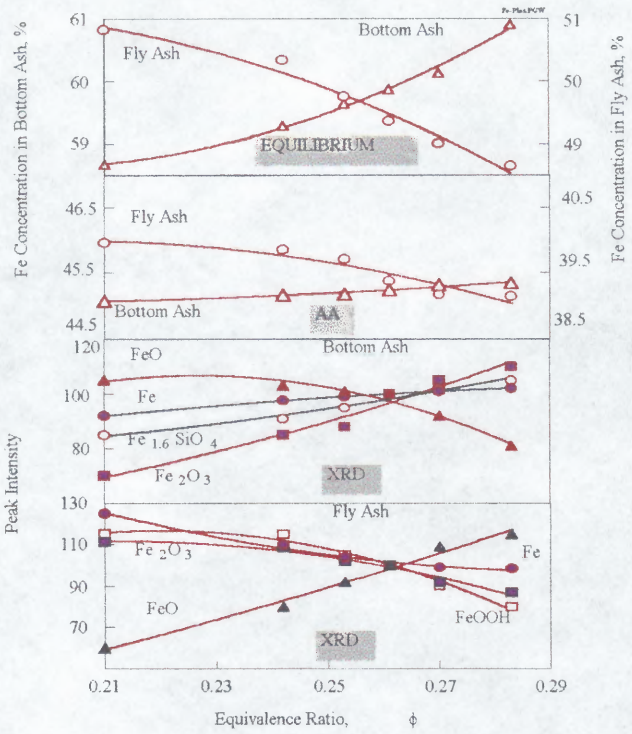

Figure 4.8 Comparison of XRD Trends, modified AA measurements and equilibrium predictions for partitioning of Iron.

The computations showed that the content of Fe_2O_3 (and thus, the overall iron content in the bottom ash) increases at higher equivalence ratios, whereas the FeOOH content, or the total iron content in the fly ash, decreases at higher equivalence ratios. This trend is in agreement with the AA measurements, as shown in Figure 4.8. Species of iron in both the bottom ash and fly ash were determined using x-ray diffraction (XRD). The XRD measurements indicated the presence of common species, Fe, Fe_2O_3 and FeO in both bottom and fly ash samples. Also, such species as $Fe_{1.6}SiO_4$ were detected in the bottom ash and FeOOH with Fe_3Si were detected in the fly ash (Figure

4.7). Perhaps, the most unexpected observation is the presence of metallic iron in the fly ash. Two mechanisms that could explain such observation can be considered. One mechanism has been discussed by Senior et al., 2000, who suggested that iron oxide formed in the primary combustion chamber could be vaporized through its reduction. Later on, the ultra fine iron particles could condense on the fly ash particles in the heat exchanger/filter area that is lean in oxygen (the gas is a mixture of nitrogen and carbon dioxide). The second mechanism could simply be the mechanical entrainment of iron particles in the flue gas.

The changes in the intensities of the x-ray diffraction peaks qualitatively reflect the changes in the relative concentrations of the Fe-containing species. Quantities of Fe and Fe_2O_3 in the bottom ash increased at higher equivalence ratios, whereas the content of FeO decreased. In contrast, quantities of Fe, Fe_2O_3 and FeOOH in the fly ash decreased at higher equivalence ratios, whereas the content of FeO increased. This behavior can be understood considering that in a typical fuel-lean system (low fuel-equivalence ratios in the primary combustion chamber), the chemical reaction rate of the iron oxidation is accelerated at higher equivalence ratios. The primary product of iron oxidation is a Fe_2O_3 layer on the Fe particle surface. Thus, the faster formation of such a layer results in a slower reactions of other iron intermediate species, e.g., volatile FeO, FeOOH, and, possibly, gaseous Fe, ultimately causing the decrease in the contents of these species in the fly ash. Thus, the observed decrease in the elemental Fe content in the fly ash at higher equivalence ratios indicates that the primary mechanism for its transfer into the fly ash is through the chemical reduction/vaporization/re-condensation route, as opposed to the simple mechanical entrainment of iron particles.

Clearly, there are more of the iron-containing species observed to be present in the ash as compared to the equilibrium predictions. A more detailed kinetic modeling and a more detailed investigation of the structure and compositions of the ash particles would be needed for an adequate interpretation of these observations important for the understanding of the overall structure and composition of the produced ash.

Silicon: The equilibrium computations predicted that SiO_2 is the only silicon-containing species in both the bottom ash and the fly ash. At the same time, the XRD measurements indicated the presence of additional silicon containing species, including SiC, $Fe_{1.6}SiO_4$ and Si in the bottom ash and Fe_3Si in the fly ash. It has been reported that the elemental Si could form in the incinerator chamber when local oxygen depleted reduction zones are developed (Wey et al., 1998). In this case, the silicon oxide SiO_2 contained on the fuel grate can be reduced to the volatile SiO and pure Si through the following reactions:

$$SiO_2 + CO \rightarrow SiO + CO_2 \quad (\Delta H_{rxn} = -510 \text{ KJ/mol}) \qquad (4.10)$$

$$SiO + CO \rightarrow Si + CO_2 \quad (\Delta H_{rxn} = -248 \text{ KJ/mol}) \qquad (4.11)$$

As shown in Figure 4.9, it is predicted by the equilibrium computations that at higher equivalence ratios the content of silicon in the fly ash increases and in the bottom ash decreases. This predicted trend is due to higher temperatures, and thus, higher overall SiO_2 vapor pressure at higher equivalence ratios. Although the experimental temperatures at higher equivalence ratios are indeed higher, the experimentally determined changes in the silicon content in the fly and bottom ashes are opposite to those predicted to occur in equilibrium (Figure 4.9). This discrepancy is most likely due to a slow kinetics of the reaction of SiO_2 contained in the fuel, which results in a faster

accumulation of the SiO_2 in the bottom ash at a faster fuel feed rate, e.g., at higher equivalence ratios.

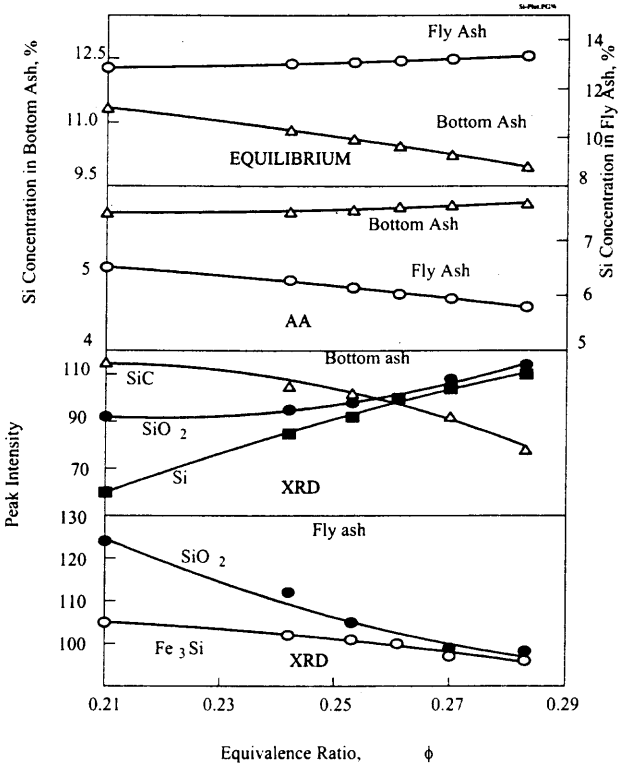

Figure 4.9 Comparison of XRD trends, modified AA results and Equilibrium predictions for Si Partitioning.

The relative changes in the intensities of the x-ray diffraction peaks show qualitatively that the contents of Si and SiO_2 in the bottom ash increase at higher equivalence ratios while the SiC content decreases. This observation can be interpreted as a result of a more complete carbon oxidation occurring at higher equivalence ratios, so that less of carbon remains available to react with silicon to form SiC. At the same time, the higher rate of chemical reaction between oxygen and SiO_2 results in a faster reduction of SiO_2 to Si, as described above.

Concentrations of both Fe_3Si and SiO_2 in the fly ash decrease at higher equivalence ratios, the trends that are likely caused by a faster rate of iron oxidation and a faster rate of oxygen reaction with hydrocarbon species in the primary combustion chamber.

Aluminum: Our equilibrium computations predicted formation of Al_2O_3 in both bottom ash and fly ash. The formation of $AlCl_3$ has been predicted by Verhulst et al, 1996 using significantly higher chlorine contents in the fuel. At the same time, the estimates of the rates of heterogeneous reaction showed that substantial amounts of unreacted aluminum should accumulate in the bottom ash. The Al contents in the bottom ash and fly ash measured by AA remain almost unchanged at varied equivalence ratios, as shown in Figure 4.10. Thus, the change in the distribution of aluminum species between the bottom ash and fly ash is smaller than the equilibrium prediction, indicative of the defining role of the slow oxidation kinetics on the aluminum behavior in the primary combustion chamber.

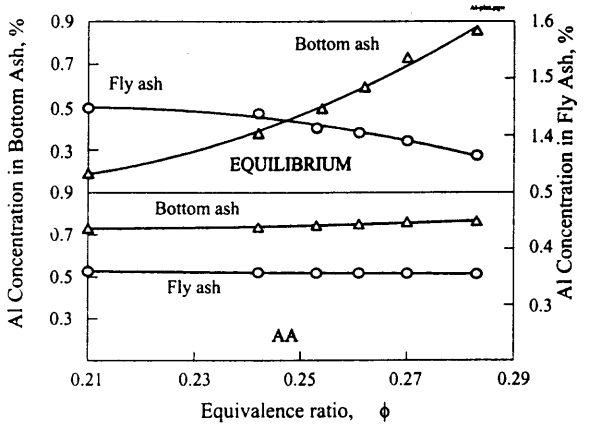

Figure 4.10 Comparison of modified AA measurements and equilibrium predictions for partitioning of aluminum.

Distributions of the aluminum-containing species between the fly ash, bottom ash, and flue gas reported in the literature (Wang, 1999, Verhulst, 1996) and in this paper are shown in Figure 4.4 on page 69. The quantity of Al in the fly ash produced in these experiments (about 5 %) is consistent with those reported in the literature (4 – 5 %). A somewhat higher aluminum content in the flue gas measured in these experiments could be explained by the presence of the ultra fine alumina particles entrained in the gas that escaped the fabric filter.

Chromium and nickel: The equilibrium computations predicted that oxides Cr_2O_3 and NiO are produced in both the bottom and fly ashes (Figure 4.11 and Figure 4.12).

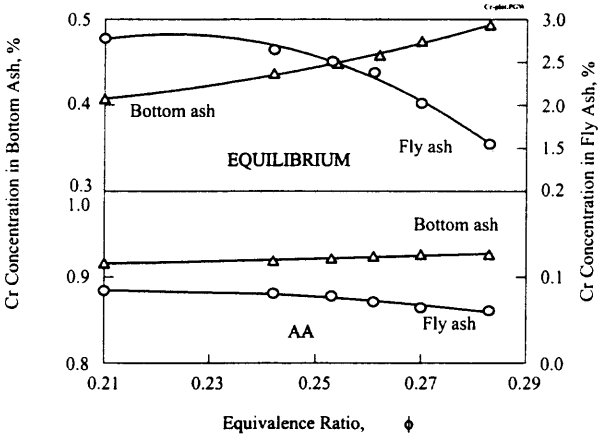

Figure 4.11 Comparison of modified AA measurements and equilibrium predictions for partitioning of chromium.

The reaction rate estimates showed that the heterogeneous reaction of oxidation is fast compared to the feed rate, and thus most of the oxides should form in the bottom ash. The rate of volatilization of these oxides at the primary combustion chamber temperature of around 1000 K is expected to be slow because of their very high boiling temperatures. The AA measurements indeed show that the amounts of chromium and

nickel in the bottom ash are greater than predicted by the equilibrium computations (Figure 4.11 and Figure 4.12). The directions of the changes in the distribution of chromium and nickel between the fly and bottom ash predicted to occur by the equilibrium computation are in agreement with the experimental trends, however the magnitude of the predicted changes significantly exceeds that observed experimentally. This discrepancy, similarly to the earlier discussion for aluminum, could be indicative of a slow chemical kinetics controlling the behavior of chromium and nickel oxides.

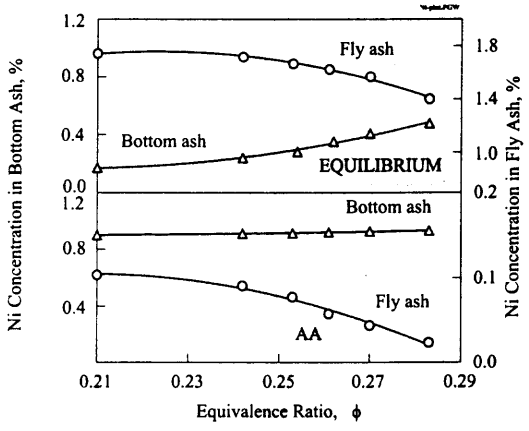

Figure 4.12 Comparison of modified AA measurements and equilibrium predictions for partitioning of Nickel.

The experimental distributions of the Cr and Ni – containing species between the bottom ash, fly ash and flue gases determined in this project are in good agreement with the results reported by Binner et al., 1997, who also used fabric filters to collect the fly ash (Figure 4.4). A noticeably higher percentage of the chromium-containing species has been found in the fly ash by Wey et al., 1998, who used electrostatic precipitator filters for capturing the fly ash. Therefore, it is possible that a significant portion of the

chromium containing species comprises of the very fine particles that escape the fabric filters used in this research and in the experiments by Binner et al., 1997.

Mercury and Lead: The equilibrium computations predicted formation of the condensed HgO and PbO oxides in the bottom and fly ashes and gaseous HgO and PbO in the flue gas. Both the mercury and lead oxide contents decrease in the bottom ash and increase in the fly ash and the flue gas at increased equivalence ratios (Figures 4.13 and 4.14).

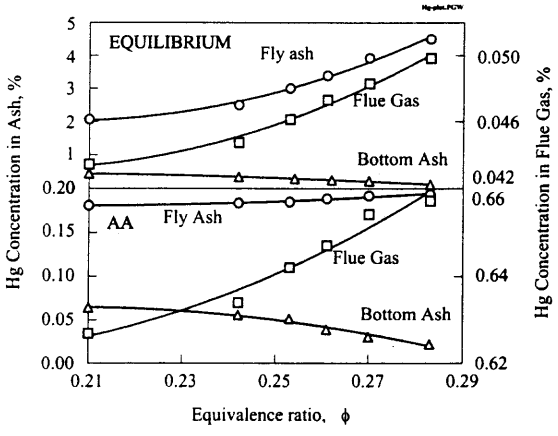

Figure 4.13 Comparison of modified AA measurements and equilibrium predictions for partitioning of mercury.

These trends are in qualitative agreement with the results of the atomic absorption measurements shown in Figures 4.13 and 4.14. However, the absolute amounts of mercury and lead found in the flue gas exceed by about an order of magnitude the amounts predicted to be gasified in equilibrium. In the overall distribution between the fly ash, bottom ash and the flue gas, a much lower percentages of both mercury and lead are found in the fly ash in these experiments as compared to the data reported in the literature (see Figure 4.4). The rates of volatilization of both metals are estimated to be higher than their feed rates into the primary combustion chamber. Thus as discussed in section 4.3, gaseous Hg and PbO_2 are produced in the primary

combustion chamber. The following reactions are accompanied by the condensation of mercury and lead oxides from the gas phase and, therefore, it is expected that significant amounts of the condensed oxides will comprise of ultra-fine particles. Therefore, using of fabric filters in this research could again account for the discrepancy in partitioning of mercury and lead between the fly ash and flue gas observed in this work and reported by other researchers using electrostatic precipitation filters (Brunner and Monch, 1986, Nakamura, et al., 1996) or wet scrubbers (Vogg et al., 1999).

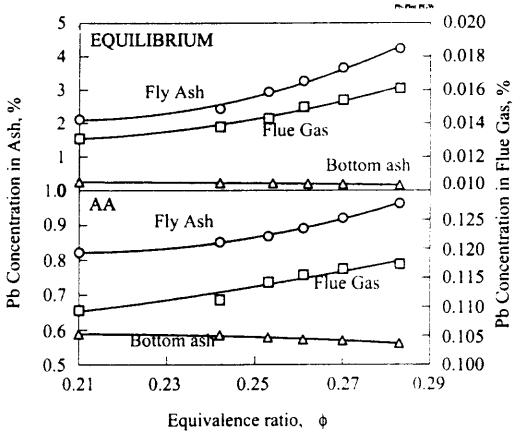

Figure 4.14 Comparison of modified AA measurements with equilibrium predictions for partitioning of lead.

4.4 Summary

An experimental technique was developed for studying metal partitioning in the products of waste incineration. The technique exploits a continuous feed, pilot-scale incinerator facility and well-characterized and reproducible synthetic fuel imitating the MSW. The total amounts of metals in different components of combustion products were determined using atomic absorption spectroscopy. The species of different metals in fly and bottom ash were determined using x-ray diffraction and compared with the

product compositions expected based on the thermodynamic equilibrium estimates. It was observed that the effect of chlorine on metal partitioning becomes important when chlorine contents in the fuel significantly exceed 0.5 %, the typical chlorine contents in the US MSW. The results on the overall metal partitioning between the fly ash, bottom ash, and flue gas are in reasonable agreement with the earlier experimental reports. One of the significant discrepancies observed was that smaller than usual metal contents were found in the fly ash.

It is suggested that the use of the fabric filters inefficient in capturing the fine particulate matter caused that discrepancy. Mechanical entrainment of metal particles in the turbulent gas flow in the primary combustion chamber was indicated to be important in transferring iron oxides into the fly ash. It has been also found that the sequence of iron oxidation, reduction, vaporization, and condensation has occurred and caused production of elemental iron in the fly ash. Because of the large absolute iron concentration in the municipal waste and its combustion products, this sequence is important for the understanding of the overall ash particle formation mechanisms. Evidence of another reduction process, formation of elemental Si from SiO_2 has also been found. Such processes need to be considered in modeling the waste incineration because of their effect on the flame exothermicity and mechanisms of the formation of bottom ash.

It has also been observed that the slow kinetics of such processes as oxidation of Al and volatilization of oxides of Cr and Ni needs to be considered to adequately describe the behavior of these metals in the furnace and caution should be exercised when the thermodynamic equilibrium predictions are used. Finally, the results indicate

that significant amounts of the lead and mercury-containing species comprise of very fine particles that are not effectively captured by the fabric filters. It is suggested that for a future research, a new electrostatic precipitation filter system should be installed in the NJIT pilot scale incinerator facility to enable capturing the fine fly ash particles.

A more detailed characterization of the species and morphology of the fly ashes is conducted in the next chapter to better understand the processes and conditions affecting the ash formation and metal species partitioning.

CHAPTER 5

PHASE DISTRIBUTION AND MORPHOLOGY OF FLY ASH

5.1 Introduction

Toxic, metallic trace elements contained in coal and refuse derived fuels present a serious environmental problem that stimulates a wide range of research (Linak and Wendt, 1993), (Niessen, 1995) and (Senior et al, 2000). Most of the studies have focused at the capturing the hazardous metal-containing particulates that escape the current filters (e.g., 0.1 – 1 μm and nanosized particles). Fewer studies have addressed the species and morphology of the ash that is being successfully collected and is known to be saturated with many metal species, most of them are often bonded to carbon. The bonding mechanisms and bond strengths are not well-known. In most cases toxic metals should be removed before the ash is buried in the landfills or used in manufacturing of cements or other commodity materials. Information on metal speciation, phase compositions, and morphology of the ash particles is needed to efficiently discard the toxic species from the collected ash. In the past decade, significant efforts have been applied to characterize the partitioning of trace metals in the ash, however, only total atomic fractions of metals have been reported in most cases. Researchers did not specify chemical compositions and morphology of the ash metal species even though such information is crucial for the development of adequate technologies for removal, neutralization, or recycling of the toxic metal species.

The lack of information on the chemical speciation and morphology of the produced ash particles is largely due to the experimental difficulties in gathering representative data using ash samples from the large scale industrial combustors. At the

same time, the complex heat and mass transfer processes occurring in different sections of the large-scale installations with continuous fuel feed systems and including primary and secondary combustion chambers, staged heat exchangers, and electrostatic or fabric filters determine the mechanisms of ash formation. These mechanisms depend on the temperature profiles and two-phase flow patterns existing in different parts of the industrial scale combustors and cannot be adequately imitated in the well-instrumented bench-scale burners.

Recently, a unique 140,000 Btu/hr pilot-scale laboratory combustor has been developed at NJIT with the primary goal of studying the mechanisms governing combustion of municipal waste and refuse derived fuels (Thipse et al., 1999). A schematic diagram of the apparatus is shown in Figure 3.1. It is a continuous solid fuel feed facility with a stationary grate with moving fingers, and capabilities to control independently the underfire and the overfire air flows, and adjust the temperatures in the primary and secondary combustion chambers. It is equipped with various diagnostics, e.g., thermocouples, gas sampling ports for the in situ gas chromatography, and windows for the optical observations and measurements. In a recent research exploiting this facility, a synthetic fuel representative of the municipal solid waste in the United States was formulated and produced in 270 kg batches (Thipse et al., 2001). The fuel composition included paper, hardwood mulch, low density polyethylene, animal feed, iron, and sand and was doped with trace amounts of Al, Ni, Cr, Hg and PbO. Experiments have been conducted on combustion of the synthetic fuel in the pilot-scale incinerator with varying fuel-air ratio. Both gaseous and condensed combustion products were sampled and analyzed. The total amounts of metals in different components of

combustion products were determined using atomic absorption spectroscopy. The species of main metal components in fly and bottom ash were determined using x-ray diffraction and compared with the product compositions expected based on the thermodynamic equilibrium estimates (Thipse and Dreizin, 2001). A number of metal-containing species were found in both bottom and fly ashes that have not been predicted as products by the equilibrium estimates. It has been also observed that the captured fly ash particles are characterized by an extremely wide particle size distribution and it was hypothesized that different mechanisms could be significant in the formation of different size particles. In addition, it was expected that if significant difference in the chemical composition is found for the particles of different sizes, an ash processing technique based on size classification could be developed to remove most of the toxic species from the ash prior to its recycling or burying in the landfills. This research was aimed to test the above hypotheses and characterize the morphology, species, and compositions of the produced fly ash particles of different sizes.

5.1 Overall Fly Ash Composition

Nine combustion experiments have been conducted with the equivalence ratio varied around 0.2 – 0.3 to imitate the lean conditions used normally in the practical incinerators (Niessen, 1995). A pilot natural gas-air flame was used to ignite the solid fuel. A steady state combustion regime was established after about one hour. The temperature in the primary combustion chamber was continuously monitored using an internally mounted thermocouple. The thermocouple was placed in the top portion of the chamber and have shown the temperature variation from 830 °C to 860 °C at different fuel to air ratios. In addition, a digital video camera and three-color pyrometer set up at a window in the

primary combustion chamber were used to monitor the flame radiation and temperature distribution in the region close to the center of the chamber. The optical measurements have indicated that the temperature at the center of the primary combustion chamber was not uniform and changed from 880 °C to 950 °C. However, once the steady state combustion regime was established, the average temperature and the range of the temperature variation remained constant.

Normally, one batch of synthetic fuel was used in three consequent experiments. The duration of each experiment was in the range of 6 to 8 hours. The overall ash composition and metal partitioning between the fly ash, bottom ash, and the flue gas were studied using the atomic absorption measurements and x-ray diffraction, as described by Thipse and Dreizin, 2001. Fly ash samples were recovered after each experiment from the "bag-house" fabric filter. Metals contents in the fly ash were determined using atomic absorption measurements; carbon, chlorine, hydrogen, nitrogen, and sulfur contents were obtained using standard ASTM chemical tests (ASTM, 1996). The remaining mass balance was assumed to be oxygen. The resulting overall composition for the fly ash is shown in Figure 4.1. In addition to the main elements, C, Fe, H, N, S, Cl, O, and Si, the ash percentage composed of the trace metals (Al, Ni, Cr, Pb, and Hg) is lumped together and is labeled M to represent the combined trace metals.

5.2 Fly Ash Particle Size Distribution and Density

The particle size distribution was obtained using optical microscopy. The fly ash samples were dispersed in oil on surfaces of microscope glass slides. A microscope was coupled to a video camera and a snappy board was used to digitize the images for further

processing. These images were processed using a UTHSCSA Imagetool software. The image processing included subtraction of background (an image acquired with no particles on the slide but with the same field illumination) to produce a uniform initial image brightness, Gaussian filtering, and boost of contrast. Each particle on the image, identified by the software as an object, was converted into a perfect circle with the same area as the original particle. The diameter of such a circle, called "Feret diameter", was measured for each object automatically so that the particle size distribution was determined. Each image included 50 – 100 particles, and at least ten images were collected and processed for each ash sample to provide an acceptable quality size distribution. An example of the representative size distribution for fly ash particles is shown in Figure 5.1. Such bimodal size distributions were consistently observed for ash samples collected after different combustion runs. The measured size distribution covers a very wide particle size range, so that some of the details, e.g., the size distribution in the range of 0 – 75 μm have not been resolved. The presence of very coarse particles, greater than 500 μm, in the fly ash was not expected. Note, that as described below, the large particles were not agglomerates of smaller particles.

In addition to the microscopic measurements, the fly ash particles were size classified using a set of four sieves with the 75, 150, 300 and 1000 μm opening sizes. A sieve shaker was used and the size classification was complete during 1 hr. The masses of each of the separated fractions of the fly ash particles were determined. As shown in Figure 5.2, the results of these measurements are consistent with the size distribution determined using optical microscopy. The densities of the different size fractions of the

fly ash particles were determined using a 10 ml glass picnometer. The results of these measurements are shown in Figure 5.3.

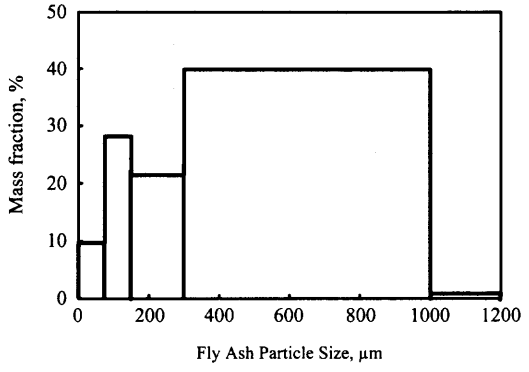

Figure 5.1 Size distribution of the fly ash particles determined using sieves.

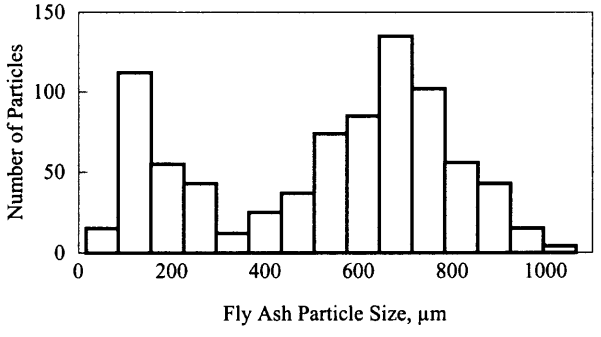

Figure 5.2 Size distribution of the fly ash particles determined using optical microscopy.

5.3 Morphology and Composition of Fly Ash Particles

The compositions of the different size fractions of fly ash particles were determined using Atomic Absorption (AA) measurements. The fly ash samples were dissolved in nitric acid and a flame AA instrument by Thermo Jarrell Ash, Inc., was used for the analysis.

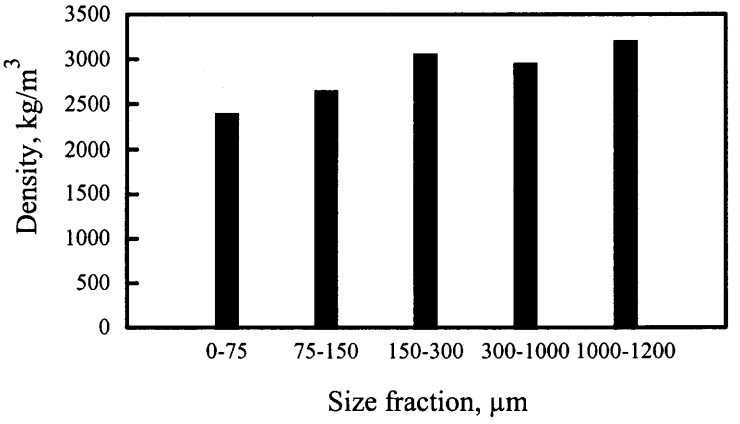

Figure 5.3 Densities of different size fractions of fly ash.

The measurements have been conducted for 6 ash samples collected after different incinerator runs. The trends observed for the changes in composition as a function of particle size were repeatable from sample to sample and are illustrated in Figure 5.4. In order to illustrate better similar trends and relative changes in metals concentrations as a function of the particle size, metal mass percents per a fly ash size fraction are plotted in Figure 5.4. Therefore, the sums of each metal's percentage in each size fraction will result in 100%. The total absolute mass percentages of different metals in ash are given in the caption of Figure 5.4. The amounts of Cr, Ni, and Fe in the particles are increasing as the particle size increases, while the opposite trend is observed for Al and Si. The intermediate size particles are observed to contain the most significant amounts of the volatile metals, Pb and Hg.

X-ray diffraction (XRD) was used to determine the species compositions of the fly ash particles of different sizes. The samples for the analyses were prepared using the size classified ash. This technique was only sensitive to the main components of the ash and the results of the measurements are illustrated in Figure 5.5.

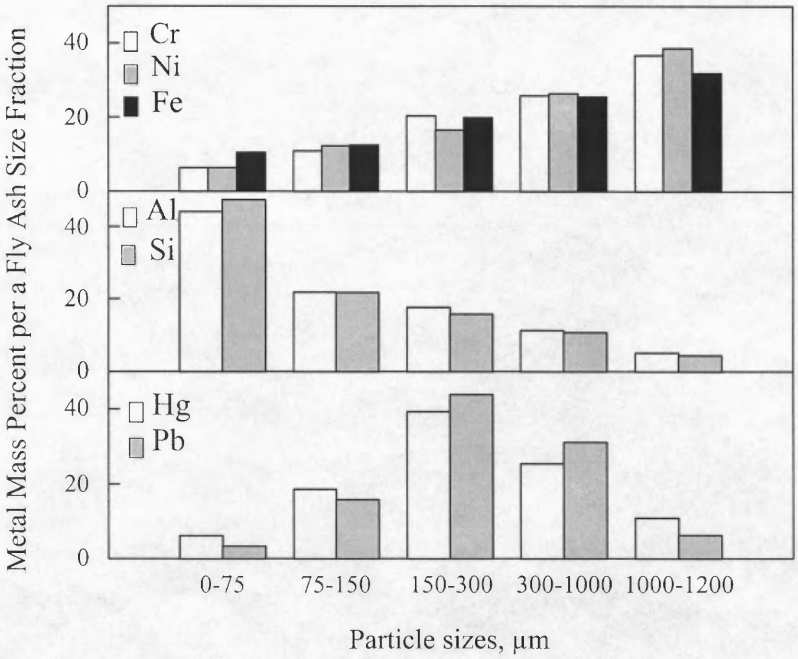

Figure 5.4 AA results on elemental compositions of different size fractions of the fly ash particles. The total metal mass concentrations in the fly ash are: Cr - 0.025%; Al - 0.12%; Ni - 0.028%; Fe - 13.35%; Si - 2.11%; Hg - 0.069%; Pb - 0.030

As the XRD patterns showed, the main fly ash components were carbon, iron, and silicon containing species, consistently with the atomic absorption and chemical measurements (Figures 4.1 and 5.4). Although the XRD results are qualitative, the heights of the observed peaks reflect the relative concentrations of the respective species. As shown in Figure 5.5, such components as FeOOH, C, and SiO_2, and somewhat unexpectedly, pure Fe, are observed in all the fly ash particles. The pure iron could occur in the fly ash as a result of vaporization and reduction of iron oxide formed in the primary combustion chamber (Senior et al., 2000).

Peaks of a metastable iron oxide FeO are observed in the particles less than 1000 μm, and peaks of a stable iron oxide, Fe_2O_3, appear in the smaller particles, less than 300 μm. It is also interesting that significant amounts of FeSi are observed in the largest

particles (> 1000 μm). According to the Fe-Si phase diagram (Massalski, 1990), this is the most high-temperature ferro-silicon phase, stable at about 1400°C. This phase is essentially absent in all the smaller size particles, in which other Fe-Si alloys are found. A phase of Fe_3Si stable at temperatures below 1196°C is present in particles less than 1000 μm. A compound Fe_5Si_3, that is normally stable in the limited temperature range of 960 – 1072 °C is found in the particles in the size range of 150 – 300 μm.

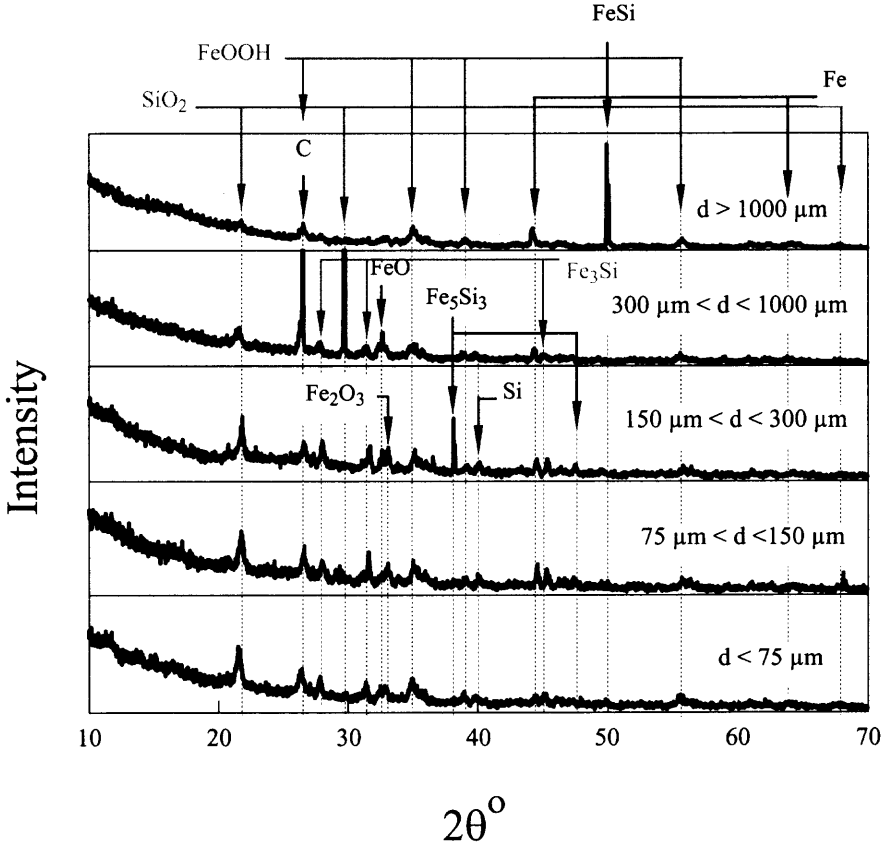

Figure 5.5 X-ray diffraction patterns of different size fractions of the fly ash particles.

In agreement with the AA measurements, the overall intensity of the SiO_2 peaks increases for the smaller particle sizes. Very strong peaks of a low-temperature modification of silica are observed in the size range of 300 – 1000 μm, that can be

interpreted by the presence of sand particles entrained in the gas flow and later captured in the filter. Note that the XRD analysis of the synthetic fuel showed the presence of cristobalite, a high-temperature silica specie, different from that found in the fly ash. Polymorphic phase transitions are known to occur in cristobalite during annealing, and such a transition could explain the difference between the species of silica present in the fuel and in fly ash.

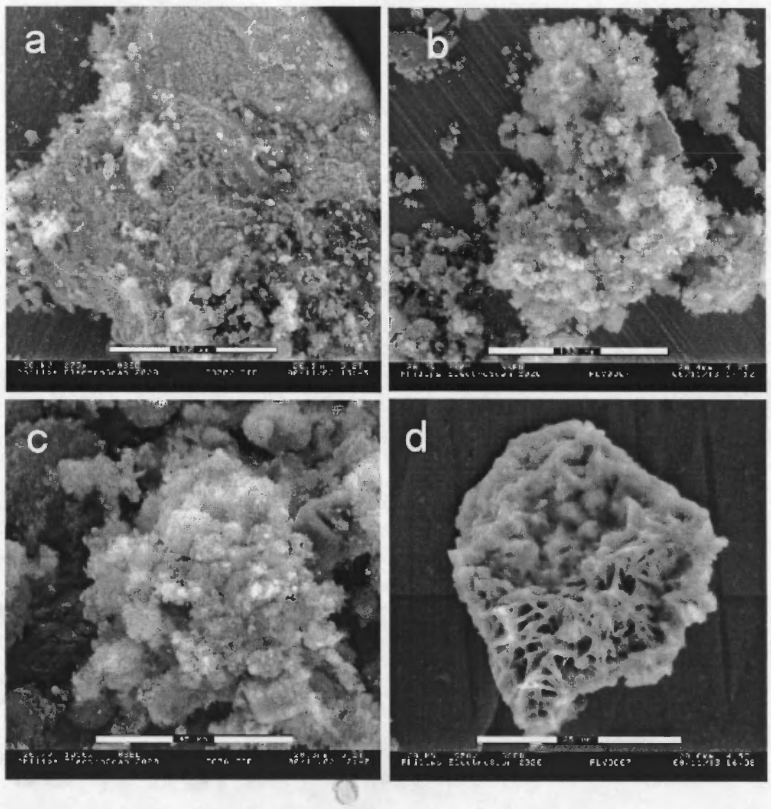

Figure 5.6 SEM Images of different size fly ash particles.
Scale bars: a,b:150 μm, c:45 μm, d:25 μm

Pure Si peaks are also observed in the particles less than 1000 μm, the strongest Si peaks are visible for the particle sizes from 75 to 300 μm. The formation of pure Si could be explained through a reduction reaction of SiO_2 with CO in the oxygen-lean gas pockets (Wey et al., 1998). However, it remains unclear why the pure Si is observed in

the particles of these specific size ranges. It is interesting that according to the XRD analyses, the decrease in the overall iron content in the smaller particles observed using atomic absorption (Figure 5.4), can be linked with the decrease in the contents (i.e., peak intensities) of the Fe-Si compounds. At the same time, the increased amounts of the iron oxides (FeO and Fe_2O_3) are observed in the smaller particles in spite of the overall decrease in the iron content.

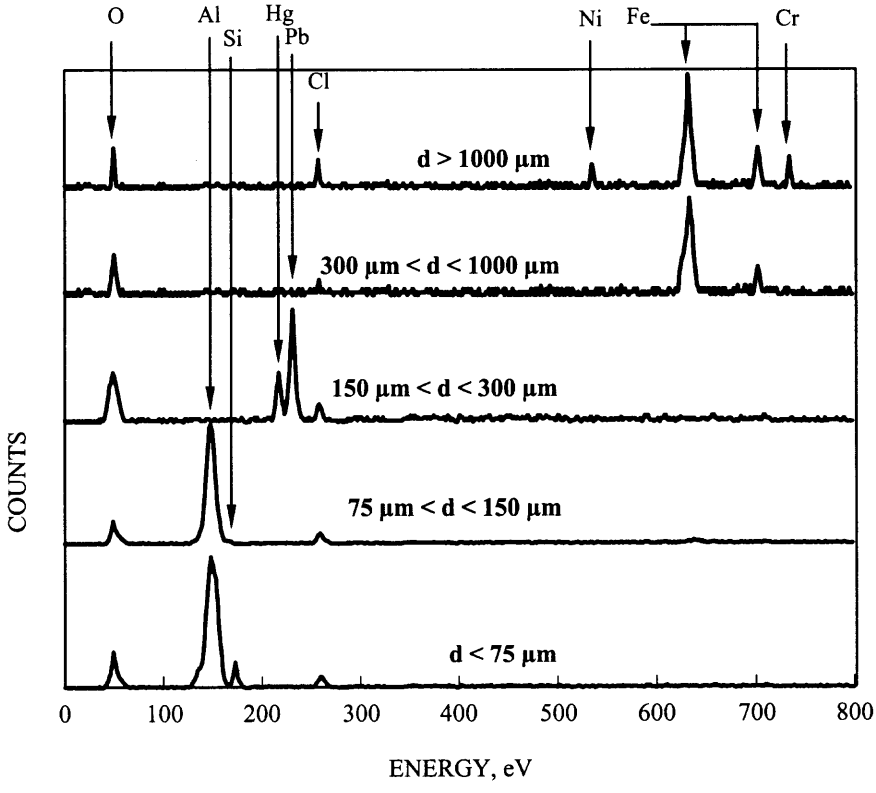

Figure 5.7 Results of Energy-Dispersive Spectroscopy for different size fly ash particles

The measurements described above and producing the information on the bulk compositions and species of different size ash particles have been supported by the elemental composition measurements for individual particles. An Electro Scan environmental scanning electron microscope integrated with Kevex Sigma 3 Energy

Dispersive X-ray Spectroscopy detector (EDS) was used to study morphology and identify compositions of individual fly ash particles. The results of these analyses are illustrated in Figures 5.6 and 5.7. A typical image of a large particle found in the fly ash is shown in Figure 5.6a. It can be noted that the core of the particle is monolithic, and thus the large particles found in the fly ash are not agglomerates of smaller particles. Indications of the layered surface morphology are visible, and a number of smaller particles are attached to the large particle surface. The EDS spectra shown in Figure 5.7 indicate strong peaks of iron (both K_α and K_β), in agreement with the AA and XRD measurements. In addition, K_α peaks of both Ni and Cr are clearly visible for this particle's spectrum. Note that the sensitivity of the EDS measurements is very high for the metals and heavier elements, so that they are readily detected even though their relative contents could be too low to be detected by XRD. Peaks of oxygen (K_α) and chlorine (K_α) are also evident in the EDS spectra for this and all other particles.

An image of a typical fly ash particle of the size in the range of 150 – 300 μm is shown in Figure 5.6b. The particle has a crystalline core and a large number of smaller, 10 – 30 μm, particles are attached to its surface. The bond between the crystalline core and the attached particles is expected to be reasonably strong because the small particles remained attached in spite of the processing of the fly ash in the sieve shaker. As shown in the EDS spectrum for this particle (Figure 5.7), iron peaks disappear, but strong Hg and Pb peaks appear indicative of the high content of these two volatile and toxic metals in the particles of this size range. As shown in Figures 5.1 and 5.2, the number of fly ash particles in this size range is relatively small, but, as shown in Figure 5.3, they contain the greatest amounts of lead and mercury. It is, therefore, suggested that size

classification of particles of this size fraction could significantly reduce amounts of these toxic metals in the reminder of the fly ash.

A typical image of a particle from the size range of 75 – 150 μm is shown in Figure 5.6c. The particle core consists of different size rectangular crystallites. In addition, a number of micron-size spherical particles can be found attached to the particle surface. A strong aluminum peak appears in the EDS spectrum measured for this particle, as shown in Figure 5.7.

Finally, an image of a 25 μm size particle is shown in Figure 5.6d. It is a crystalline particle with porous structure, no smaller particles can be seen attached to it. Strong Al and Si peaks are observed at the EDS spectrum (Figure 5.7) measured for this particle, in agreement with the AA measurements showing the highest Al and Si contents in the particles of less than 75 μm size.

5.4 Summary

The nature of the observed difference in the compositions of the different size fly ash particles is not immediately clear. It is suggested that the comparison of the oxidation and volatilization rates of different species with their feed rate into the combustion chamber might indicate the mechanisms responsible for the observed trends. Sampling of the fly ash from different locations of the incinerator is also suggested to be useful. While additional research is needed to better understand the processes leading to the partitioning of metal species between the fly ash particles of different sizes, the practical implications of the reported here experimental results could be exploited almost immediately. For example, an inexpensive and straightforward technique of ash processing based on the particle size classification could be developed. Applying such a

technique could result in the efficient removal of the lead and mercury-rich particulates from the produced ash. The processed, environmentally benign ash portions will therefore be useful for a variety of the recycling-based manufacturing technologies. At the same time, mercury and lead can be recovered from the separated ash fractions rich with these metals and used in the manufacturing employing mercury and lead. Other materials, e.g., iron, silica, or iron-silicon alloys could also be recovered effectively if the collected fly ash is preliminary size classified.

In order to start development of new ash processing technologies, it would be important to find out how similar or dissimilar the compositions of the different size ash particles are when the ash samples are produced in different combustors. It would also be interesting to determine whether the trends in the morphology and composition found for the ash of synthetic fuel imitating solid waste are also valid for coal-based fuels.

CHAPTER 6

CONCLUSIONS

6.1 Dissertation Conclusions

In the previous studies of incineration metal partitioning, only few researchers have been able to compare the amounts of metals fed to and exiting from the incinerator. Numerous studies have been published, focused on partitioning of a few toxic metals like Hg, Pb, Cr, Cd, As and Ni. Most of the times the partitioning results for the metals have been reported as percentage distribution in bottom ash, fly ash and flue gas without discussing the phases of metals distributed. This is due to the difficulties of identifying the trace metal phases and measuring concentrations, usually in the order of parts per million (ppm). The effects of some of the experimental conditions, such as chlorine content, combustion temperature, and incinerator design on metal partitioning have been extensively studied. The kinetic data available for chemical transformations occurring during incineration in general and metal reactions in particular is very limited. In many of the theoretical studies of metal partitioning, predictions have been made and effects of incinerator operating parameters e.g., combustion temperature, chlorine content of the fuel, and flue gas residence time on metal phase distribution have been discussed based on the results of the equilibrium modeling. However, in most cases the fuels used by researchers in equilibrium modeling did not have a formula representative of MSW.

In this research, a pilot-scale incinerator has been constructed for emulating large-scale incinerators. The capability of the unit to operate at steady state conditions after a transient startup phase has been demonstrated. A well-characterized synthetic co-fired fuel has been fabricated and utilized. The synthetic includes all the typical components of

MSW, its parameters and composition are characterized using standard ASTM methods developed for the refuse-derived fuels. Density, heat of combustion, and composition of the synthetic fuel are found to be similar to those of MSW. Preliminary combustion experiments were conducted using synthetic fuel and pilot-scale incinerator research facility and it has been observed that steady state operation regimes can be achieved and reproduced using repeatable fuel feed rates and airflows. Thus, the new synthetic fuel can be used in the future experiments aimed at the parametric characterization of the MSW incineration processes. Thermodynamic equilibrium computations were conducted for a wide range of fuel/air ratios using chemical species representative of each synthetic fuel component. Comparisons of the equilibrium computation results with the limited experimental measurements of the combustion product gas species show that chemical kinetics must be considered for an adequate modeling of the MSW incineration processes.

An experimental technique was developed for studying metal partitioning in the products of waste incineration. The technique exploits a continuous feed, pilot-scale incinerator facility and well-characterized and reproducible synthetic fuel imitating the MSW. The total amounts of metals in different components of combustion products were determined using atomic absorption spectroscopy. The phases of different metals in fly and bottom ash were determined using x-ray diffraction and compared with the product compositions expected based on the thermodynamic equilibrium estimates. It was observed that the effect of chlorine on metal partitioning becomes important when chlorine contents in the fuel significantly exceed 0.5 %, the typical chlorine contents in the US MSW. The results on the overall metal partitioning between the fly ash, bottom ash, and flue gas are in reasonable agreement with the earlier experimental reports.

Mechanical entrainment of metal particles in the turbulent gas flow in the primary combustion chamber was indicated to be important in transferring iron oxides into the fly ash. It has been also found that the sequence of iron oxidation, reduction, vaporization, and condensation has occurred and caused production of elemental iron in the fly ash. Because of the large absolute iron concentration in the municipal waste and its combustion products, this sequence is important for the understanding of the overall ash particle formation mechanisms. Evidence of another reduction process, formation of elemental Si from SiO_2 has also been found. Such processes need to be considered in modeling the waste incineration because of their effect on the flame exothermicity and mechanisms of the formation of bottom ash. It has also been observed that the slow kinetics of such processes as oxidation of Al and volatilization of oxides of Cr and Ni needs to be considered to adequately describe the behavior of these metals in the furnace and caution should be exercised when the thermodynamic equilibrium predictions are used.

Finally, the results indicate that significant amounts of the lead and mercury-containing species comprise of very fine particles that are not effectively captured by the fabric filters. It is also suggested that a more detailed characterization of the species distribution and morphology of the fly and bottom ashes be conducted to better understand the processes and conditions affecting the ash formation and metal species partitioning. It is also suggested that for a future research, a new electrostatic precipitation filter system should be installed in the NJIT pilot scale combustor facility to enable capturing the fine fly ash particles.

It has been observed that the fly ash particles have bimodal size distribution and that the particles of different sizes have different elemental and phase compositions.

Concentrations of Al and Fe are greater in the coarse particles (up to 1 mm diameter), whereas concentrations of Cr, Ni and Si are higher in the finer particles (less than 75 μm). Concentrations of the volatile metals (Pb and Hg) were observed to peak for the particles in the 150-300 μm diameter range. The nature of the observed difference in the compositions of the different size fly ash particles is not immediately clear. It is suggested that the comparison of the oxidation and volatilization rates of different species with their feed rate into the combustion chamber might indicate the mechanisms responsible for the observed trends. Sampling of the fly ash from different locations of the incinerator is also suggested to be useful.

While additional research is needed to better understand the processes leading to the partitioning of metal species between the fly ash particles of different sizes, the practical implications of the reported here experimental results could be exploited almost immediately. For example, an inexpensive and straightforward technique of ash processing based on the particle size classification could be developed. Applying such a technique could result in the efficient removal of the lead and mercury-rich particulates from the produced ash. The processed, environmentally benign ash portions will therefore be useful for a variety of the recycling-based manufacturing technologies. At the same time, mercury and lead can be recovered from the separated ash fractions rich with these metals and used in the manufacturing employing mercury and lead. Other materials, e.g., iron, silica, or iron-silicon alloys could also be recovered effectively if the collected fly ash is preliminary size classified. In order to start development of new ash processing technologies, it would be important to find out how similar or dissimilar the compositions of the different size ash particles are when the ash samples are produced in different

combustors. It would also be interesting to determine whether the trends in the morphology and composition found for the ash of synthetic fuel imitating solid waste are also valid for coal-based fuels.

6.2 Claim of Originality

1) The research was carried out using a unique pilot scale incinerator. This apparatus has two combustion chambers, a heat exchanger, and a fabric filter baghouse. Its primary combustion chamber is equipped with a moving grate, facility for overfire air and underfire air, a continuous solid fuel feed mechanism and air pollution controls. This enabled the author to replicate actual municipal incinerator conditions, which was not possible in bench scale units.

2) A unique synthetic fuel was formulated to represent MSW in the United States and was characterized both physically and chemically.

3) For most of the previous metal partitioning studies, the metals have been introduced in the lab scale incinerators by spraying solutions in natural gas flames. However in municipal incinerators metals are present in the waste in solid form. To replicate the entry of metals in actual incinerators, the solid synthetic fuel was doped with metal powders in this study.

4) Although metal partitioning has been investigated before, very few researchers have been able to complete metal mass balance for MSW incinerators. Such balance of metals in the fuel and combustion products was established in the present work.

5) For a number of metals, metal phases in bottom ash and fly ash have been experimentally identified by XRD and characterized for the first time.

6) Link between the metal partitioning and fly ash particle size distribution and morphology has been investigated in this study for the first time.

APPENDIX A

ATOMIC ABSORPTION SPECTROSCOPY

1.0 Introduction

Atomic absorption spectroscopy (AA) has become an important tool in environmental analysis. Almost every known metallic element can be determined by this method. In most cases, trace amounts of an element can be identified in the presence of much higher concentrations of other elements.

2.0 Operation of Flame Atomic Absorption Unit (AA)

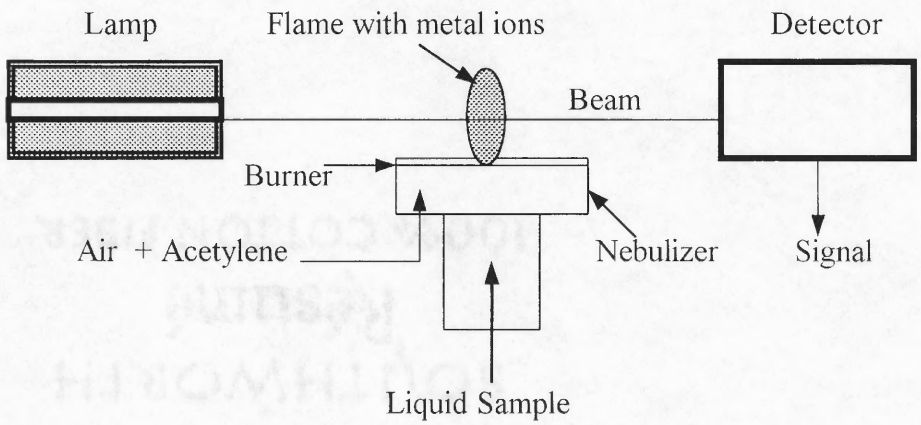

Figure A1 Block Diagram of Atomic Absorption Unit.

The principle of operation of AA is based on the Beer's law of absorption $A = \epsilon bc$ where, A = Absorbance of the medium, b = path length (cm), ϵ = molar absorptivity (L mol^{-1} cm^{-1}), c = concentration (mol L^{-1}). In the flame atomic absorption unit the liquid sample is first mixed with air and a gaseous fuel such as acetylene (Skoog et al., 1997). This is done in a nebulizer, which mixes the sample solution with the fuel and oxidizer to form an aerosol (see Figure A1). The solution is then aspirated into a burner flame. The

flame emerges from a flat slot in the burner. Metallic atoms are released in the flame after aspiration. A hollow cathode lamp emitting wavelength specific to a particular metal is used for absorbance measurement. The beam from the lamp passes through the flame and a detector measures the absorbance of the atomized species in the flame. The absorbance is proportional to the concentration of the ground state atoms in the flame. The monochromatic beam passes along the entire length of the flame for a higher sensitivity and longer absorbing path. The absorbance of the metal species measured by the detector is displayed on an electronic display. The same procedure is applied to standard solutions of known concentrations and their absorbances are measured. The absorbances of the standard solutions are plotted against the concentration and a calibration curve is obtained. Based on the calibration curve, the unknown concentration of a metal can be calculated from the measured absorbance.

3.0 Description of the AA Instrument Accessories

Lamps: The light source for the AA analysis must give narrow line spectra of the element of interest. The requirements for such light sources are stability, long life, brightness, and a narrow line width. In the AA instrument, hollow cathode lamps usually serve as light sources. The cathode of such a lamp is a hollow cup, which contains the same element as that to be determined. This hollow cup is usually filled with an inert gas (usually neon or argon) under low pressure. Approximately 600 volts at 1 to 50 milliamperes are applied between the anode and cathode. This operating current is a critical parameter in optimizing the atomic absorption measurement. High absorbance

and good signal to noise ratio occur at currents of about one third of the maximum lamp current.

Burners: Two different types of burners, a long path Air/Acetylene burner and a nitrous oxide burner are used depending on the element to be analyzed. The Air-Acetylene burner has a single slot with dimensions optimized to yield the maximum sensitivity. Its interior faces are polished to allow it to be used with sample solutions containing dissolved solids. The nitrous oxide burner is designed for the high temperature work in atomic absorption. It has a single slot design and is constructed out of titanium. It is designed to permit an increased ambient airflow to reduce carbon build up common in the high temperature organic flames. It is important to measure and adjust the burner height for the correct operation of the AA instrument. The burner height is the distance from the center of the focal point of the hollow cathode lamp beam to the top of the burner. Three types of flames are used: rich, stoichiometric and lean flames.

Nebulizer: It is the premix system of the AA instrument. It is designed to provide a uniform mixture of fuel, oxidizer and sample mist fed to the flame. The best accuracy can be obtained only when the flame stoichiometry and the sample aspiration rate are carefully optimized. The nebulizer is equipped with a corrosion resistant orifice and a stainless steel capillary. The nebulizer is adjusted to deliver the liquid mist at a rate of 0 to 12 ml/minute. An impact bead adjusts the flow of the liquid mist from the nebulizer. The position of the impact bead relative to the orifice has a strong effect on the nebulizer sensitivity and performance. The optimum bead position is 0.3 to 0.5 mm from the fully choked position (no flow).

APPENDIX B

X-RAY DIFFRACTION

1.0 Introduction

X-ray diffraction provides a convenient and practical means for the qualitative identification of crystalline compounds. X-ray diffraction is widely used in the industry for elucidating the structures of such complex natural products as steroids, vitamins and antibiotics. X-ray powder methods are based upon the fact that an X-ray diffraction pattern is unique for each crystalline substance. Thus, if an exact match can be found between the pattern of an unknown and an authentic sample, chemical identity can be assumed. The operation principle of X-ray diffraction equipment is based on the Bragg's law, $n\lambda = 2d \sin \theta$, Where θ is the diffraction angle, λ is the wavelength of radiation, n is peak number and d is the interplanar distance of the powder sample (Skoog et al., 1997). When an X-ray beam strikes a crystal surface at some angle θ, a portion is scattered by the layer of atoms at the surface. The unscattered portion of the beam penetrates to the second layer of atoms where again a fraction is scattered, and the remainder passes on to the third layer and so on. As a result of the cumulative effect of this scattering from the regularly spaced centers of the crystal, a diffraction pattern is produced. The requirements for the X-ray diffraction are: 1) The spacing between the layers of atoms must be the same order of magnitude as the wavelength of the X-ray radiation. 2) The scattering centers must be spatially distributed in a highly regular way.

2.0 Preparation of Samples for the X-Ray Diffraction (XRD) Analyses

For analytical diffraction studies, the crystalline sample is ground to a fine homogenous powder. In such a form, a large number of small crystallites are oriented in every possible direction; thus, when an X-ray beam traverses the material, a significant number of the particles can be expected to be oriented in such a way as to fulfill the Bragg's law for reflection from every possible interplanar spacing. The sample may be held in the beam in a thin-walled glass or metallic containers. Alternatively specimens can be mixed with binders and molded to appropriate shape. The container for the powder placement used in this project consisted of a flat 3" X 5" glass substrate covered with a metallic plate with a rectangular window (see Figure A2). The powder sample was packed in the window. This container was placed on the X-ray diffractometer positioning table.

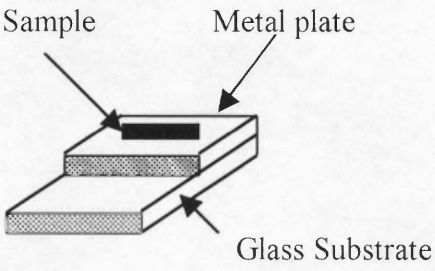

Figure A2 XRD Sample Metallic Container

3.0 Measurement by X-Ray Diffraction Instrument

A Phillips X-Ray diffraction instrument (model X-PERT) was used for testing of bottom and fly ash samples. The instruments for these applications contain components that are analogous in function to the five components of instruments for the optical spectroscopic measurements. These components include a source, a device for restricting the wavelength range of incident radiation, a sample holder, a radiation

detector and a signal processor with readout. These components are different in details from the optical counterparts but their function is the same. The detector senses the monochromatic radiation and sends out a measurement signal, which is recorded by a PC data acquisition system. The Instrument operation is controlled by a PC based software developed by Phillips Inc. Once the sample is prepared and loaded in the instrument, the parameters such as scan step size, range of scanning angles and time per step are specified as the input data to the software. Once an operator starts the measurement, the X-ray diffraction pattern scanning is done automatically. The final XRD spectrum is plotted and peaks are identified by comparison with the library spectra. In this study, the XRD was used to obtain spectra of the bottom ash, the size classified fly ash and the synthetic fuel components.

APPENDIX C

SAMPLE INCINERATOR DATA

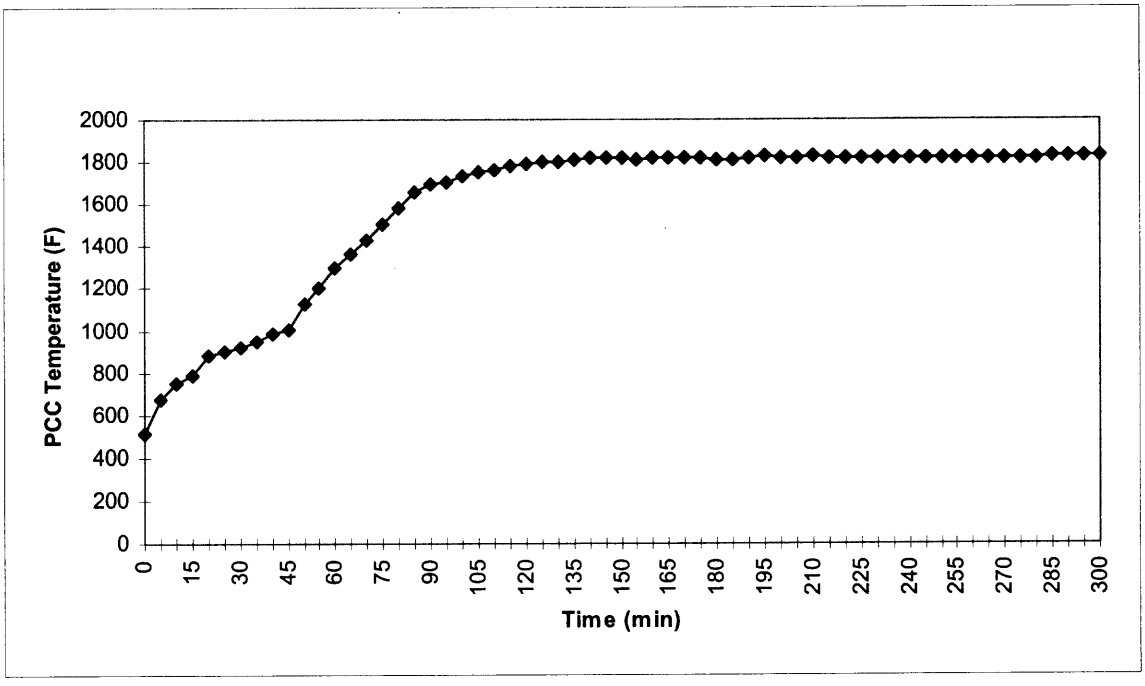

PLOT 1 Primary Combustion Chamber Temperature Profile

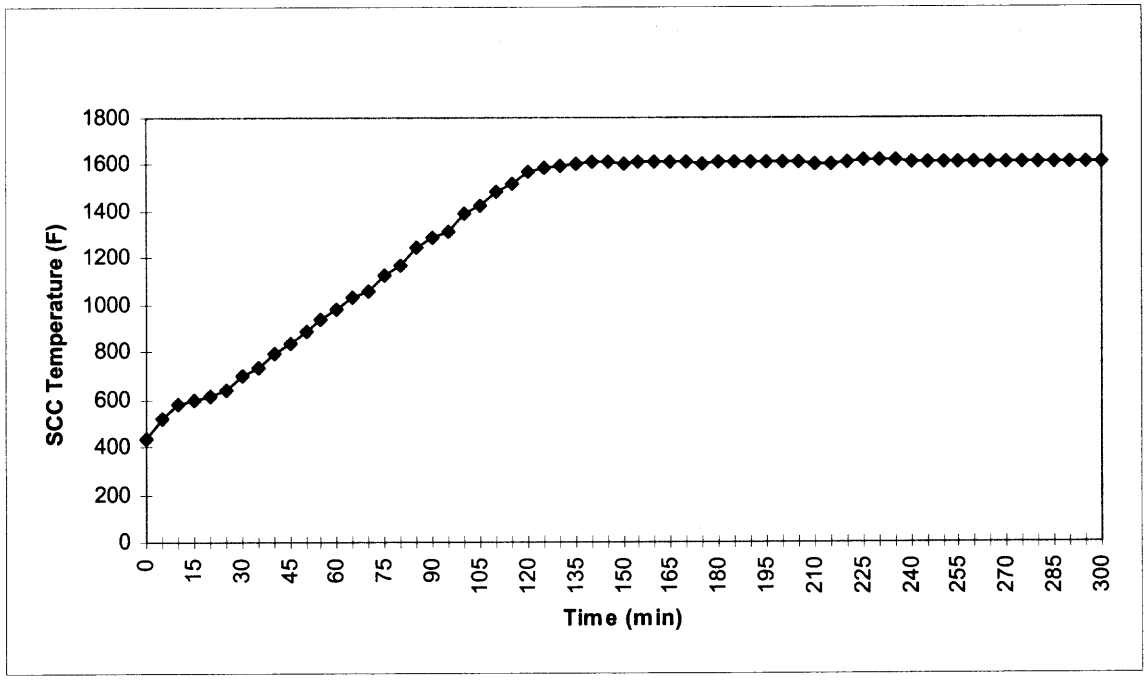

PLOT 2 Secondary Combustion Chamber Temperature Profile

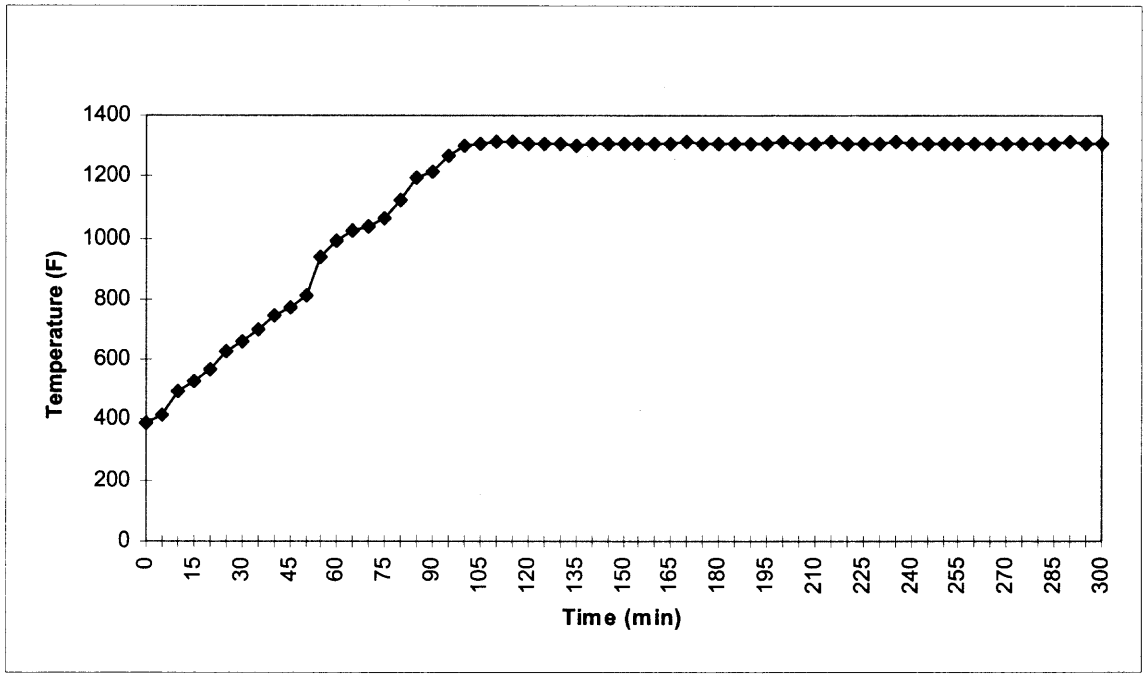

PLOT 3 Temperature Profile at CEMS Sampling Port 1
(Located after Secondary Combustion Chamber)

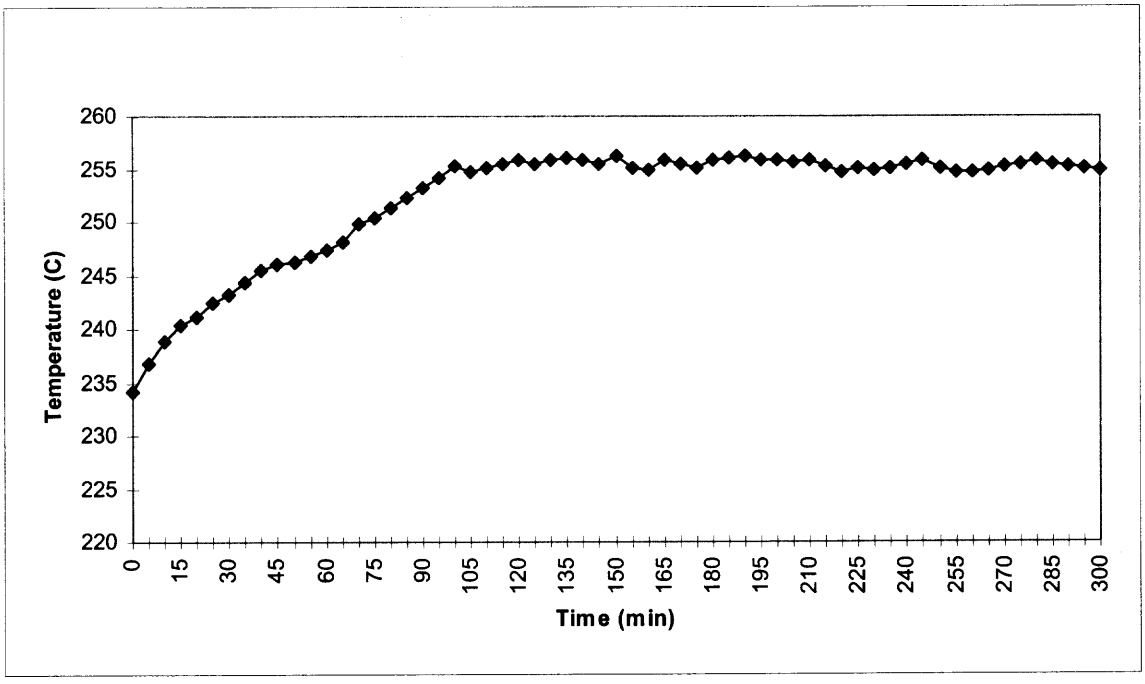

PLOT 4 Temperature Profile at CEMS Sampling Port 2
(Located after Heat Exchanger)

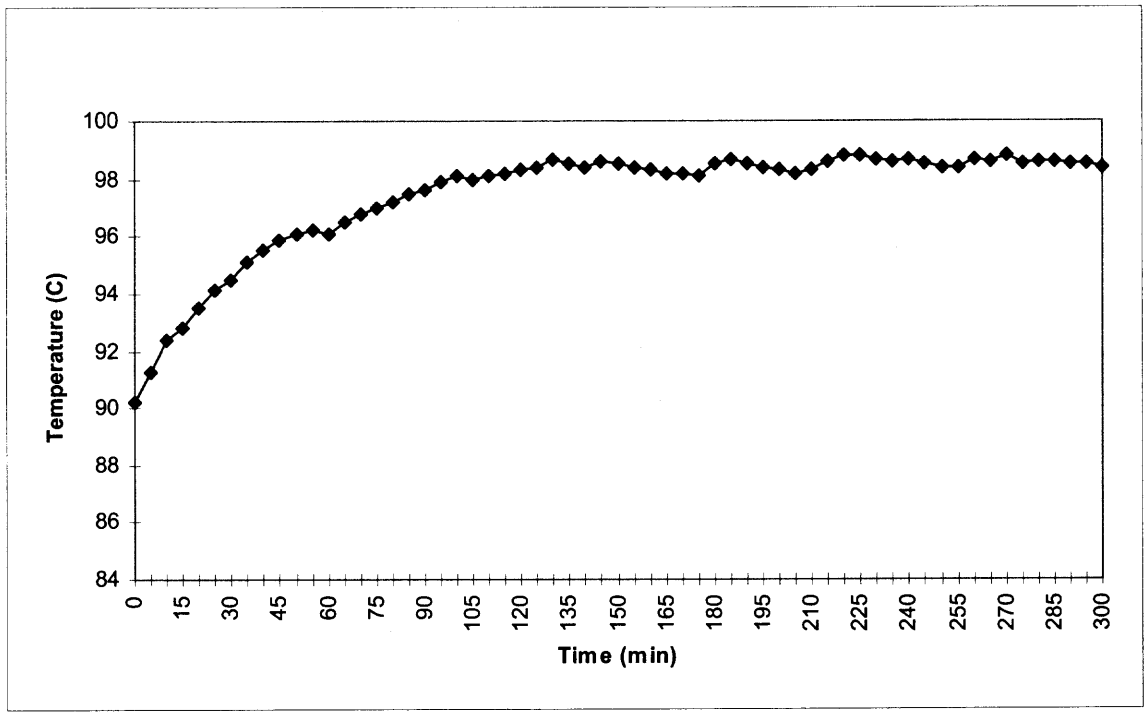

PLOT 5 Temperature Profile at CEMS Sampling Port 3
(Located after Baghouse)

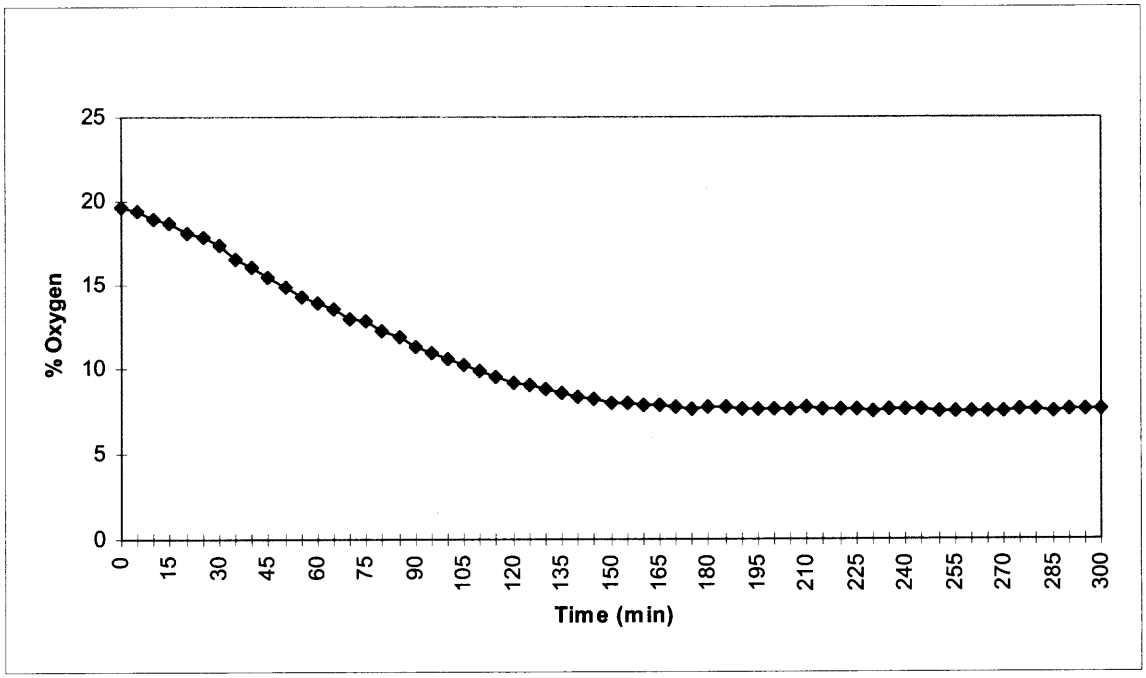

PLOT 6 Oxygen Profile at CEMS Sampling Port 3
(Located after Baghouse)

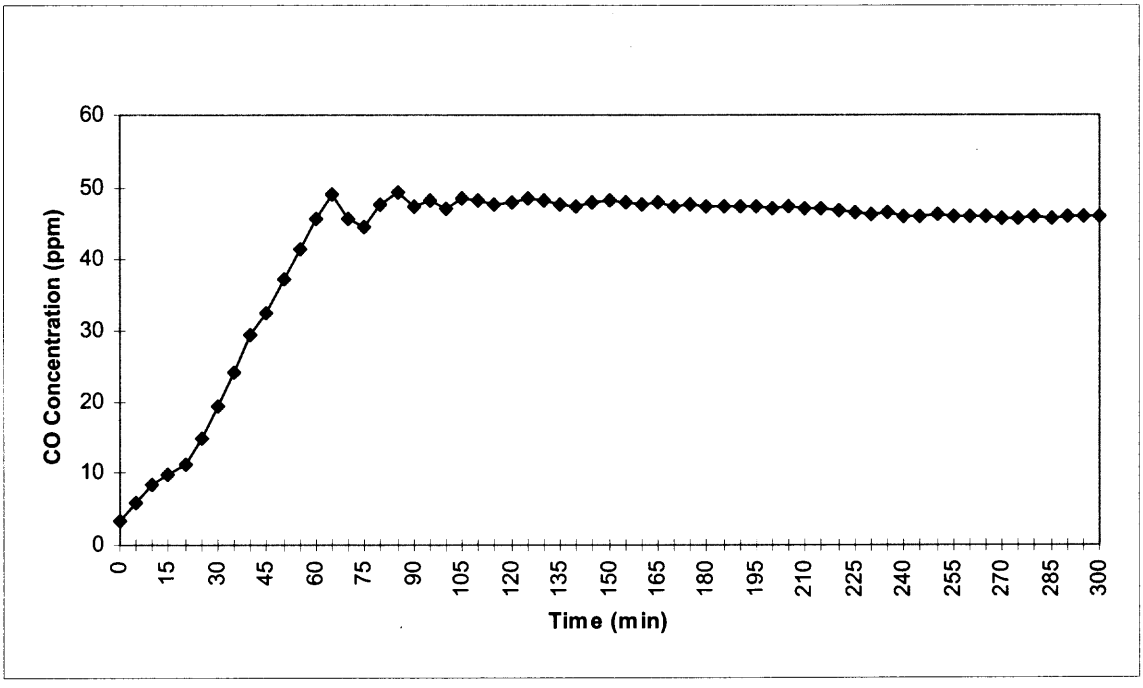

PLOT 7 Carbon Monoxide Profile at CEMS Sampling Port 3
(Located after Baghouse)

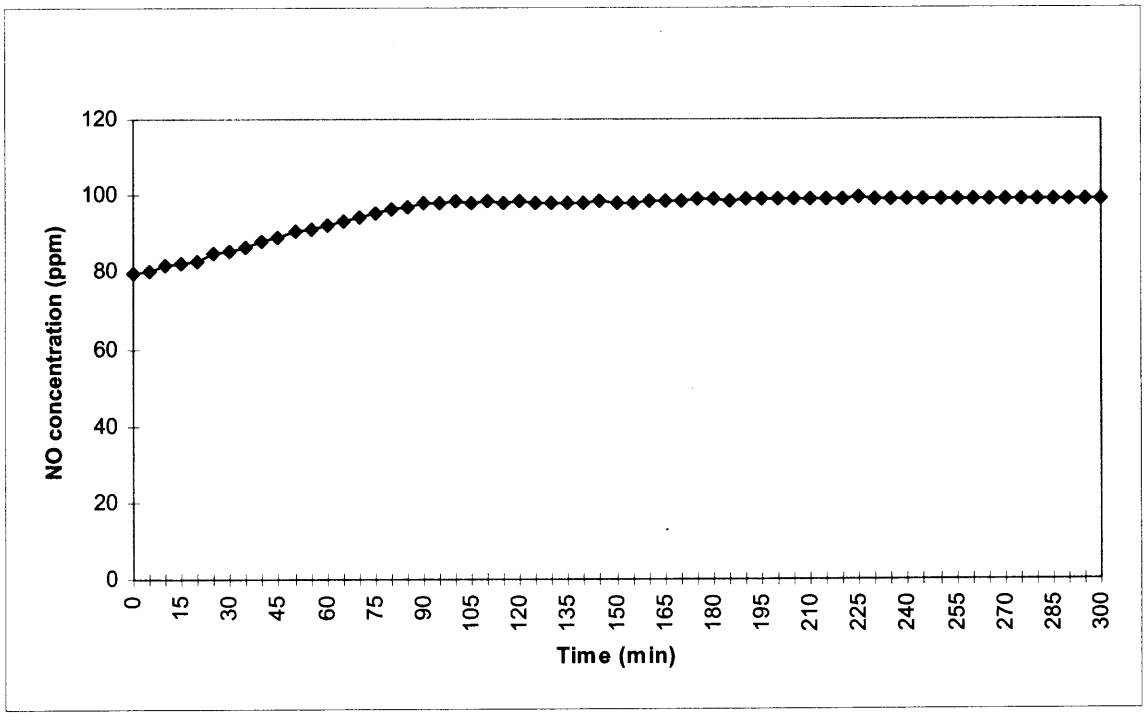

PLOT 8 Nitrous Oxide Profile at CEMS Sampling Port 3
(Located after Baghouse)

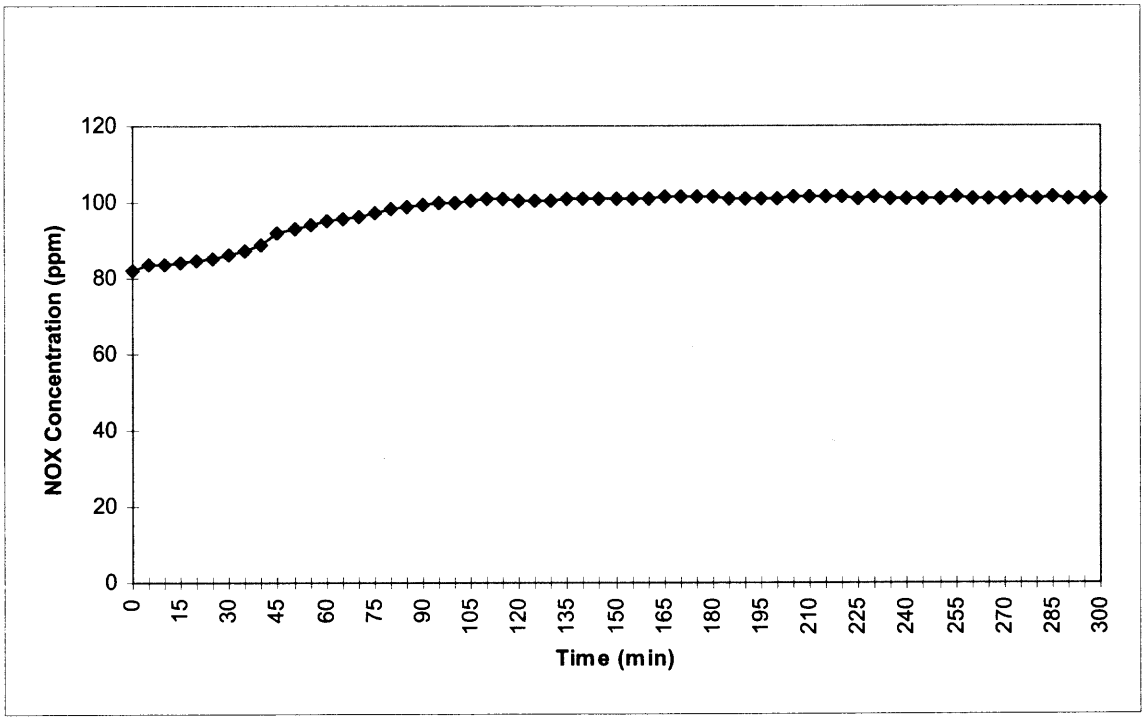

PLOT 9 NOx Profile at CEMS Sampling Port 3
(Located after Baghouse)

Incinerator Data Summary Sheet

Date of Run : 11/09/99

Run time : 7 Hrs (Including warm up time)

Fuel feed rate : 27 lbs/hr (4.5 lbs every 10 minutes)

Total feed : 135 lbs (for 5 hours)

Overfire air : 3 SCFM

Underfire air : 0.3 in H_2O column.

Grate cooling water flow rate : 10 gallons per minute

Fuel residence time on grate : 25 minutes

Incinerator draft : 0.06 in H_2O column on magnahelic

Pitot tube reading : 0.8 in H_2O column on manometer.

Flue gas velocity : 3340 feet per minute.

Sampling :

Flue gas sampled from sampling manifold.

Fly ash sampled from fabric filters in baghouse.

Bottom ash sampled from the incinerator grate.

Bottom Ash Weight : 28 lbs

Fly Ash Weight : 6 lbs

APPENDIX D

XRD MEASUREMENTS ON FUEL COMPONENTS

The synthetic fuel and its components namely paper, plastic, sand, metal, wood and organic food were analyzed individually by X-ray diffraction. The total fuel spectrum and the individual fuel component spectra are shown in Figure A4. A brief description of each component spectra is given below.

Sand: This is the inert component of the fuel. The major constituent is Silica (SiO_2) with multiple peaks observed at different angles. The 100 % intensity peak is observed at angle 26.64 and a 35% intensity peak is observed at 20.83. Smaller peaks of 12% intensity are observed at angles 36.52 and 39.45.

Metal: The metallic content of the fuel is represented by iron. Two peaks of intensity 100 % and 20 % at angles 44.67 and 65.02 are visible. Trace metal species are not detected due to their low concentrations.

Plastic: Polyethylene represents the plastic content of the fuel. Two major peaks of intensity 100 % and 35 % are detected at angles 21.48 and 23.84 respectively.

Wood: The major component of the hardwood mulch used to simulate wood is cellulose ($C_6H_{10}O_5$). Three major peaks of intensities 100, 27 and 17 % are observed at angles of 27.3, 22.48 and 31.66 respectively.

Paper: The major constituent of newsprint used to simulate paper is cellulose ($C_6H_{10}O_5$). Presence of 3 strong peaks of % intensity 100, 27 and 17 are observed at angles 27.3, 22.48 and 31.66 respectively.

Food: This is the organic content of the fuel containing nitrogen. The major constituent is α-Diperidyl ($C_{10}H_8N_2$). This species shows 5 strong peaks of % intensity 90, 100, 90, 80 and 70 at angles 16.90, 17.90, 20.68, 26.74 and 22.96 respectively.

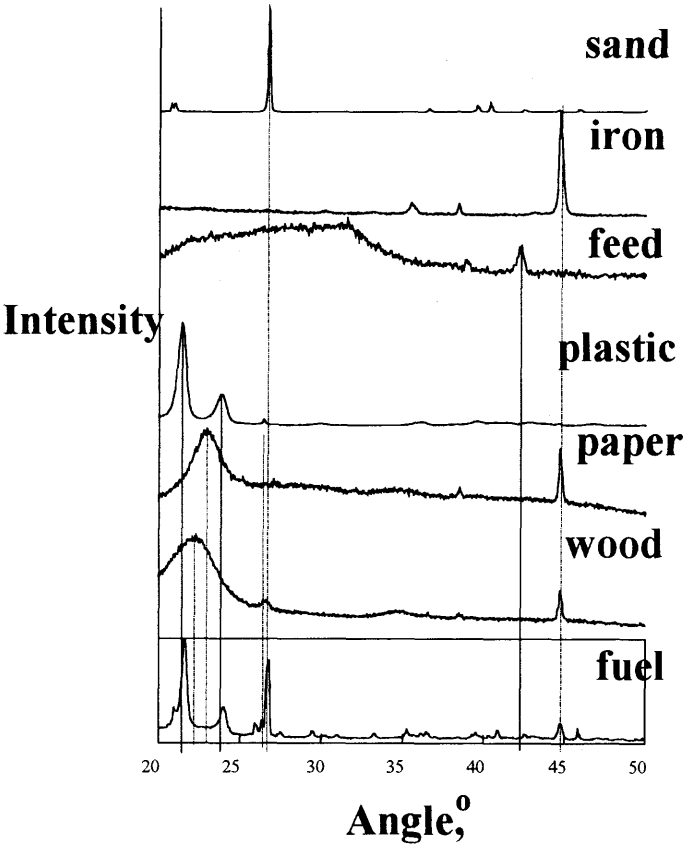

Figure A3 Total fuel and individual component XRD spectra

APPENDIX E

COMPUTATION OF HEAT OF FORMATION OF SOLID POLYETHYLENE

In order to simulate the combustion of fuel by equilibrium modeling, it was required to estimate the enthalpy of formation of solid polyethylene. The estimates for heat of formation of solid polyethylene were obtained by the following two methods.

Method 1: The enthalpy of formation of solid ethylene was obtained as 42.2 kJ/mol from the literature (Cox and Pilcher, 1970). The enthalpy of formation of solid polyethylene was obtained by adding the negative enthalpy of polymerization (Q) per mer –93.4 kJ/mol (Whiteley et al., 1992) to the enthalpy of formation of ethylene. The equation can be written as $\Delta h_f\ (C_2H_4)_n = \Delta h_f\ (C_2H_4) + Q$. This equation leads to a final value of enthalpy of formation of solid polyethylene $\Delta h_f\ (C_2H_4)_n$ as **–51.2 kJ/mol.**

Method 2: The reaction for combustion of polyethylene can be written in equation form as $(C_2H_4)_n + 3nO_2 \rightarrow 2nCO_2 + 2nH_2O$ ---(A). The enthalpy of combustion of polyethylene ΔH_C from literature is 11718 kJ/mol (Niessen et al, 1995). Number of mers in polyethylene polymer is calculated by dividing entire polymer (polyethylene) molecular weight by unit molecular (ethylene) weight. The molecular weight of polyethylene ranges from 145 to 350 and averaging near 265 as reported by Niessen et al., 1995 and CRC handbook of chemistry, 1999. Thus the number of mers (n) in polyethylene ranges from 5.2 to 12.5 averaging 9.5 The enthalpies of formation of water, carbon dioxide and gaseous ethylene are given by NIST to be –241.82 kJ/mol, –393.51 kJ/mol and 52.46 kJ/mol respectively (Eremenko et al., 1998). To estimate the enthalpy of formation of solid polyethylene we write the following equation, where X is the enthalpy of polymerization.

$\Delta h_f (C_2H_4) + X + 3\ \Delta h_f(O_2) = 2\ \Delta h_f (H_2O) + 2\ \Delta h_f (CO_2) + (\Delta H_C / n)$ ---(B)

Substituting values in the equation B (All units kJ/mol),

$52.46 + X + 3(0) = 2(-241.82) + 2(-393.51) + (11718/9.5)$

The enthalpy of polymerization obtained = X = -93.69 kJ/mol

Thus final enthalpy of formation of solid polyethylene = $\Delta h_f (C_2H_4)_n$

$= 52.46 + X = 52.46 - 93.69 =$ **-41.23 kJ/mol.**

Results: Δh_f solid polyethylene (estimate from method 1) = -51.2 kJ/mol.

Δh_f solid polyethylene (estimate from method 2) = -41.23 kJ/mol.

Conclusions: There is slight difference between the values calculated by two methods for enthalpy of formation of solid polyethylene.

APPENDIX F

CONTENTS OF ATTACHED COMPACT DISK

The attached compact disk (CD) contains three main sections. A brief explanation of the contents of each section is explained below.

A) Atomic Absorption spectroscopy: The AA results are divided in two data folders. The first data folder includes results for elemental metal partitioning in the bottom ash, fly ash and the flue gas. The sheet "AAdata1" includes absorbance and concentration measurements for Fe and Si, and the sheet "AAdata2" includes similar measurements for Hg, Pb, Al, Ni and Cr. The calculation of elemental metal concentrations (considering ash weights) is reported in "Metal-partitioning" sheet, and the mass balance data for all metals is reported in "Mass-balance" sheet. The second data folder includes AA measurements on the size classified fly ash ("FlyashAA" sheet).

B) X-ray Diffraction: The XRD results are divided in three data folders. The first data folder includes spectra for six samples of bottom ash and fly ash along with identification algorithm reported in the sheet "Ashtable". The second data folder includes spectra for fuel along with its components and the identification algorithm reported in the sheet "Fueltable". The third data folder includes XRD spectra of size classified fly ash.

C) Equilibrium Modeling: The equilibrium results are divided in two data folders. The first data folder includes input and output files of computations to determine stoichiometric F/A ratio. The second folder includes input and output files of computations to determine adiabatic flame temperature and equilibrium species distribution at different experimental conditions.

REFERENCES

Abe, S., Kanabayashi, F., Kimura, T., and Kokado, M., 1997. Organohalogen Compounds, v31, pp 348.

Andersson, P., and Marklund, S., 1998. Emissions of organic compounds from biofuel combustion and influence of different control parameters using a laboratory scale incinerator, *Chemosphere,* v36, pp1429-1443.

ASME, 1979. Thermodynamic data for waste incineration. American society of mechanical engineers, East 47th Street, New York 10017.

ASTM, 1996. Annual book of ASTM standards, Sections 5 and 11, American Society for Testing and Materials, 100 Barr Harbor Drive, West Conshohocken, PA.

Barton, R.G., Maly, P.M., Clark, W.D., and Seeker, W.R., 1998. Prediction of the fate of toxic metals in waste incineration. *Proceedings of 1998 National Waste Processing Conference,* v1, pp379-386.

Bergstrom, J.J., 1986. Mercury behavior in flue gases. *Waste Management and Research,* v4, pp57-64.

Binner, S., Galeotti, L., Lombardi, F., Mogensen, E., and Srini, P., 1997. Heavy metal distribution in municipal solid waste incineration. *Journal of Solid Waste Technology and Management,* v24, pp45-52.

Biswas, P., and Wu, C., 1998. Control of toxic metal emissions from combustors using sorbents: a review. *Journal of Air and Waste Management Association,* v48, pp113-127.

Blumenstock, M., Zimmerman, R., Schramm, K., and Kettrup, A., 2000. Influence of combustion conditions on the PCDD/F, PCB, PCBz and PAH concentrations in the post combustion chamber of a waste incineration pilot plant. *Chemosphere*, v40, pp987-993.

Bool, L., Peterson, T., and Wendt, J.O.L., 1995. The partitioning of iron during combustion of pulverized coal. *Combustion and Flame,* v100, pp262-270.

Brunner, C., and Monch, H., 1986. The flux of metals through municipal solid waste incinerators. *Waste management and research,* v4, pp105-119.

Brunner, C., 1989. Handbook of hazardous waste incineration. Tab books, Blue Ridge Summit, PA 17294.

Burgess, D.R. Jr., Zachariah, M.R., Tsang, W., Westmoreland, P.R., 1996. *Progress in Energy and Combustion Science,* v21, pp 453-529.

Carrol, G., Thurnau, R., and Fournier, D., 1995. Mercury emissions from a hazardous waste incinerator equipped with a state-of-the-art wet scrubber. *Journal of Air and Waste Management Association*, v45, pp730-736.

Catallo, J., 1998. Polycyclic aromatic hydrocarbons in combustion residues from 1,3-Butadiene, *Chemosphere*, v37, pp143-157.

Çengel, Y.A., 1997. Heat Transfer, A Practical Approach, WCB/McGraw Hill, Boston.

Chen, J., Wey, M., Liu,Y., and Chang, B., 1998. Dynamic adsorption of heavy metals under various incineration temperatures. *Journal of Environmental Engineering,* v124, pp776-779.

Chen, J., Wey, M., Jeng, S., and Hsieh, S., 1998. Two stage simulation of major heavy metal species under various incinerator conditions. *Environment International,* v24, pp451-466.

Chiang, K.Y., Wang, K.S., Lin, F.L., 1997. The effect of inorganic chloride on the partitioning and speciation of heavy metals during a simulated municipal solid waste incineration process. *Proceedings of the Air and Waste management Association's 90th Annual Meeting,* WA88-03, Toronto, Canada.

Cox, J.D., Wagman, D.D., and Medvedev, V.A., 1989. CODATA Key Values for Thermodynamics, Hemisphere Publishing Corporation, New York.

Cox, J.D., Pilcher, G., 1970. Thermochemistry of Organic and Organometallic Compounds, v1 pp 636 Academic Press, New York.

Davis, S.B., Gale T.K., Wendt, J.O.L., and Linak, W.P., 1998. Multicomponent coagulation and condensation of toxic metals in combustors. *Proceedings of Twenty-Seventh Symposium (International) on Combustion*, v1, pp1785-1791.

Dempsey, C.R., and Oppelt, E.T, 1993. Incineration of Hazardous Waste: A Critical Review Update, *Air and Waste*, v43, pp25-73.

Eckert, J., Guo, Q., and Moscati, A., 1999. Mass balance of toxic metals in cement and aggregate kilns co-fired with fossil and hazardous waste-derived fuels. *Environmental Engineering Science,* v16, n1, pp31-56.

Eremenko, L.T., Korolev, A.M., Miroshnichenko, E.A., Lebedev, Yu.A., Apin, A.Y., 1998. In *NIST Chemistry WebBook*, NIST Standard Reference Database Number 69, (Editors. W.G. Mallard and P.J. Linstrom,) National Institute of Standards and Technology, Gaithersburg MD 20899. (http://webbook.nist.gov.)

Fernandez, M., Martinez, L., Segerra, M., Garcia, J., and Esplell, F., 1992. Behavior of heavy metals in the combustion gases of urban waste incinerators. *Environmental Science and Technology*, v26, pp1040-1047.

Furimsky, E., 2000. Characterization of trace element emissions from coal combustion by equilibrium calculations. *Fuel Processing Technology,* v63, pp29-44.

Goodman, D., Ohlsson, O., Sosa, J., 1997. American Plastics Council and Booty, M.R., NJIT, Personal Communication.

Gordon S., and Mcbride B., 1991. CET-89 Equilibrium Code. *NASA Report.*

Gulbransen, E., and Andrew, K., 1958. Oxidation rate measurement for metals and alloys, *Journal of Electrochemical Society*, v105, pp4-20.

Gupta, A.K., and Rohrbach, E.M., 1992. Refuse-derived fuels: technology, processing, quality and combustion experiences. *ASME Proceedings of the Fifteenth National Waste Processing Conference*, Detroit, v1, pp49-59.

Hinton, W.S., and Lane, A.M., 1991. Characteristics of municipal solid waste incinerator fly ash promoting the formation of polychlorinated dioxins, *Chemosphere*, v22, pp473-483.

Ho, T.C., Lee, H.T., Kuo, T.H., Chen, D., and Bostick, W.D., 1994. Analysis of incinerator performance and metal emissions from recent trial and test burns. *Hazardous Waste and Hazardous Materials,* v11, n1, pp53-70.

Jakob, A., Stucki, S., and Kuhn, P., 1995. Evaporation of heavy metals during heat treatment of municipal solid waste incinerator fly ash. *Environmental Science and Technology,* v29, pp2429-2436.

Karimanal, K., and Hall, M., 1996. Effect of temperature and flow on the volatilization of Pb and Cd. *Journal of Hazardous Waste and Hazardous Materials,* v13, pp63-71.

Kiser, J., 1991. Municipal waste combustion in the United States: an overview. *Waste Age,* v22, pp27-29.

Korpiel, J., and Vidic, R., 1997. Effect of sulfur impregnation method on activated carbon uptake of gas phase mercury. *Environmental Science and Technology*, v31, pp2319-2325.

Kubachewski, O., and Hopkins, B., 1962. Oxidation of metals and alloys, Butterworths Publishers, London, UK.

Lee, C.C., 1988. A model analysis of metal partitioning in a hazardous waste incineration system. *Journal of Air Pollution Control Association*, v38, n7, pp941-945.

Linak, W.P., and Wendt, J.O.L., 1993. Toxic metal emissions from incineration: mechanisms and control. *Progress in Energy and Combustion Science,* v19, pp145-185.

Linak, W.P., Ryan, J.V., and Wendt, J.O.L., 1996. Formation and destruction of hexavalent chromium in a laboratory swirl flame incinerator. *Combustion Science and technology*, v116-117, pp479-498.

Lind, T., Valmari, T., Kauppinen, E., Sfiris, G., Nilsson, K., and Maenhaut, W., 1999. Volatilization of heavy metals during circulating fluidized bed combustion of forest residue. *Environmental Science and Technology*, v33, pp496-502.

Ljung, A., and Nordin, A., 1997. Theoretical feasibility for ecological biomass ash recirculation: chemical behavior of nutrient elements and heavy metals during combustion. *Environmental Science and Technology*, v31, pp2499-2503.

Manninen, H., Peltola, K., and Ruskannen, J., 1997. Co-combustion of Refuse-Derived and Packaging-Derived Fuels (RDF and PDF) with Conventional Fuels, *Waste Management and Research*, v15, pp137-147.

Massalski, T.B., Okamoto, H., Subramanian, P.R., and Kacprzak, L., 1990, *Binary Alloy Phase Diagrams*, ASM Publishers, Materials Park, OH.

Mills, A., 1995. Heat and Mass Transfer, Irwin Publishers, Chicago.

Nakamura, K., Kinoshita, S., and Takatsuki. H., 1996. The origin and behavior of lead, cadmium and antimony in a MSW incinerator. *Waste Management Journal*, v16, pp509-517.

Niessen, W., 1995. Combustion and Incineration processes, applications in environmental engineering. Marcel Dekker Publishers, New York.

NIST, 1993. Certificate of Analysis for NIST Standard Reference Material 1657, Synthetic Refuse-Derived Fuel, Gaithersburg, MD 20899.

O'Leary, P., Walsh, P., Ham, R., 1988. Managing solid waste. *Scientific American*, v259, pp36- 42.

Park, B., Bozzelli, J.W., and Booty, M.R., 2000. Polymer pyrolysis and oxidation in a continuous feed and flow reactor: Polyethylene. *Environmental Science and Technology*, In press.

Parr, 1994. Operating manual for the 1341 oxygen bomb calorimeter, Parr Instrument Company, Moline, IL 61265.

Reger, D., Goode, S.R., Mercer, E.E., 1993. Chemistry Principles and Practice, Saunders College Publishing, New York, pp110.

Reimann, D.O., 1986. Mercury output from garbage incineration. *Waste Management and Research*, v4, pp45-56.

Reimann, D.O., 1989. Heavy metals in domestic refuse and their distribution in incineration residues. *Waste Management and Research,* v7, pp57-62.

SANDIA, 1995. Chemkin code for PFR and PSR analysis. *Report- Sandia National Laboratories,* New Mexico.

Selph, C., and Hall, R., 1992. ISP Thermodynamic Equilibrium Code, Air Force Astronautics Laboratory, Edwards AFB, California.

Senior, C., Helble, J., and Sarofim, A., 2000. Emissions of mercury, trace elements, and fine particles from stationary combustion sources, *Fuel Processing Technology*, v65-66, pp263-288.

Shin, D., and Choi, S., 2000. The combustion of simulated waste particles in a fixed bed, *Combustion and Flame*, v121, pp167-180.

Skoog, D.A., Holler, F.J., and Nieman, T.A., 1997. Principles of Instrumental Analysis, Saunders College Publishers, Chicago.

Stanley, J., Von Hoene, J., and Huntoon, R., 1951. *Transactions of American Society of Metals*, v43, pp426-435.

Thipse, S.S., Sheng, C., Sun, H., Bozzelli, J.W., Booty, M.R., and Magee, R.S., 1999. A Pilot-Scale Incinerator for Evaluating the Combustion of Co-fired Plastics, *Proceedings of the Joint meeting of the U.S sections of the Combustion Institute,* v1, pp857-860, George Washington University, Washington, D.C.

Thipse, S.S., Sheng, C., Booty, M.R., Magee, R.S., and Dreizin, E.L., 2001. Characterization of a synthetic fuel for the imitation of municipal solid waste, *Chemosphere* (In Press).

Thipse S.S., and Dreizin, E.L., 2001. Metal partitioning in the products of incineration of municipal solid waste, *Chemosphere* (Submitted).

Tillman, D.A., Rossi, A.J., and Vick, K.M., 1989. Incineration of Municipal and Hazardous Solid Wastes, Academic Press Inc., New York.

Tuttle, K.L., 1998. Combustion generated particulate emissions, *Fuel and Energy*, v39, pp218.

USEPA, 1996. Characterization of municipal solid waste in the United States: 1996 update. *Report* EPA 530-R-97-015, Washington D.C.

Verhulst, D., Buekens, A., Spencer, P., and Eriksson, G., 1996. Thermodynamic behavior of metal chlorides and sulfates under the conditions of incineration furnaces. *Environmental Science and Technology*, v30, pp50-56.

Vogg, H., Braun, H., Metzger, M., and Schneider, J., 1986. The specific role of cadmium and mercury in MSW incineration. *Waste Management and Research,* v4, pp65-74.

Wallis, M., and Watson, A., 1994. MSW incineration: a critical assessment. *Energy World,* v12, pp14-18.

Wang, K., and Chiang, K., 1999. Metal leachability and species analysis in municipal solid waste incinerator ashes. *National Waste Conference, Taiwan ROC.*

Wang, K.S., Chiang, K.Y., Lin, S.M., Tsai, C.C., and Sun, C.J., 1999. Effects of chlorides on emissions of toxic compounds in waste incineration: study on partitioning characteristics of heavy metal. *Chemosphere*, v38, pp1833-1849.

Wey, M., Hwang, J., and Chen, J., 1998. Mass and elemental size distribution of chromium, lead and cadmium under various incinerator conditions. *Journal of Chemical Engineering of Japan*, v31, pp506-517.

White, R., 1987. Effect of lignin content and extractives on the higher heating value of wood, *Wood and Fiber Science*, v19, pp446-452.

Whiteley, K.S., Heggs, T.G., Koch, H., Mayer, R.L., and Immel, W., 1992. In Ulmann's Encyclopedia of Industrial Chemistry, A21, pp487-499.

Winter, M., 2000. WebElements [http://www.webelements.com], University of Sheffield, UK. (Reference Date: 01/02/2000).

Wu, C.Y., and Biswas, P., 1993. An equilibrium analysis to determine the speciation of metals in an incinerator. *Combustion and Flame,* v93, pp31-40.

Wu, C., Biswas, P., and Fendinger, N., 1994. Model to assess heavy metal emission from municipal solid waste incineration. *Journal of Hazardous Waste and Hazardous Materials*, v11, pp71-91.